AN EVALUATION OF HF IONOSPHERIC BACKSCATTER ECHOES

R75EMH19

George H. Millman

November 1975

General Electric Company
Syracuse, New York 13201

DISCLAIMER NOTICE

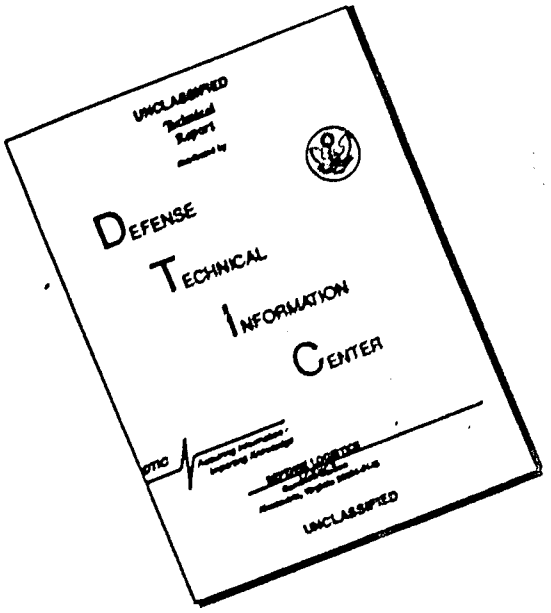

THIS DOCUMENT IS BEST QUALITY AVAILABLE. THE COPY FURNISHED TO DTIC CONTAINED A SIGNIFICANT NUMBER OF PAGES WHICH DO NOT REPRODUCE LEGIBLY.

GENERAL ELECTRIC COMPANY TECHNICAL INFORMATION

Within the limitations imposed by Government data export regulations and security classifications, the availability of General Electric Company technical information is regulated by the following classifications in order to safeguard proprietary information:

CLASS 1: GENERAL INFORMATION

Available to anyone on request.
Patent, legal and commercial review required before issue.

CLASS 2: GENERAL COMPANY INFORMATION

Available to any General Electric Company employee on request.
Available to any General Electric Subsidiary or Licensee subject to existing agreements.
Disclosure outside General Electric Company requires approval of originating component.

CLASS 3: LIMITED AVAILABILITY INFORMATION

Original Distribution to those individuals with specific need for information.
Subsequent Company availability requires originating component approval.
Disclosure outside General Electric Company requires approval of originating component.

CLASS 4: HIGHLY RESTRICTED DISTRIBUTION

Original distribution to those individuals personally responsible for the Company's interests in the subject.
Copies serially numbered, assigned and recorded by name.
Material content, and knowledge of existence, restricted to copy holder.

GOVERNMENT SECURITY CLASSIFICATIONS, when required, take precedence in the handling of the material. Wherever not specifically disallowed, the General Electric classifications should also be included in order to obtain proper handling routines.

TIS Distribution Center
CSP 4-Lobby, X7712
Syracuse, New York 13201

GENERAL ELECTRIC

HEAVY MILITARY EQUIPMENT DEPARTMENT

TECHNICAL INFORMATION SERIES

Author	Subject Category	No.
G.H. Millman	HF Radar, Field-Aligned Backscatter	R75EMH19
		Date Nov 75

Title: AN EVALUATION OF HF IONOSPHERIC BACKSCATTER ECHOES

121 P.

Copies Available at	GE Class	No. of Pages
HMED TIS Distribution Center Box 1122 (CSP4-Lobby) Syracuse, New York 13201	1	
	Govt Class: Unclassified	125

Summary

The characteristics of HF radar echoes reflected from ionization irregularities aligned along the lines of force of the earth's magnetic field are discussed. The spatial-geographical extent of ionospheric backscatter echoes is estimated for an HF radar located in the midlatitudes with the antenna beam oriented toward the polar region. Utilizing experimental radar-ionospheric data acquired at frequencies between HF and UHF, an analysis is made of the amplitude and the cross-sectional area statistics of HF field-aligned echoes. The Doppler frequency variation, the frequency of occurrence and the diurnal and seasonal variation of ionospheric backscatter echoes and their correlation with solar geophysical conditions are also discussed.

Key Words

Ionospheric irregularities	Radar-aurora
Field-aligned ionization	Auroral oval
E-layer backscatter	Spread-F
F-layer backscatter	Polar region
Doppler frequency shift	HF propagation

408 969

Send to _____

-A-

GENERAL ELECTRIC COMPANY
HEAVY MILITARY EQUIPMENT DEPARTMENT
TECHNICAL INFORMATION SERIES

SECTION Advanced Systems and Technology

UNIT 570

HMED ACCOUNTING REFERENCE

COLLABORATORS

APPROVED M. A. Johnson TITLE Mgr., AS&T LOCATION CSP 4-58

M. A. Johnson

TIS R75EMH19

MINIMUM DISTRIBUTION - Government Unclassified Material (and Title Pages) in G.E. Classes 1, 2, or 3 will be the following.

Copies	Title Page Only	To
0	1	Legal Section, HMED (Syracuse)
0	1	Manager, Technological Planning, HMED (Syracuse)
5	6	G-E Technical Data Center (Schenectady)

MINIMUM DISTRIBUTION - Government Classified Material, Secret or Confidential in G.E. Classes 1, 2, or 3 will be the following.

1	1	Classified Section, Electronics Park Library
1	0	Manager, Technological Planning, HMED (Syracuse)

ADDITIONAL DISTRIBUTION (Keep at minimum within intent of assigned G.E. Class.)

COPIES	NAME	LOCATION
S (CLASS 1 ONLY)	DEFENSE DOCUMENTATION CENTER	CAMERON STATION, ALEXANDRIA, VA. 22314

TABLE OF CONTENTS

LIST OF ILLUSTRATIONS

LIST OF ILLUSTRATIONS (CONT)

LIST OF ILLUSTRATIONS (CONT)

LIST OF TABLES

GLOSSARY

AFCRL	Air Force Cambridge Research Laboratories
cm	centimeter
dB	decibel
dBm	decibel referenced to a milliwatt
esu	electrostatic unit
gm	gram
HF	High Frequency
IAGA	International Association of Geomagnetism and Aeronomy
IGRF	International Geomagnetic Reference Field
IGY	International Geophysical Year
kHz	kilohertz
km	kilometer
LT	Local Time
MHz	Megahertz
m/s	meters per second
nmi	nautical mile
RAC	Radar Auroral Clutter
rad	radian
SNR	Signal-to-Noise Ratio
SRI	Stanford Research Institute
SSN	Sunspot Number
UHF	Ultra High Frequency
VHF	Very High Frequency

SECTION I

INTRODUCTION

Reflections from ionospheric irregularities can be an important source of clutter for an HF backscatter radar located in the midlatitude with the antenna beam oriented towards the polar region. Although theoretical and experimental investigations of radar reflections from E-layer auroral and F-layer ionization irregularities have been conducted extensively at frequencies between the HF and UHF band, only limited experimental data on the statistical characteristics of HF ionospheric echoes are available which would be directly applicable for HF backscatter radar design and performance determination. However, sufficient information and knowledge concerning ionospheric backscatter reflections do exist to provide, to a first approximation, a model for the synthesis of an HF backscatter radar.

Radar reflections from auroral ionization occur in a region which satisfies the condition of near orthogonality of the incident radiation with the magnetic field lines of force, the amplitude of the auroral echo being aspect-angle sensitive (Leadabrand, et al., 1967; Chesnut, et al., 1968; Bates and Albee, 1969).

Although radar returns from auroral ionization at VHF and UHF are normally confined to E-layer heights of about 110 km (Unwin, 1959; Watkins and Sutcliffe, 1965; Leadabrand, et al., 1965; Abel and Newell, 1969), 106-MHz auroral echoes have been detected as high as 300 km (Schlobohm, et al., 1959).

In the case of HF radar transmissions, reflections extending up to F-layer heights, i.e., 300-400 km altitude, have been observed as well as in the E-layer (Malik and Aarons, 1964; Bates and Albee, 1969, 1970; Baggaley, 1970; Au and Hower, 1970).

In addition to the F-layer reflections, an HF radar should be capable of detecting ionospheric echoes from over the horizon as a result of the normal ionospheric refraction phenomenon. The HF radar backscatter soundings by Bates (1969, 1970) in Alaska confirmed the presence of over-the-horizon ionospheric echoes at extremely long ranges corresponding to regions in space where the propagation direction-magnetic field line perpendicularity condition is satisfied.

A number of theories, which are summarized by Booker (1960) and Moorcroft (1961a, 1961b) have evolved invoking magnetic field-aligned ionization to explain the aspect sensitivity. The earliest theories of the HF radar aurora suggest field aligned sheets of ionization with critical frequency exceeding that of the transmitted frequency. Subsequent observations at VHF and UHF resulted in apparent critical frequencies much higher than physically realizable. Booker, et al. (1955) postulated that the auroral reflections occurred from columns of ionization with critical frequency below the operating frequency (weak scattering). The investigation by Lyon and Forsyth (1962) indicated that the critical frequencies in the auroral ionization columns may be as high as 100 MHz.

The analysis of radar-auroral clutter data collected at six frequencies from 50 to 3000 MHz simultaneously at Homer, Alaska, by Chesnut, et al. (1968) has revealed the following:

1. Aspect sensitivity is nearly independent of frequency;
2. Scattering cross section decreases about 10 dB per degree of aspect angle;
3. Scattering cross section varies exponentially with frequency, the slope being time-variant with an average of 33 dB per 1000 MHz; and
4. There is a moderate correlation between the radar aurora and the visual aurora.

The existence of two types of auroral echoes, which have been termed diffuse and discrete, have been reported (Presnell et al., 1959; Leadabrand, 1960). The discrete echoes appear to result from auroral ionization which is restricted in space to a small reflecting region and is prevalent at night. Diffuse echoes, on the other hand, appear to originate from large reflecting regions and, most often, are present during the day. Discrete echoes exhibit little pulse lengthening while, for the diffuse echoes, the pulse lengthening could be on the order of hundreds of kilometers.

In this report, an estimate is made of the characteristics of HF radar ionospheric echoes reflected from the polar ionosphere. The experimental radar data acquired at frequencies between HF and UHF are employed in the analysis. The topics which are discussed are the spatial-geographical extent of the HF echoes for a midlatitude location, the amplitude and backscatter cross-sectional area, the Doppler frequency variation, the frequency of occurrence, the diurnal and seasonal variation and the correlation with solar-geophysical conditions.

SECTION II

IONOSPHERIC BACKSCATTER ECHO REGIONS

2.1 INTRODUCTION

E-layer auroral and F-layer echoes are the result of radio wave scattering from electron density irregularities aligned along the magnetic field lines. The characteristics of the field-aligned scatterers are such that the radar echoes are observed from a small range of angles about perpendicular incidence to the geomagnetic field lines and that the echo magnitude is aspect angle sensitive. In addition to the perpendicularity requirement, it is necessary that this geometric configuration take place at ionospheric altitudes, i.e., 80 km and above.

The probability of observing radar reflections from ionization irregularities is also dependent upon the frequency of occurrence of E-layer auroral, or spread-F irregularity activity in the region of interest. Reflections can be expected to occur in regions where both the conditions of near-perpendicularity at ionospheric heights and high auroral or spread-F irregularity activity are satisifed. The fulfillment of only one requirement is not sufficient to warrant a radar reflection.

An appropriate model which is used to define the condition of auroral activity is the Feldstein and Starkov (1967) auroral belt (oval) model. According to Bates, et al. (1966, 1969), the spatial extent of the HF radio aurora compares closely with the optical auroral ovals of Feldstein and Starkov.

Since the location and extent of the auroral ovals are a function of time and geomagnetic activity (Feldstein and Starkov, 1967) it can be expected that the auroral echoes could appear over a wide area during magnetically disturbed periods for an HF backscatter radar located at high latitudes.

The computational procedure discussed in Appendix A is employed in the determination of the magnetic field-aspect angles presented in this report.

2.2 ELECTRON DENSITY MODELS

The refractive index in the ionosphere is expressed by the relationship

$$n = \left[1 - \frac{4\pi N_e e^2}{m_e \omega^2} \right]^{\frac{1}{2}} \qquad (2\text{-}1)$$

where N_e is the electron density (electrons/cm^3), e is the electron charge (4.8×10^{-10} esu), m_e is the electron mass (9.1×10^{-28} gm) and ω is the angular frequency of the transmitted wave (rad/s).

The distribution of electron density with height is assumed to follow the Chapman model of the form

$$N_e = N_m \exp\left\{\frac{1}{2}\left[1 - \frac{h - h_m}{H_s} - \exp\left(\frac{-(h - h_m)}{H_s}\right)\right]\right\} \qquad (2\text{-}2)$$

where H_s is the scale height of the neutral particles and N_m is the electron density at the level of maximum ionization, h_m. The values of the parameters defining the daytime and nighttime electron density profiles and the equivalent plasma frequencies of the maximum ionization levels employed in this analysis are presented in Table 2-1.

Plots of the vertical distribution of electron density are shown in Figures 2-1 and 2-2. For the daytime ionosphere models, the F-layer plasma frequency is 9.3 MHz and, for the nighttime, 4.9 MHz. The difference between the two daytime profiles is the height of the peak of the F-layer maximum. For model A, h_{max} = 250 km and model B, h_{max} = 300 km. Similarly, for the nighttime profiles, for model A, h_{max} = 250 km and model B, h_{max} = 350 km. For simplicity of data presentation, the E-layer echoes are assumed to originate at altitudes below 150 km altitude and the F-layer echoes above 150 km.

It should be noted that the ionospheric index of refraction is also a function of both the electron collision frequency and the earth's magnetic field. In order to simplify the analysis, both parameters are neglected in the computations.

For frequencies on the order of 10 MHz and above, and at altitudes greater than 80 km, the effect of the collision frequency term on the index of refraction is negligible (Davies, 1965).

The refractive index is slightly in error when the magnetic field is neglected. The maximum error in the refractive index occurs at the peak of the F-layer and, at 30 MHz, is less than 0.4 percent. At 20 MHz, the maximum deviation increases to slightly greater than 1 percent (Millman, 1975).

2.3 E-LAYER BACKSCATTER ECHO REGIONS

The contours of zero degree aspect angle (i.e., zero degree off-perpendicular angle, propagation direction is orthogonal to the magnetic field lines), for the E-layer echoes, as viewed from a midlatitude location, are plotted in Figures 2-3 through 2-8 for both daytime ionospheric models and as a function of transmission frequency (10, 20 and 30 MHz) and the various states of magnetic activity.

TABLE 2-1

ELECTRON DENSITY PROFILES

Model	Time	Layer	H_s (km)	h_m (km)	N_m (Electrons/cm^3)	Plasma Frequency (MHz)
A	Day	E	10	100	7.387×10^4	2.44
		F	45	250	1.0732×10^6	9.3
	Night	E	10	120	3.586×10^4	1.7
		F	45	250	2.979×10^5	4.9
B	Day	E	10	100	7.387×10^4	2.44
		F	70	300	1.0732×10^6	9.3
	Night	E	10	120	3.586×10^4	1.7
		F	80	350	2.979×10^5	4.9

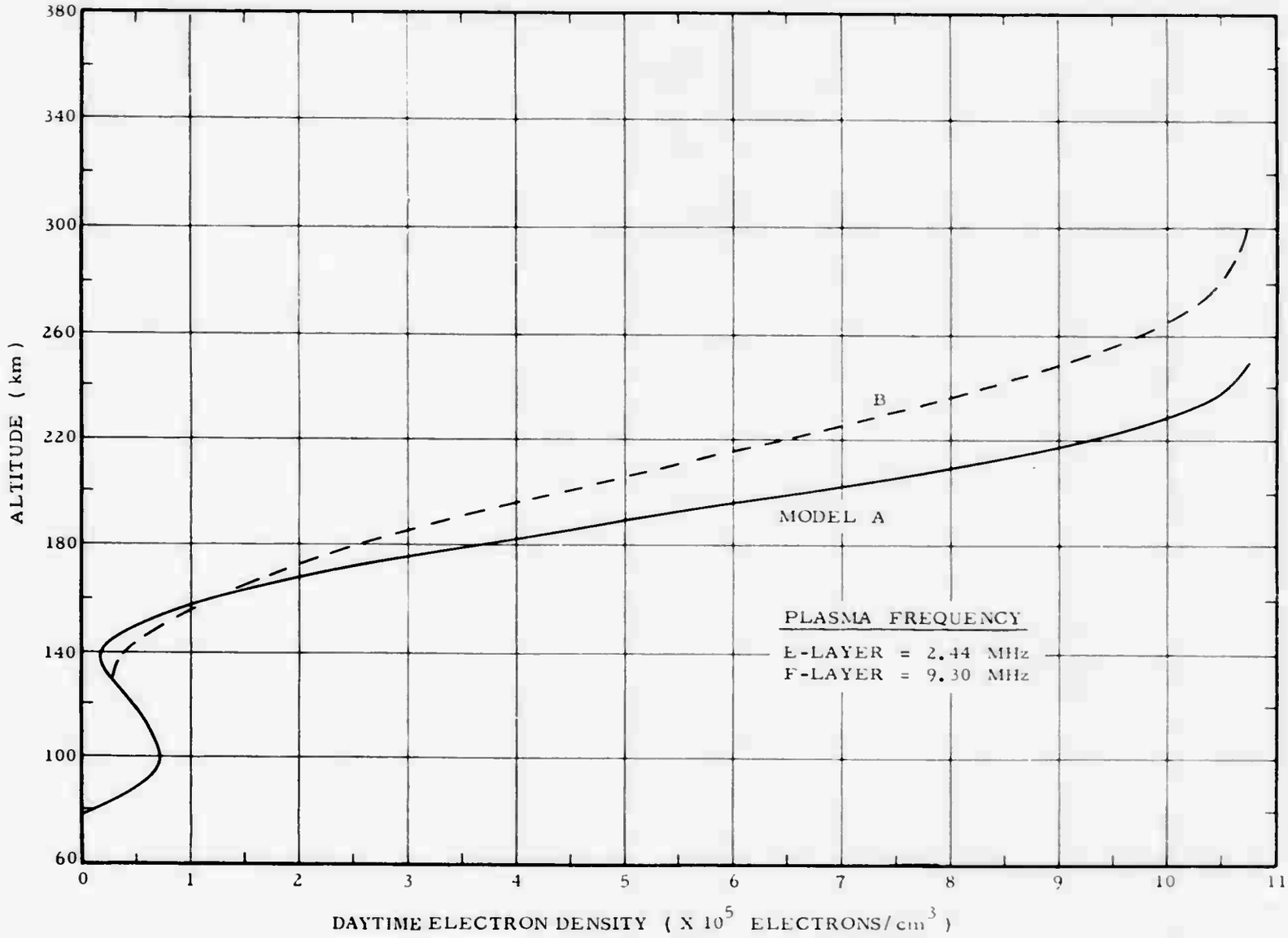

Figure 2-1. Chapman Model of Daytime Electron Density Profiles

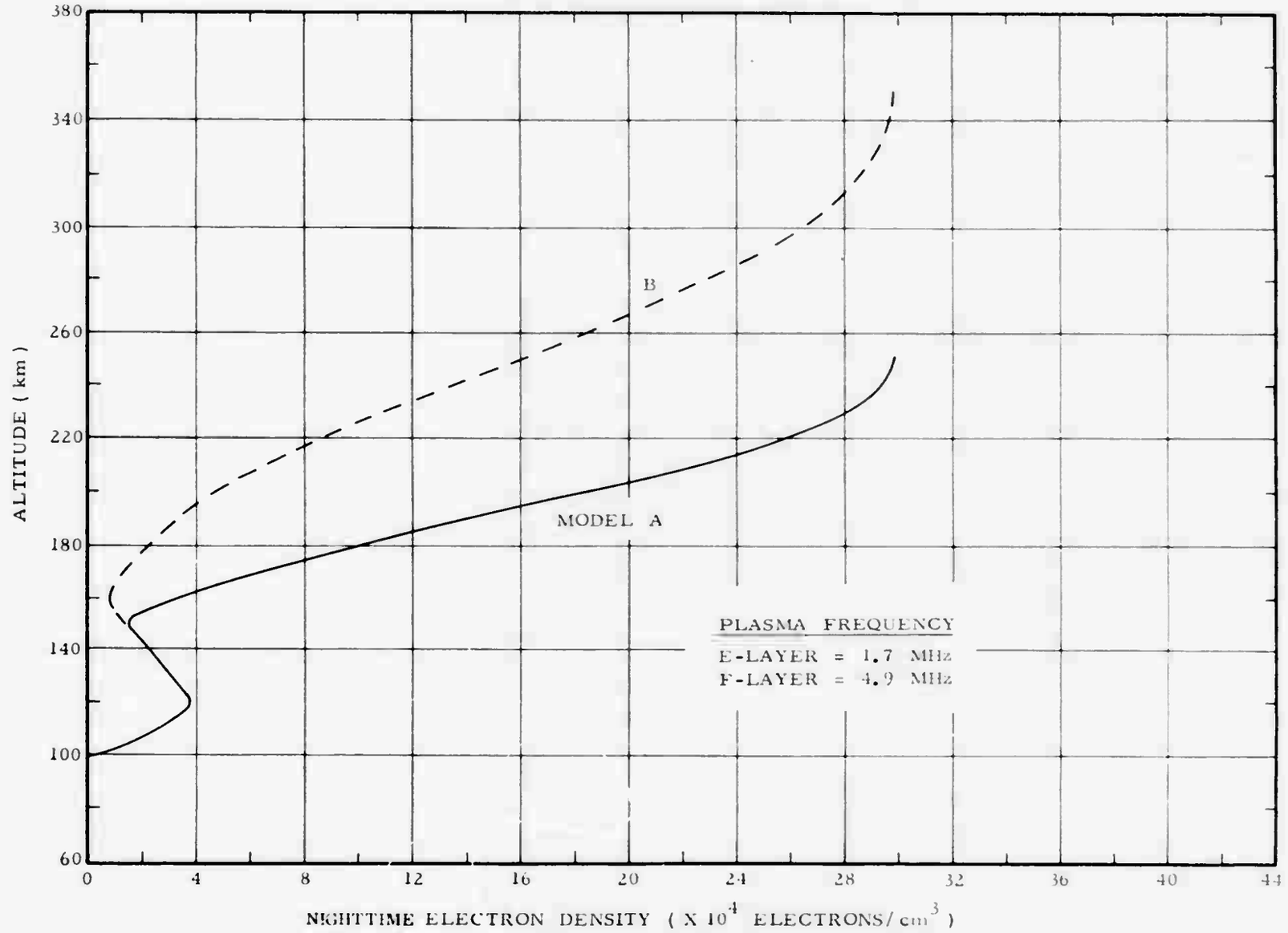

Figure 2-2. Chapman Model of Nighttime Electron Density Profiles

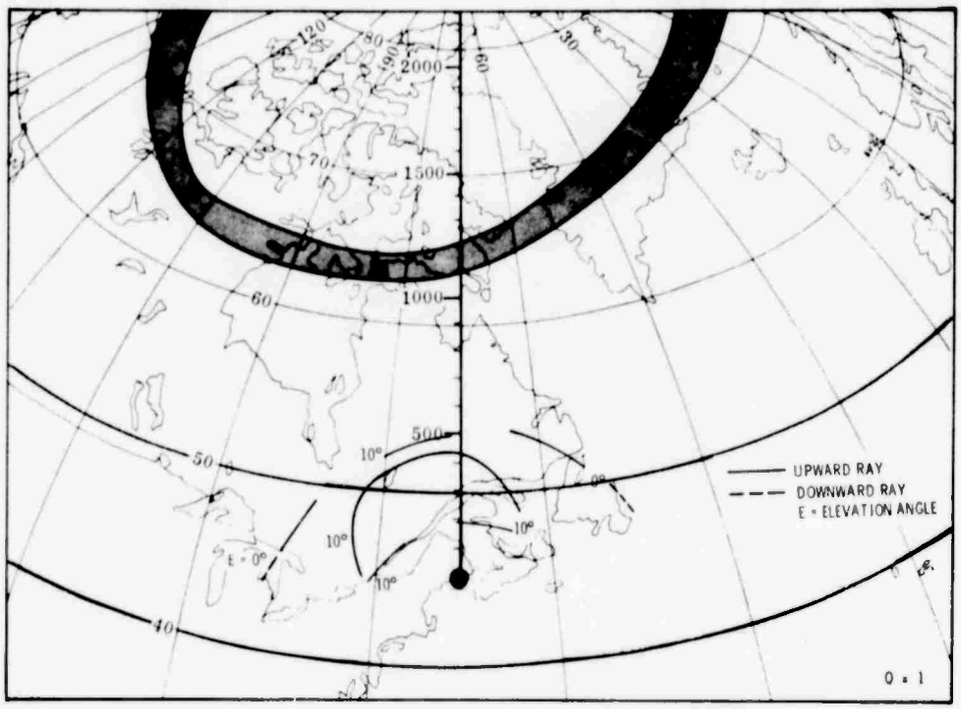

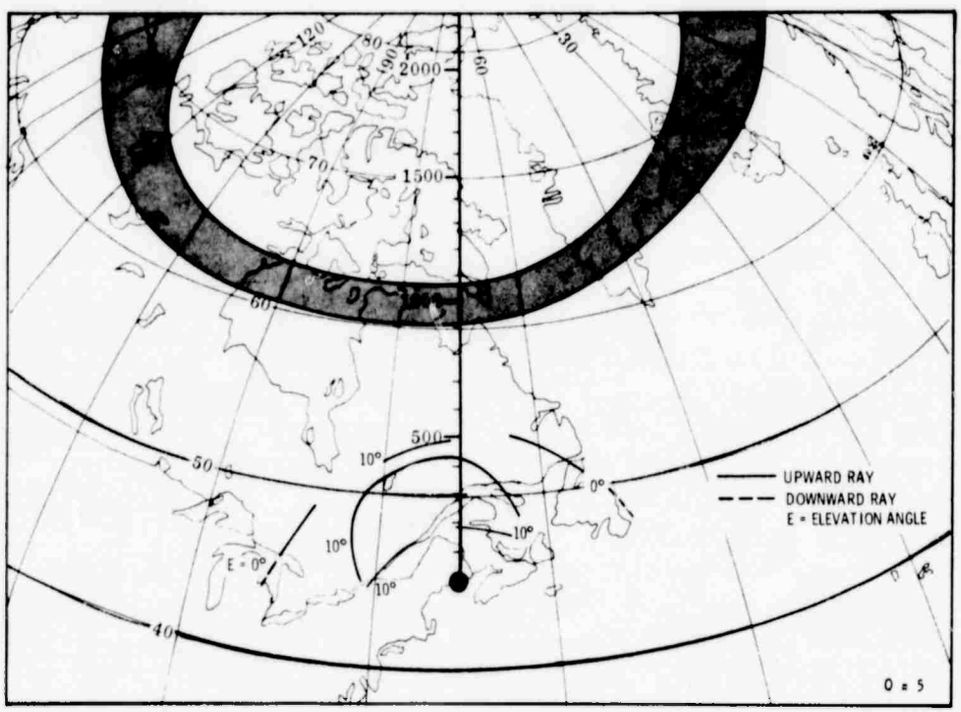

Figure 2-3. Contours of Z
as Viewed fro
Auroral Belt
1200 Hours Lo

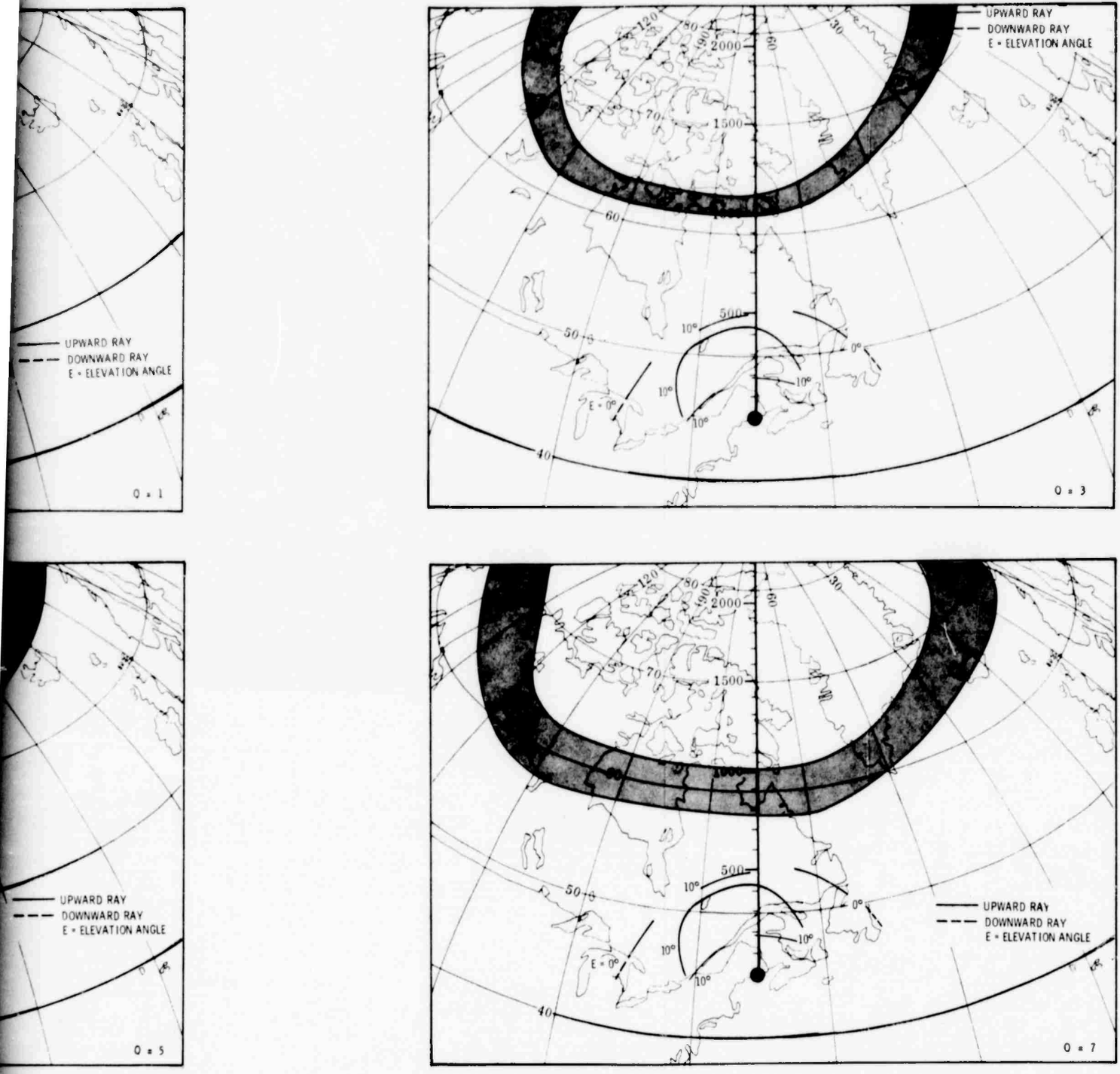

Figure 2-3. Contours of Zero-Degree Aspect Angle for 10 MHz E-Layer Echoes as Viewed from a Midlatitude Location, with Feldstein-Starkov Auroral Belt Model for Various Levels of Magnetic Activity at 1200 Hours Local Time, Daytime Ionospheric Model A

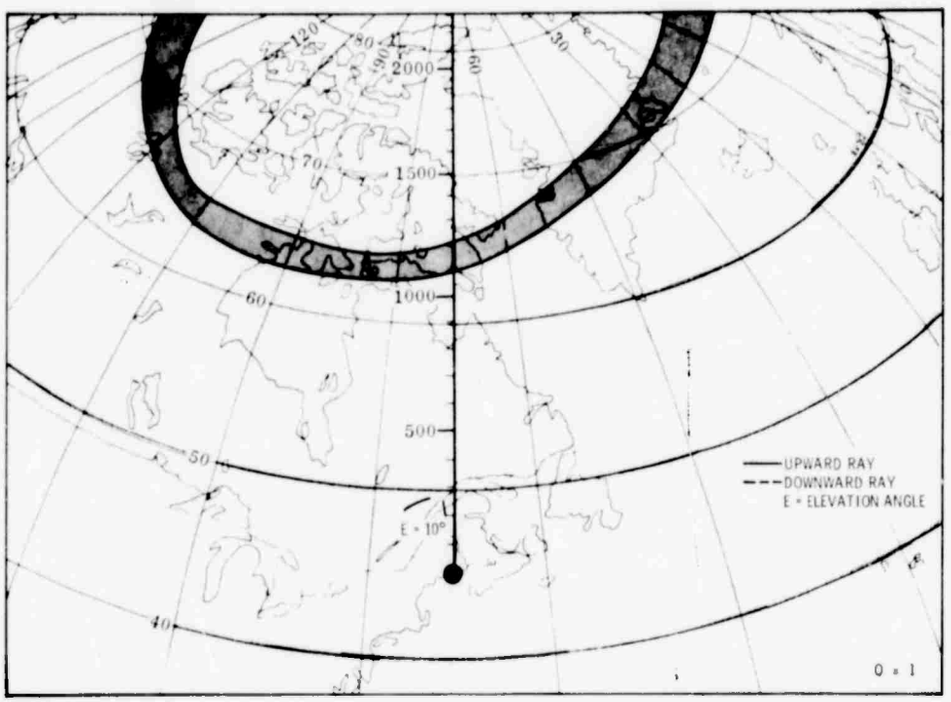

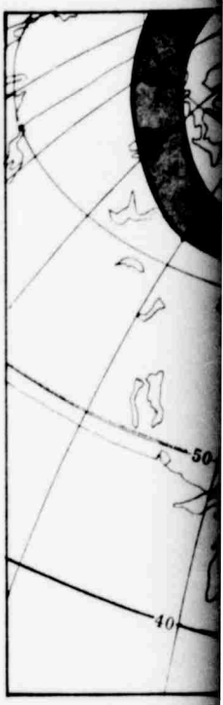

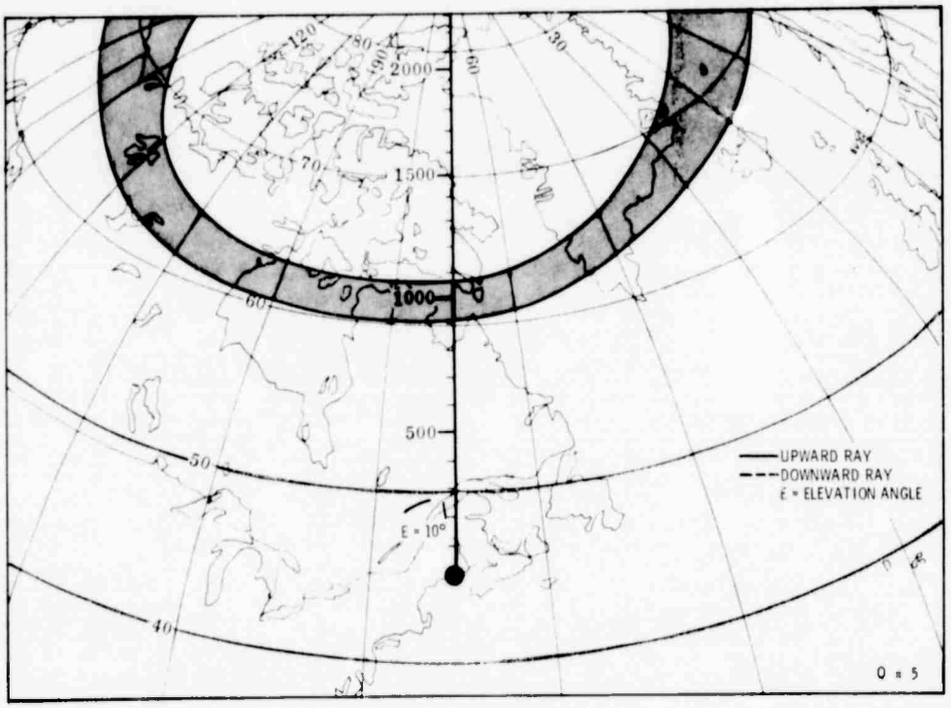

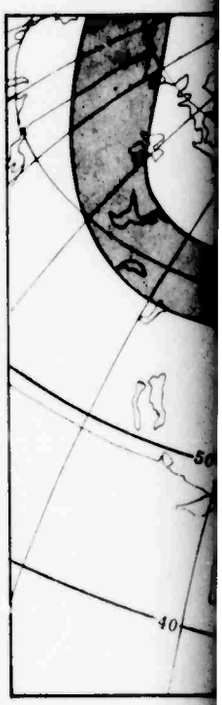

Figure 2-4. Contours of Z
as Viewed fr
Auroral Belt
1200 Hours L

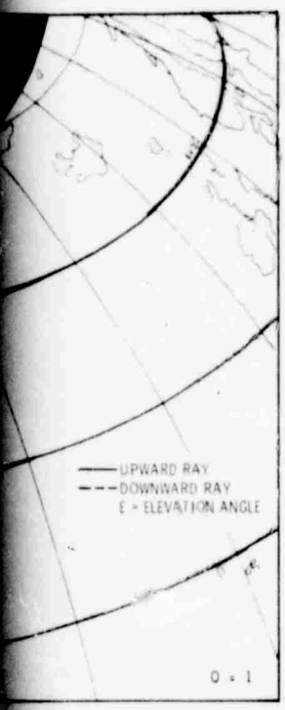

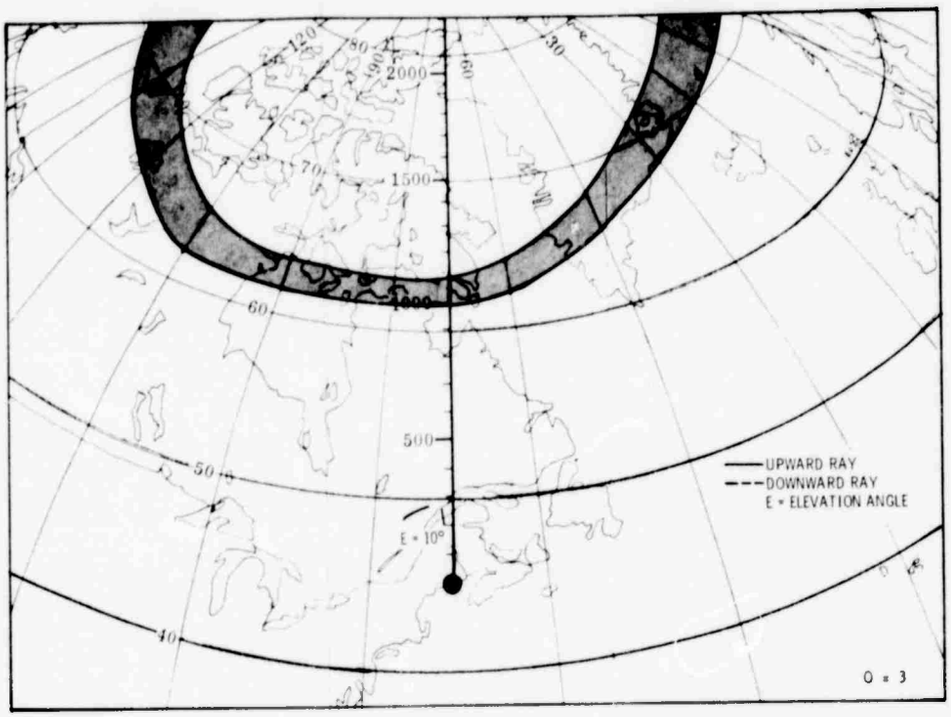

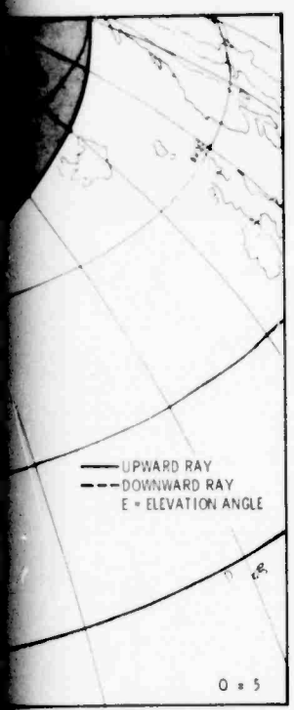

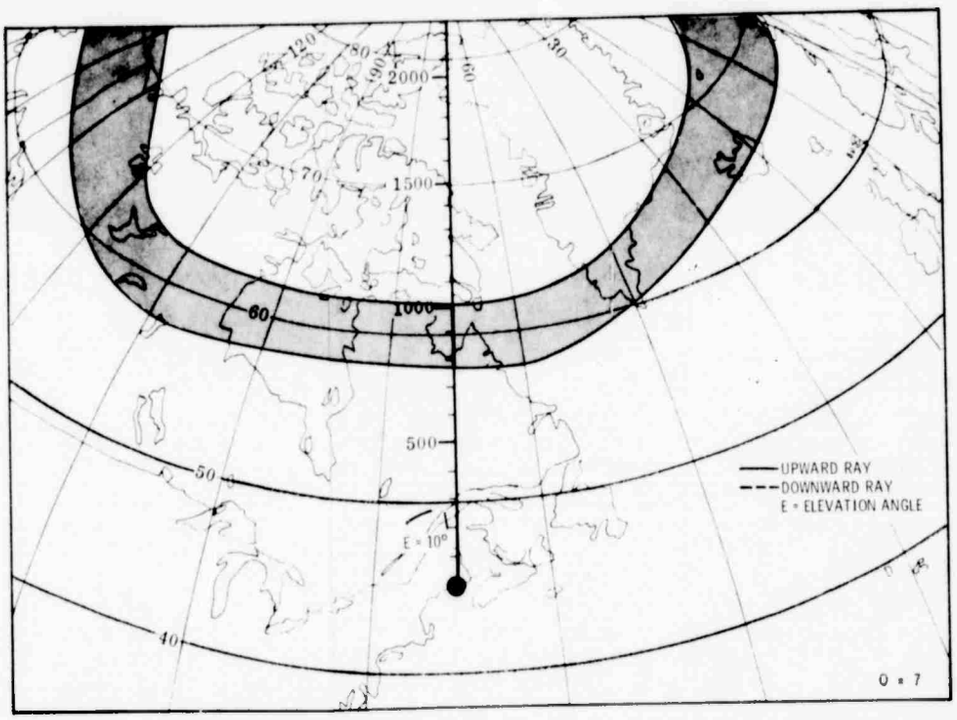

Figure 2-4. Contours of Zero-Degree Aspect Angle for 20 MHz E-Layer Eehoes as Viewed from a Midlatitude Location, with Feldstein-Starkov Auroral Belt Model for Various Levels of Magnetic Aetivity at 1200 Hours Local Time, Daytime Ionospheric Model A

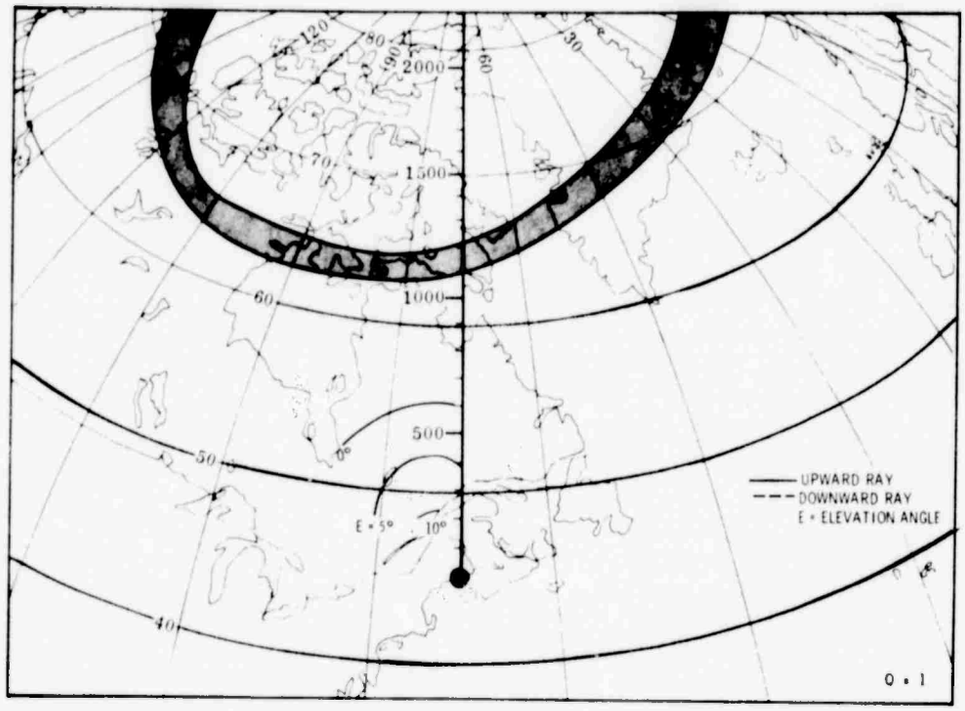

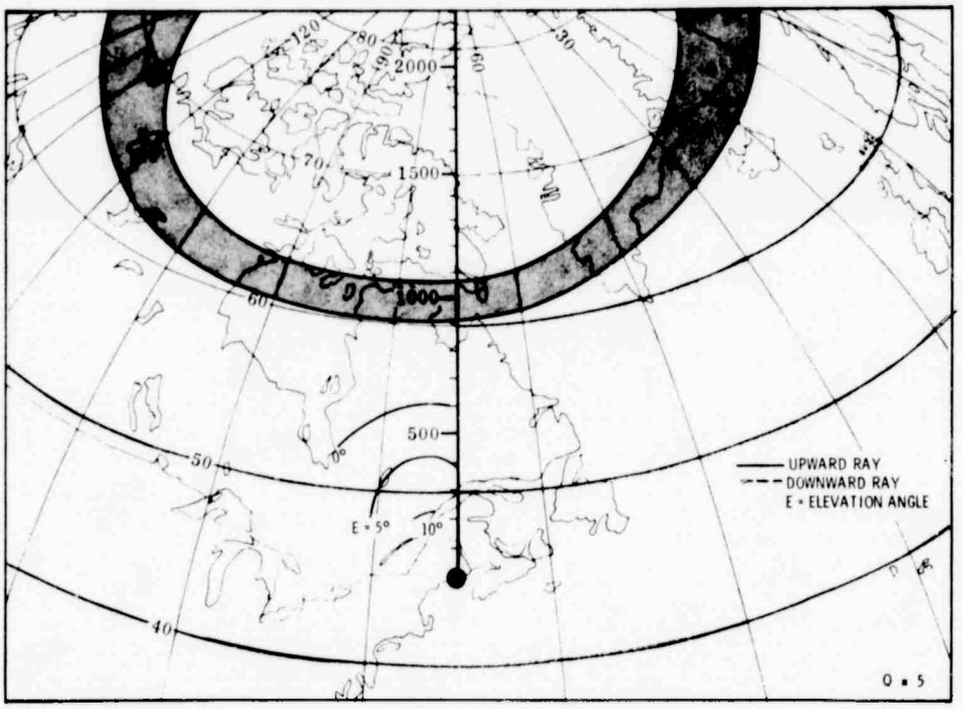

Figure 2-5. Contours of
as Viewed fr
Auroral Belt
1200 Hours L

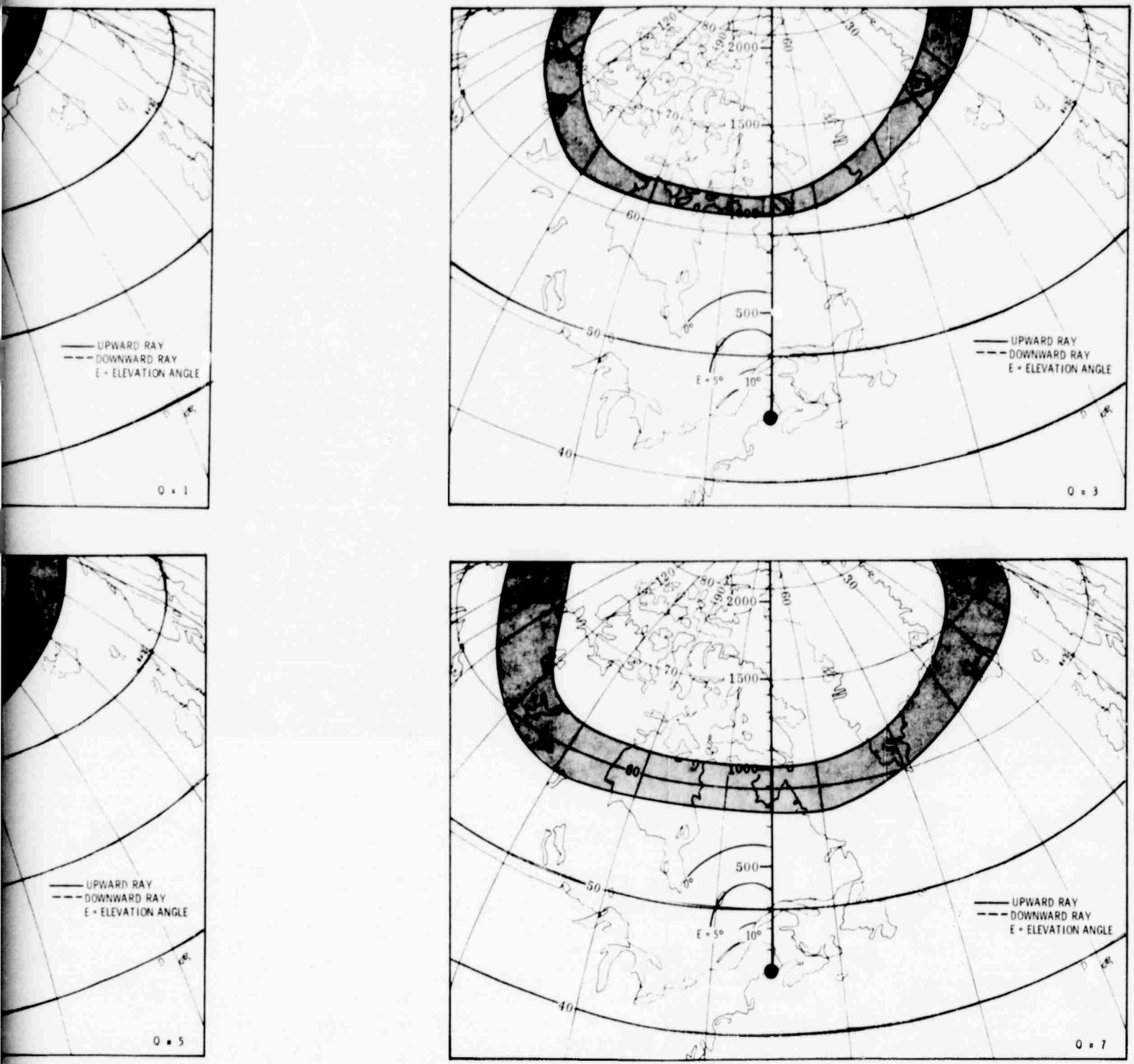

Figure 2-5. Contours of Zero-Degree Aspect Angle for 30 MHz E-Layer Echoes as Viewed from a Midlatitude Location, with the Feldstein-Starkov Auroral Belt Model for Various Levels of Magnetic Activity at 1200 Hours Local Time, Daytime Ionospheric Model A

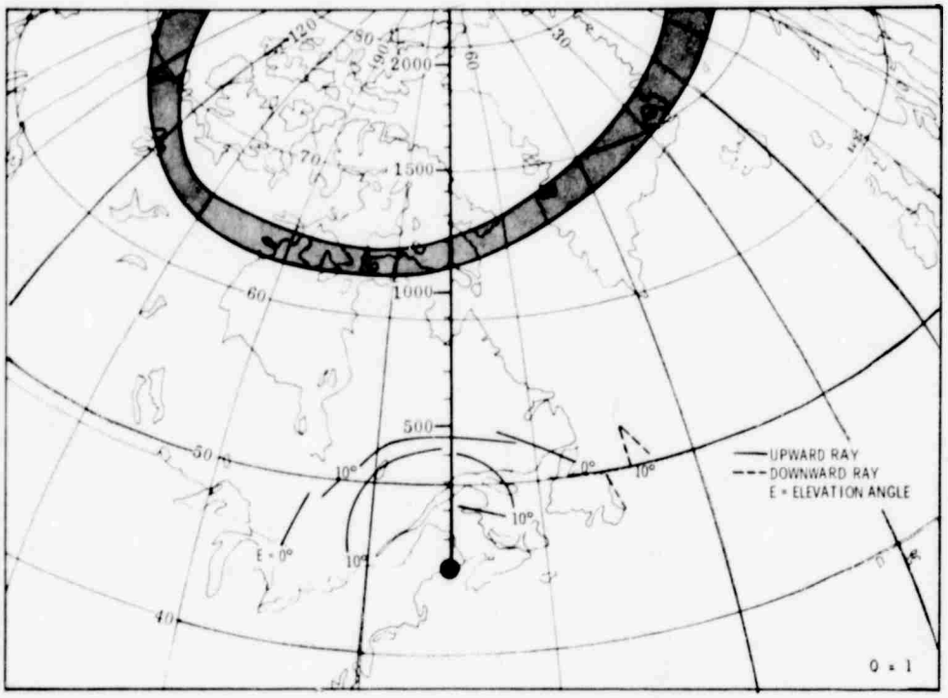

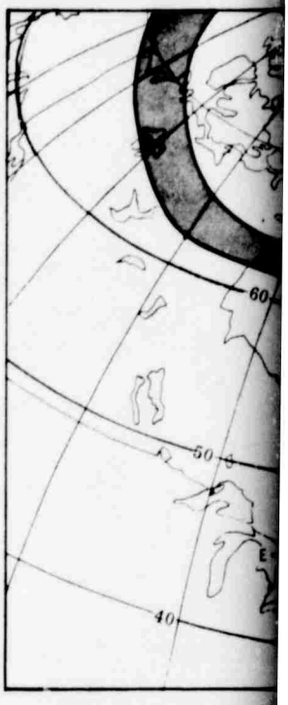

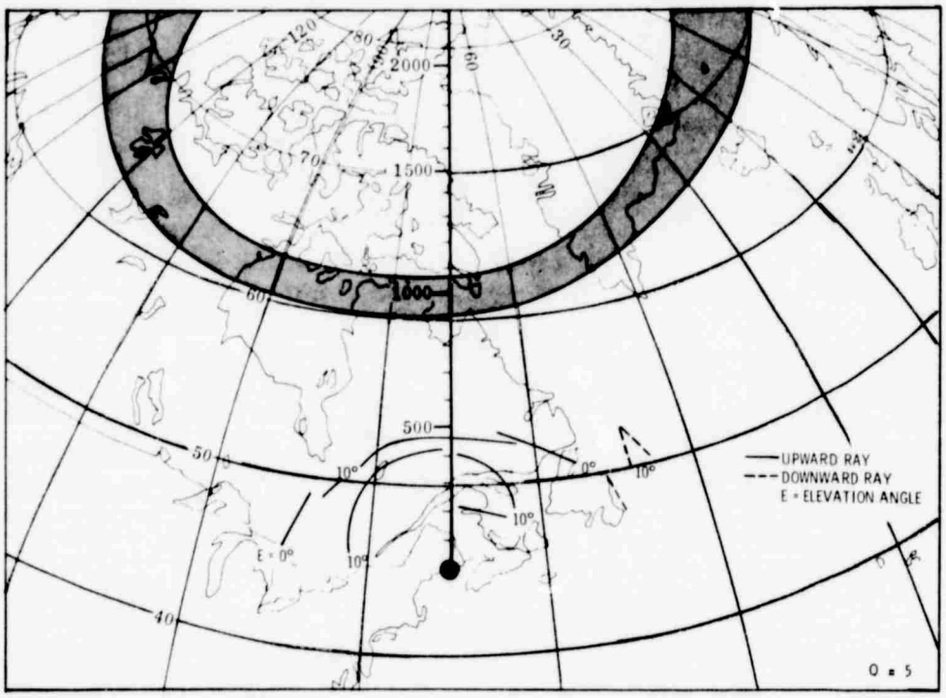

Figure 2-6. Contours of Zero-
as Viewed from a
Auroral Belt Mod
1200 Hours Local

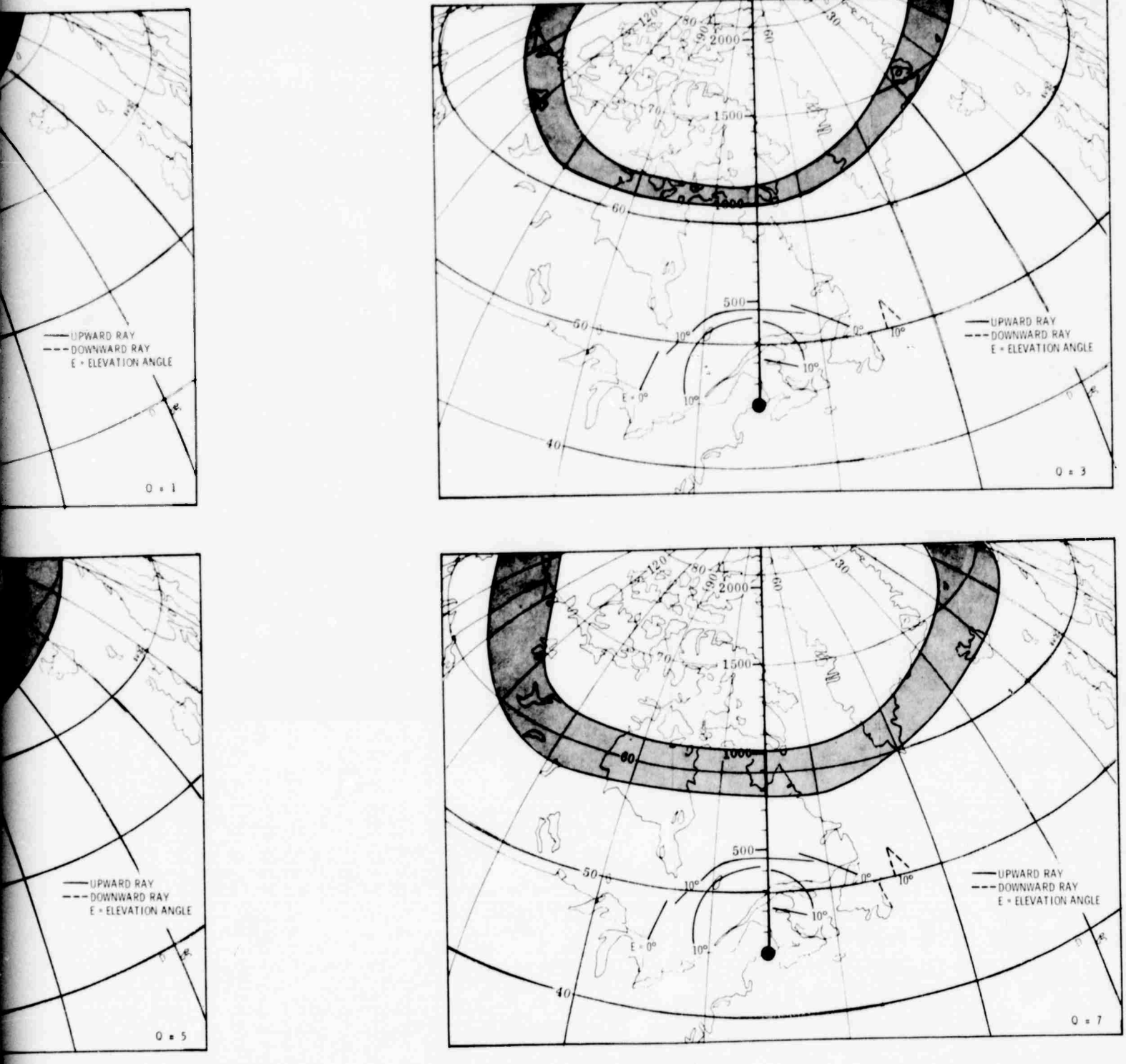

Figure 2-6. Contours of Zero-Degree Aspect Angle for 10 MHz E-Layer Echoes as Viewed from a Midlatitude Location, with the Feldstein-Starkov Auroral Belt Model for Various Levels of Magnetic Activity at 1200 Hours Local Time, Daytime Ionospheric Model B

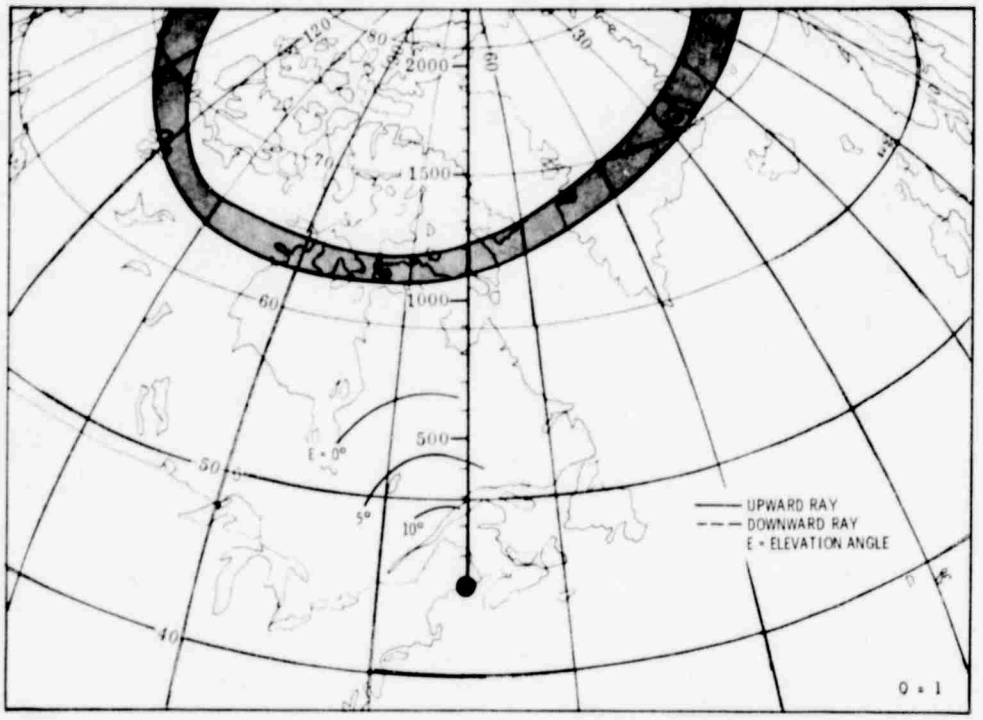

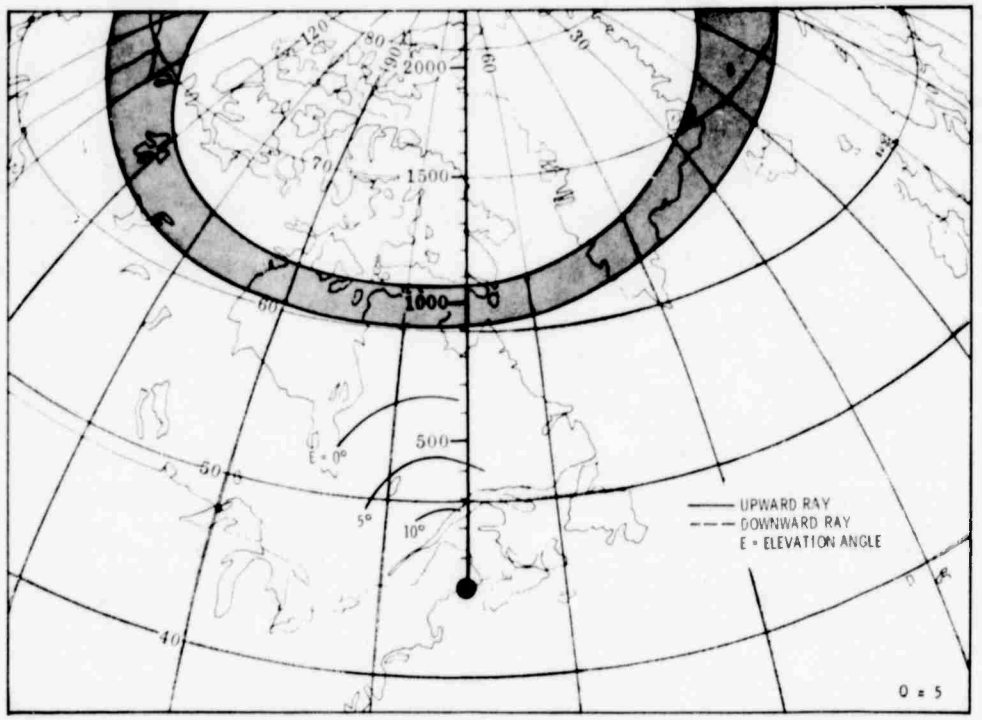

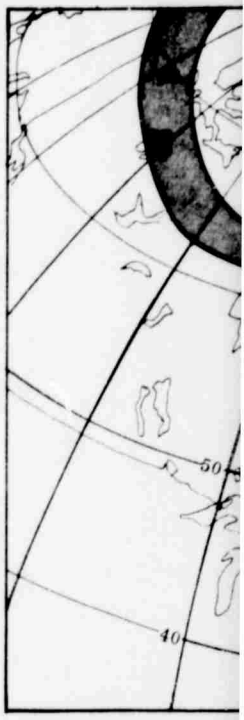

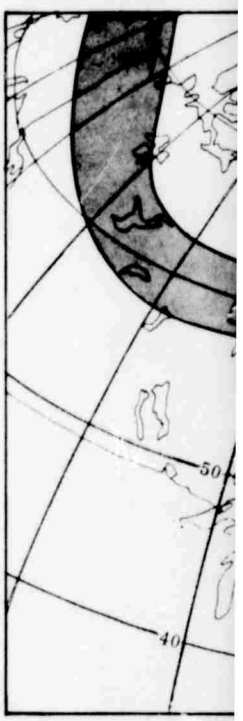

Figure 2-7. Contours of Ze
as Viewed fron
Auroral Belt M
1200 Hours Lo

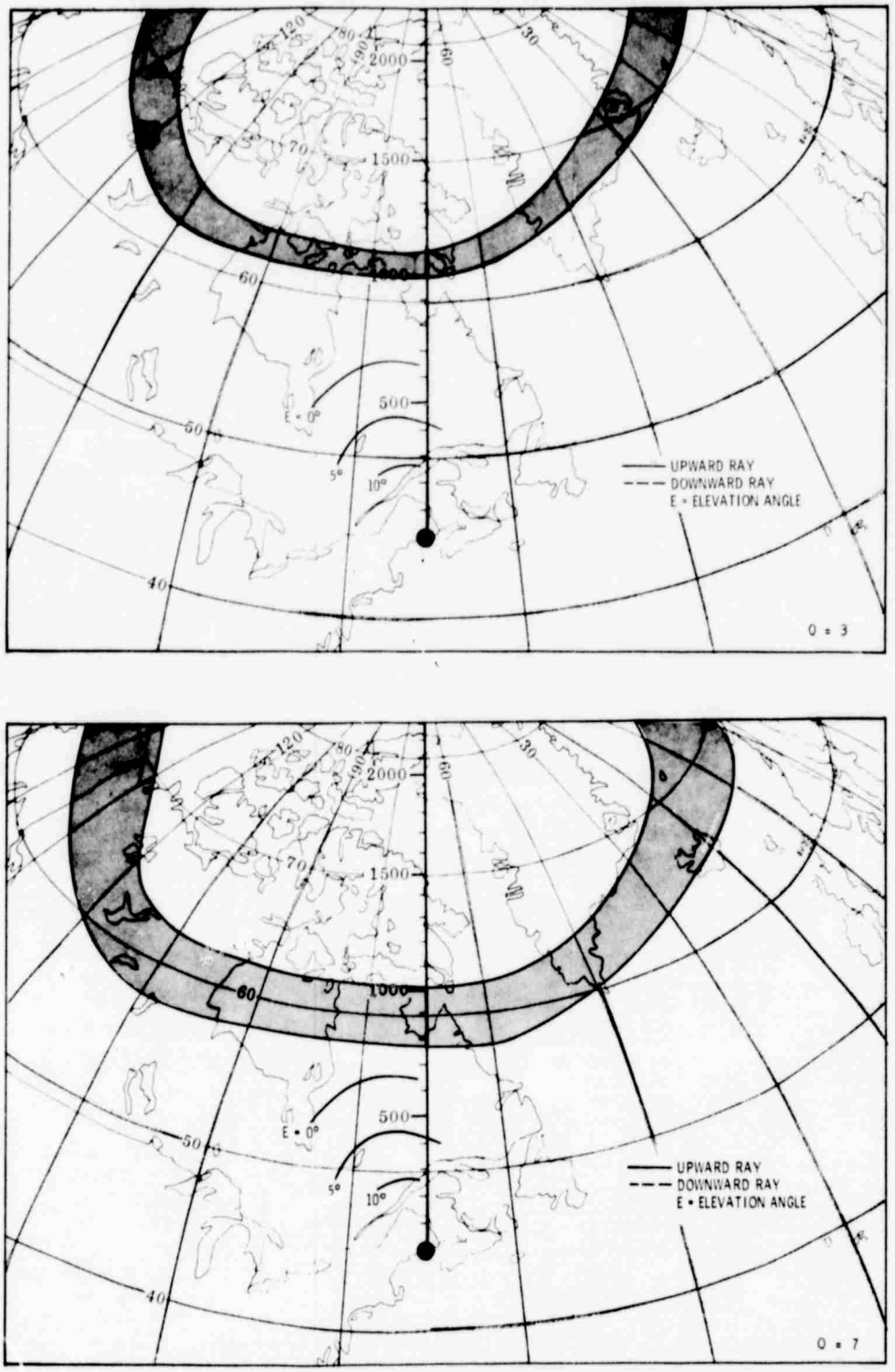

Figure 2-7. Contours of Zero-Degree Aspect Angle for 20 MHz E-Layer Echoes as Viewed from a Midlatitude Location, with the Feldstein-Starkov Auroral Belt Model for Various Levels of Magnetic Activity at 1200 Hours Local Time, Daytime Ionospheric Model B

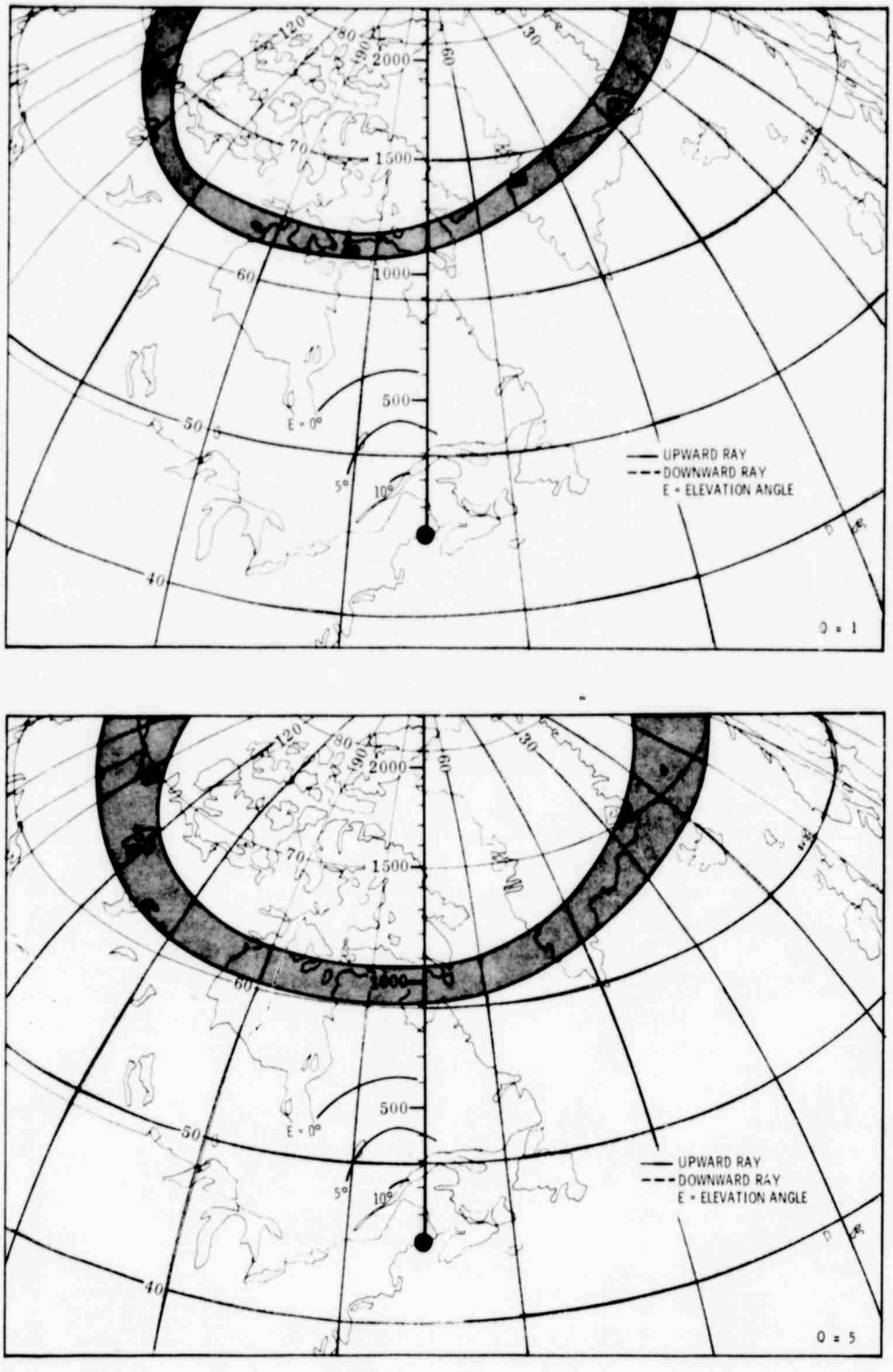

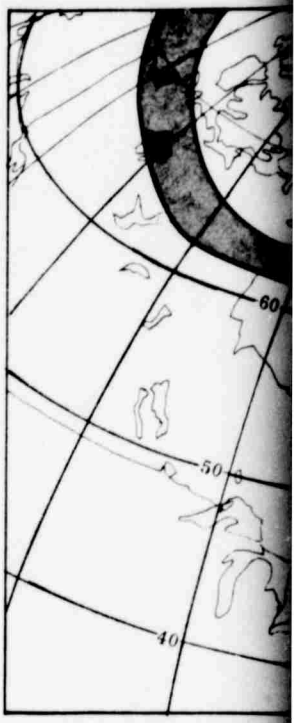

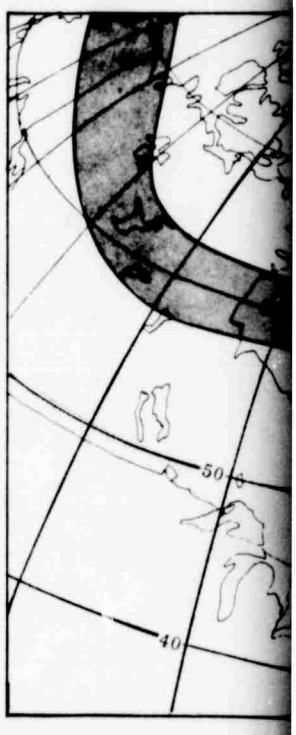

Figure 2-8. Contours of Zero-
as Viewed from a
Auroral Belt Mode
1200 Hours Local

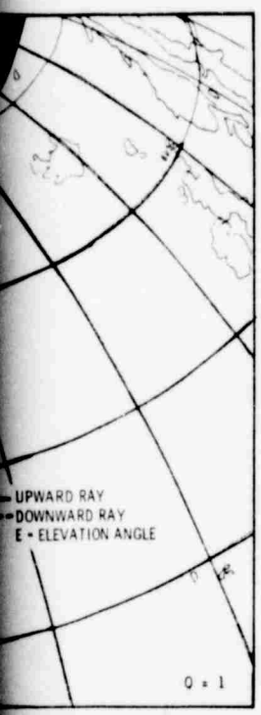

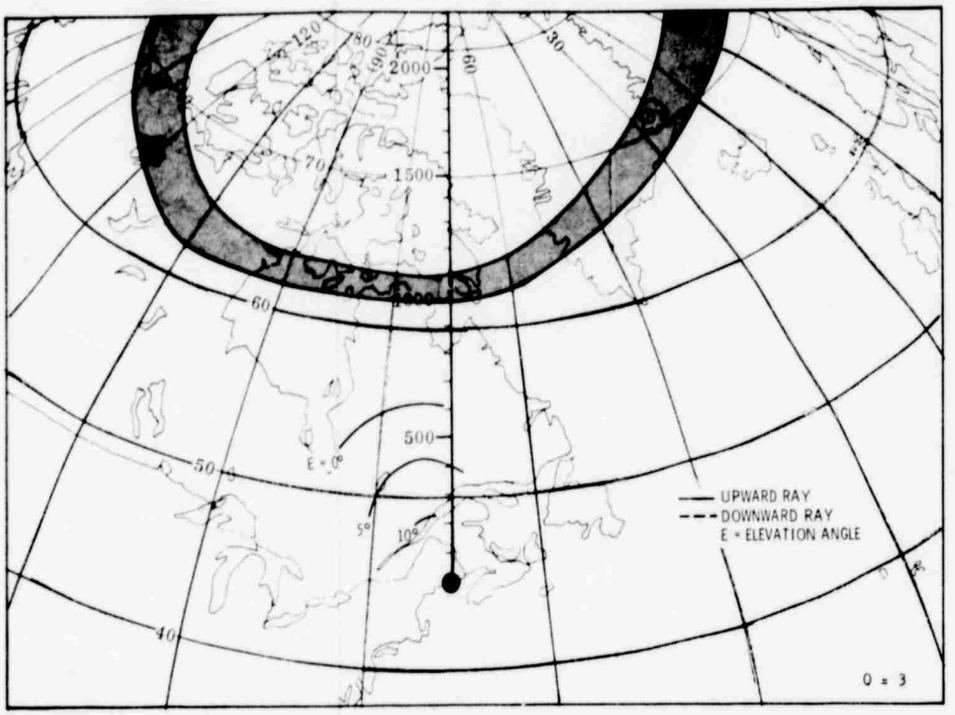

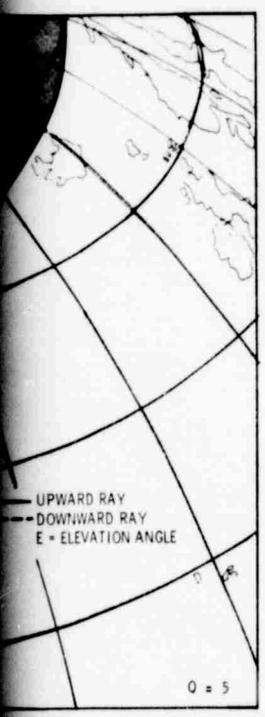

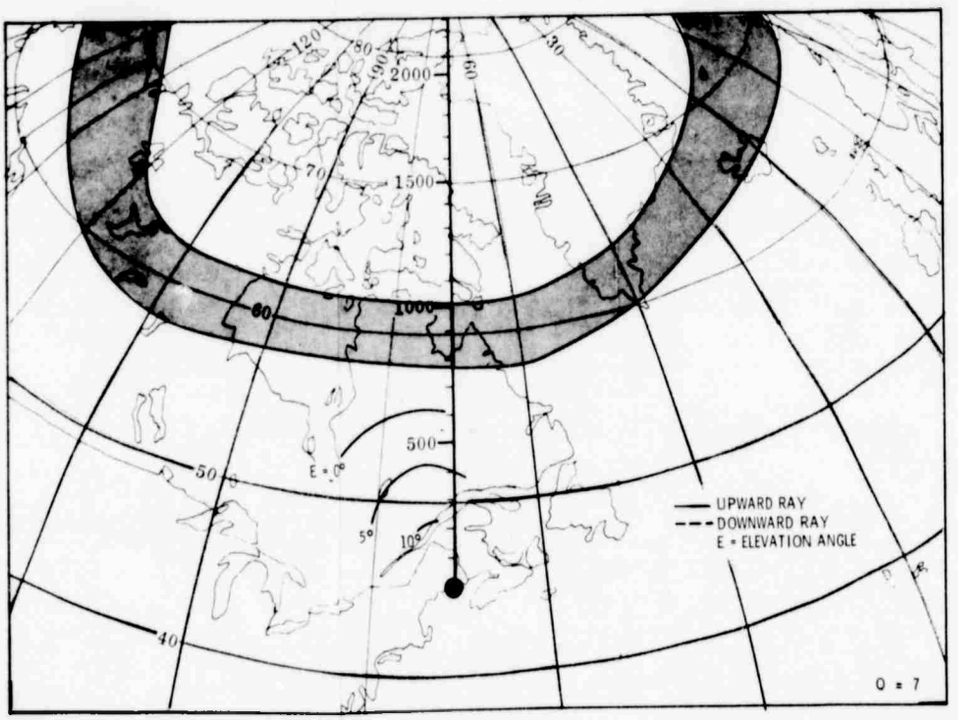

Figure 2-8. Contours of Zero-Degree Aspect Angle for 30 MHz E-Layer Echoes as Viewed from a Midlatitude Location, with the Feldstein-Starkov Auroral Belt Model for Various Levels of Magnetic Activity at 1200 Hours Local Time, Daytime Ionospheric Model B

It is evident that the spatial distribution of the perpendicular contour lines is a function of the transmission frequency and the electron density profile. In addition, it is seen that it is also a function of the azimuth-elevation angle orientation which, in turn, specifies the magnetic inclination and declination angles in space. Magnetic field orthogonality can be attained on both the upward and downward ray, i.e., after the ray has undergone ionospheric reflection. In fact, normality can be reached at multiple altitudes (Millman, 1975).

As a first approximation, it is assumed that radar-auroral echoes can be expected to appear in the areas formed by the intersection of the Feldstein-Starkov auroral ovals and the spatial positions where the magnetic field orthogonality is attained. The geographic coordinates of the boundaries of the Feldstein-Starkov auroral ovals were deduced by the nomograph method developed by Whalen (1970).

It is apparent that daytime E-layer HF radar-auroral echoes should not be observed. However, as shown in Figures 2-9 and 2-10, E-layer auroral echoes could be present during the nighttime up to approximately 780 nmi range in a northwesterly direction.

2.4 F-LAYER BACKSCATTER ECHO REGIONS

Contour plots of where spread-F was present 40, 60 and 80 percent of the time at 1300 hours local standard time for July and September 1957 (Penndorf, 1962) are shown in Figures 2-11 through 2-16 together with magnetic field perpendicular contour lines. The area formed by the intersections of the spread-F regions and the normality contours defines the region where spread-F echoes are expected to occur.

It is evident that the 40 percent contour lines do not intersect the orthogonality regions which would indicate that the probability of spread-F echoes existing during the daytime should be less than 40 percent.

The occurrence of radar echoes from the F-layer can also be examined in terms of the irregularity region which was derived from scintillation measurements by Aarons (1973b). As shown in Figures 2-17 and 2-18, echoes from F-layer irregularities during the daytime could exist over a wide azimuthal extent and to ranges out to over 1200 nmi.

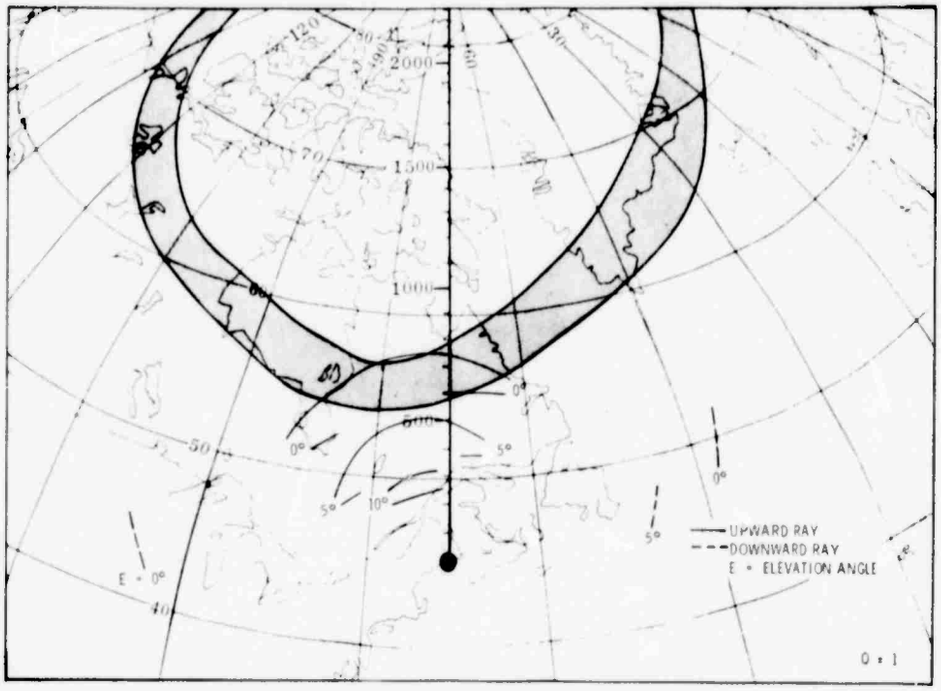

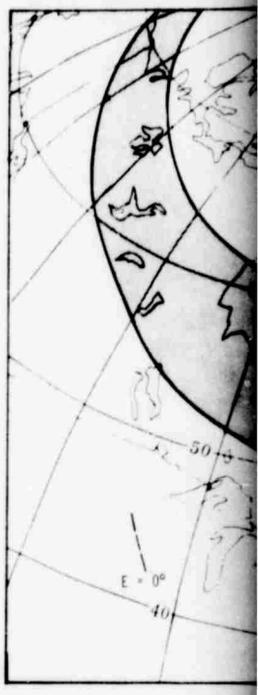

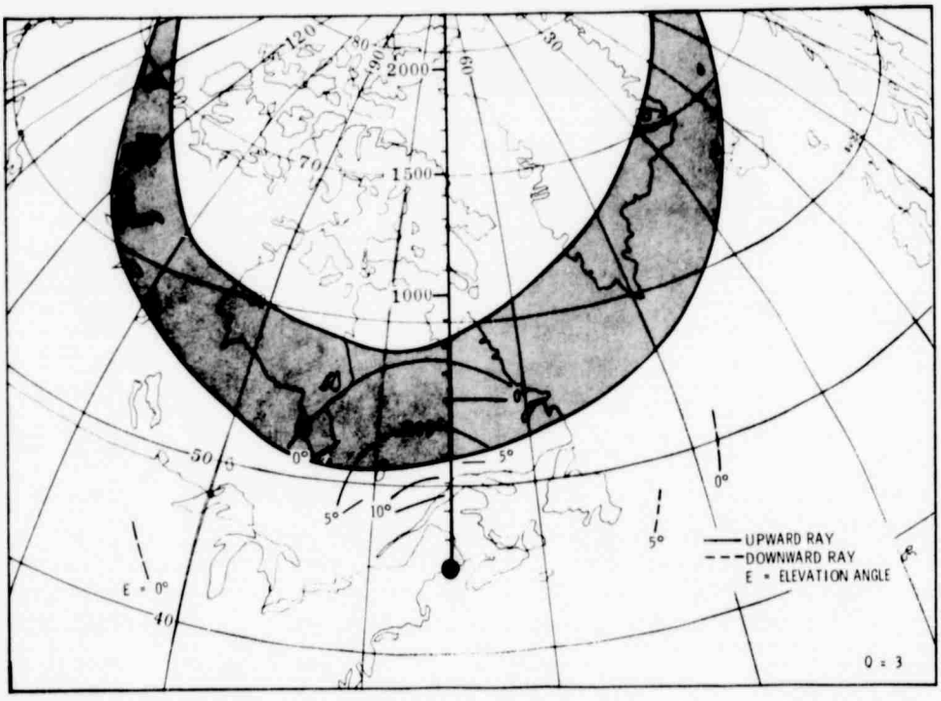

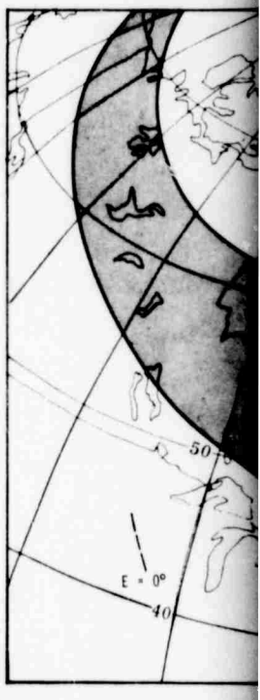

Figure 2-9. Contours of Zero-
as Viewed from a
Auroral Belt Mod
0000 Hours Local

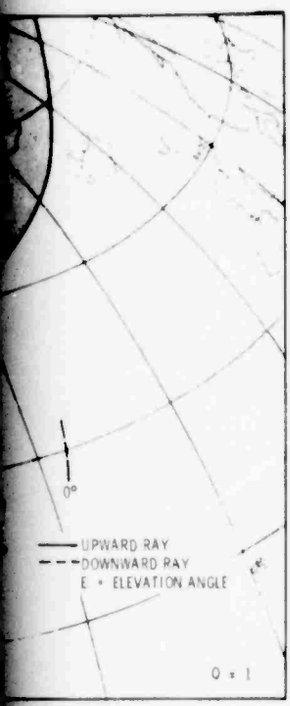

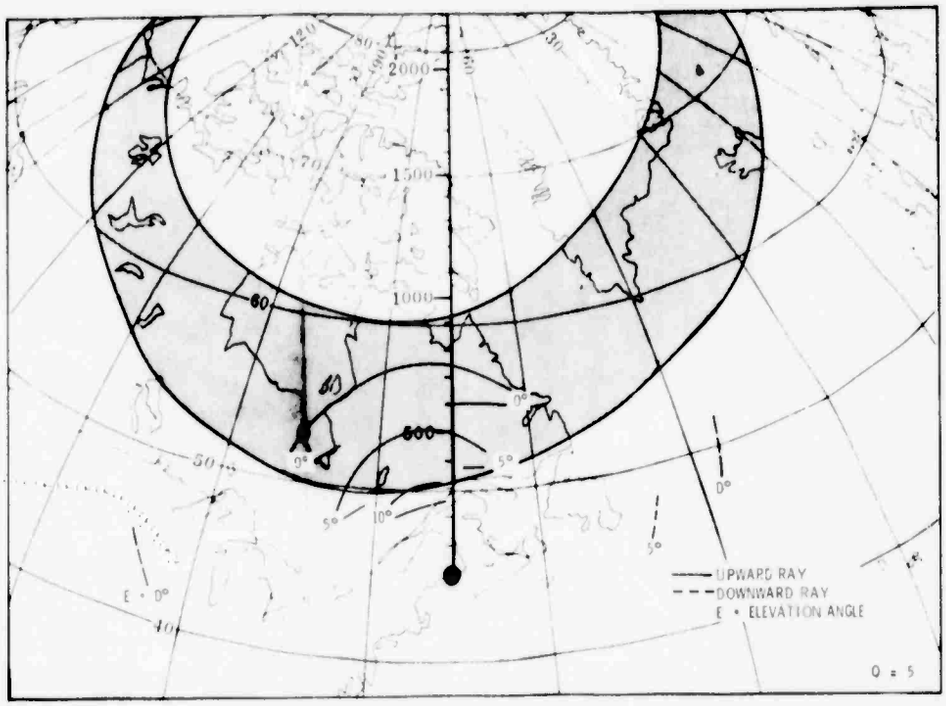

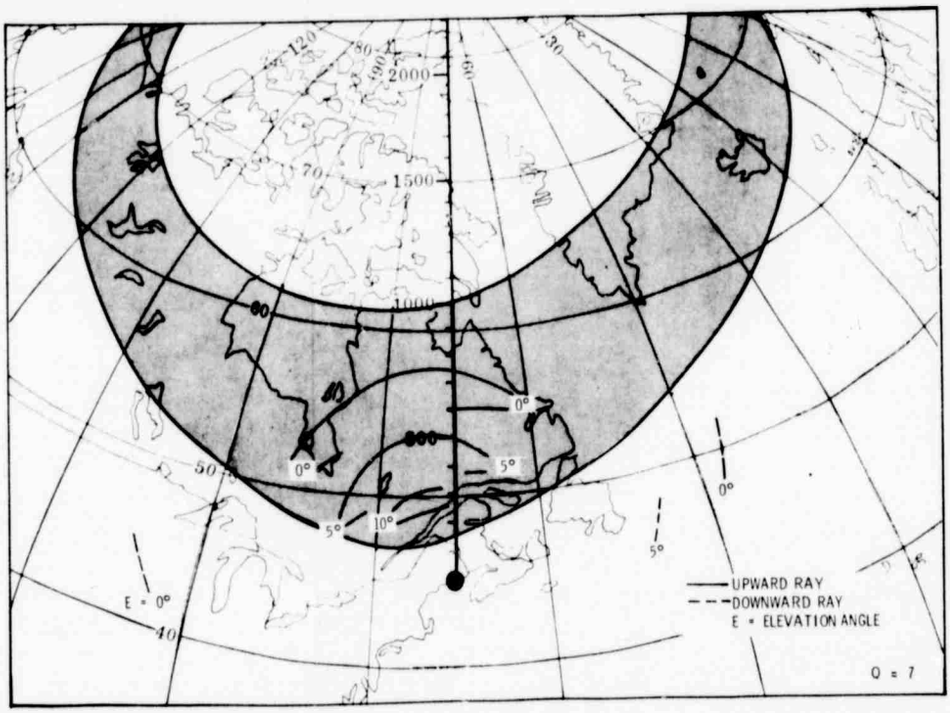

Figure 2-9. Contours of Zero-Degree Aspect Angle for 10 MHz E-Layer Echoes as Viewed from a Midlatitude Location, with the Feldstein-Starkov Auroral Belt Model for Various Levels of Magnetic Activity at 0000 Hours Local Time, Nighttime Ionospheric Model A

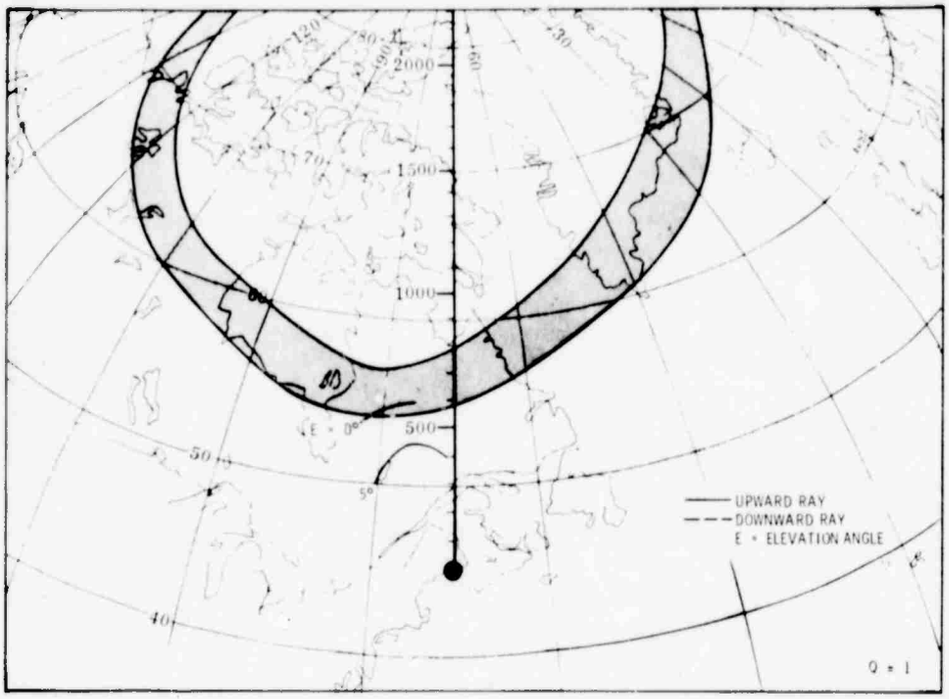

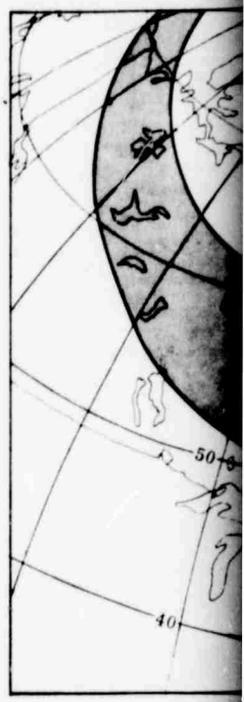

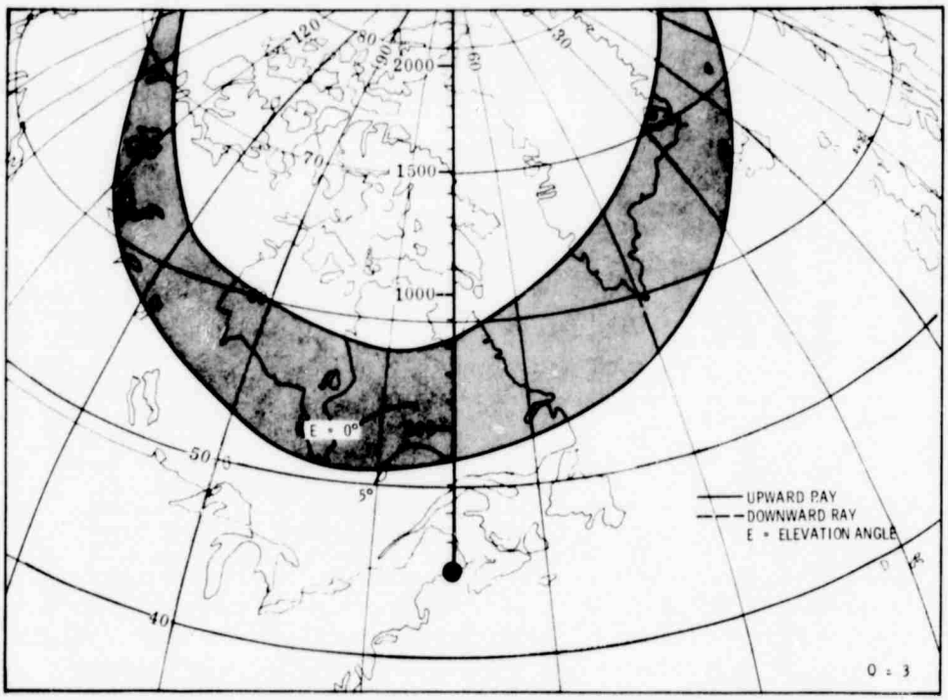

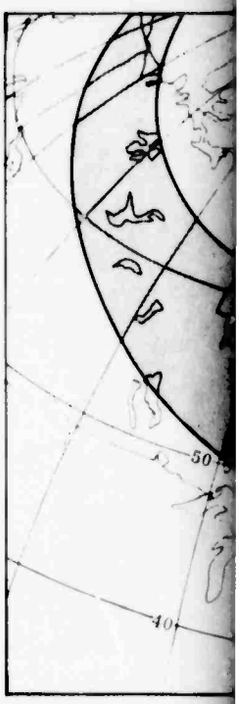

Figure 2-10. Contours of Ze
as Viewed from
Auroral Belt M
0000 Hours Loc

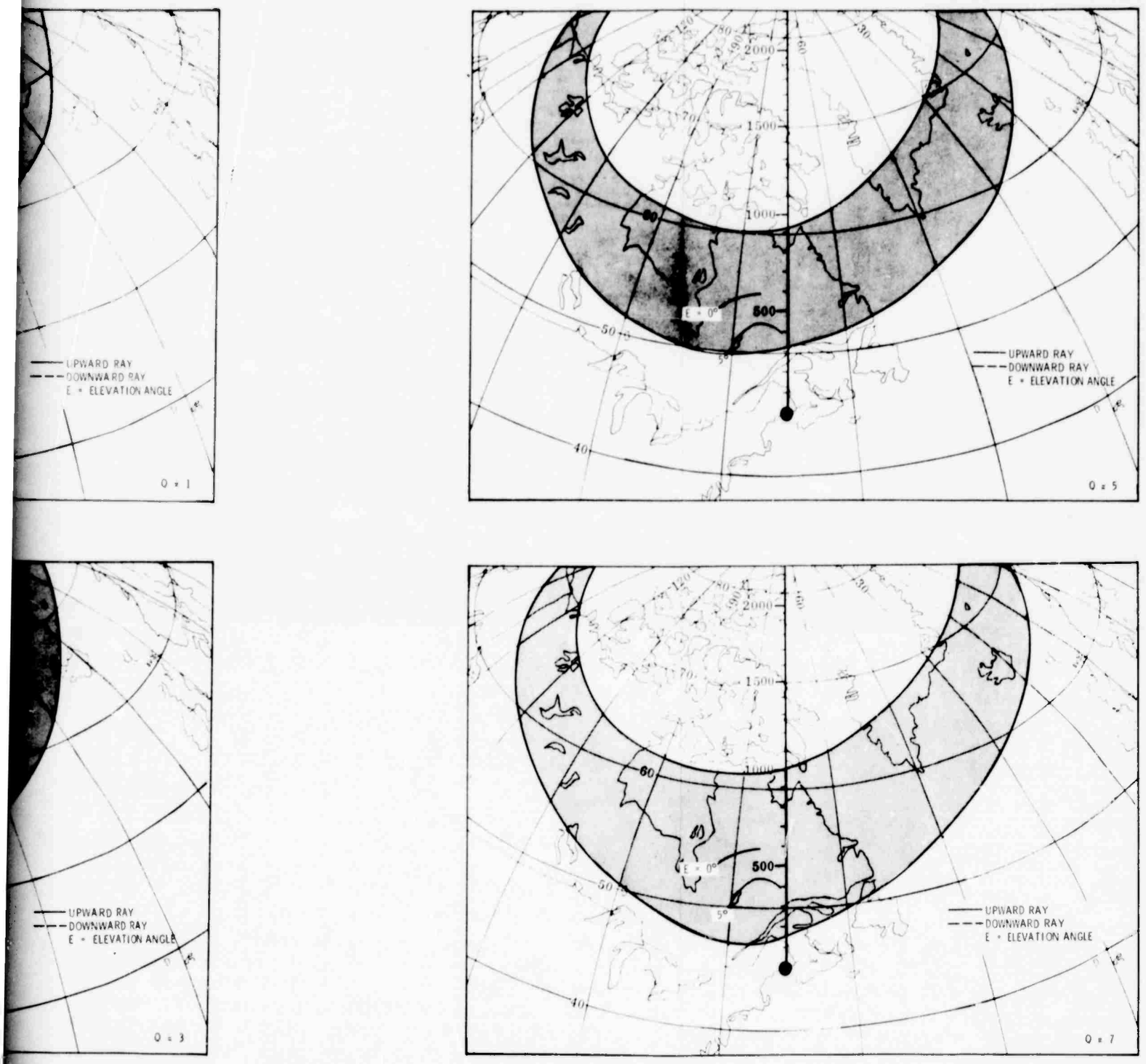

Figure 2-10. Contours of Zero-Degree Aspect Angle for 10 MHz E-Layer Echoes as Viewed from a Midlatitude Location, with the Feldstein-Starkov Auroral Belt Model for Various Levels of Magnetic Activity at 0000 Hours Local Time, Nighttime Ionospheric Model B

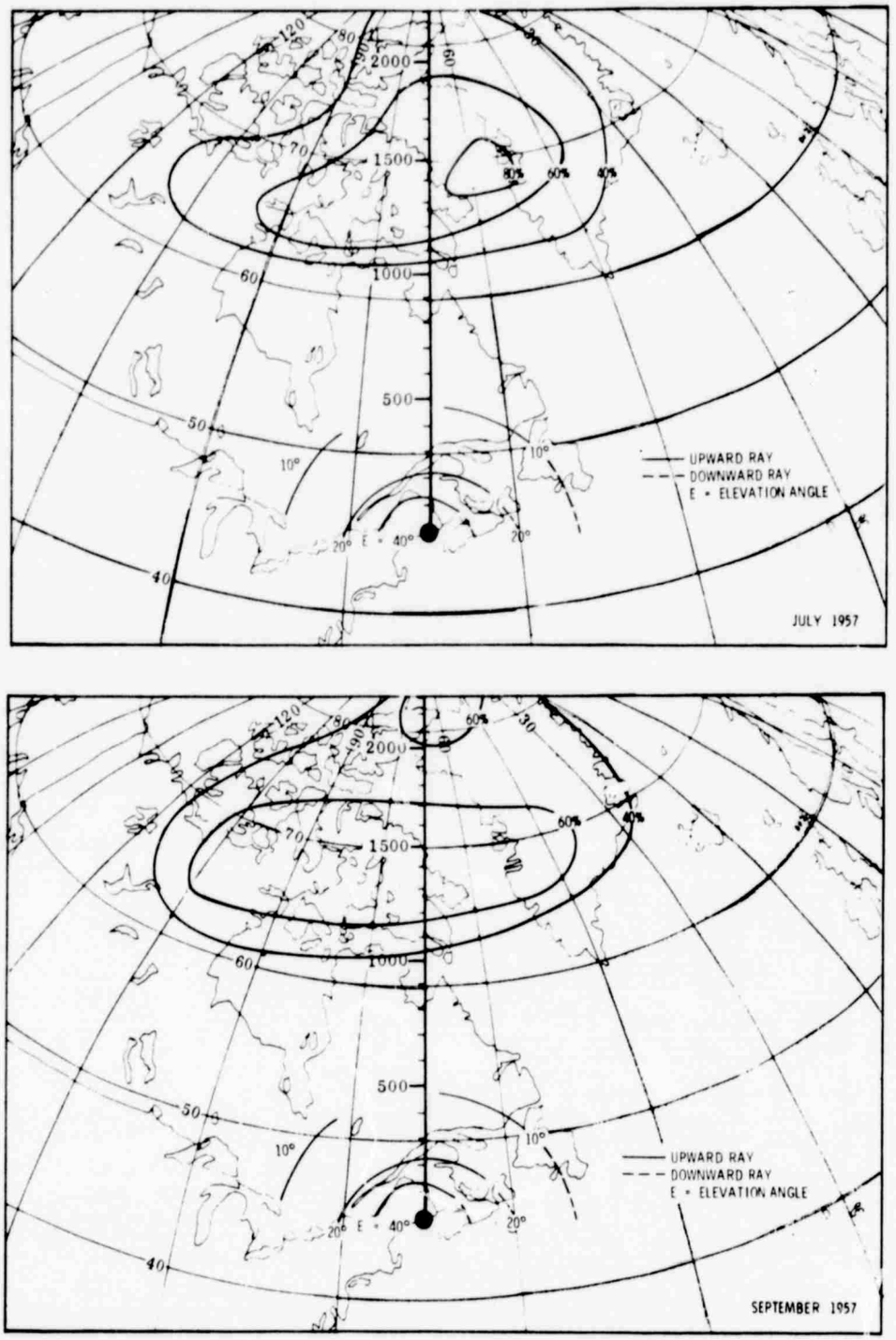

Figure 2-11. Contours of Zero-Degree Aspect Angle at 10 MHz and Penndorf's Probability of Occurrence of Spread-F as Viewed from a Mid-latitude Location, at 1300 Hours Local Time, Daytime Ionospheric Model A

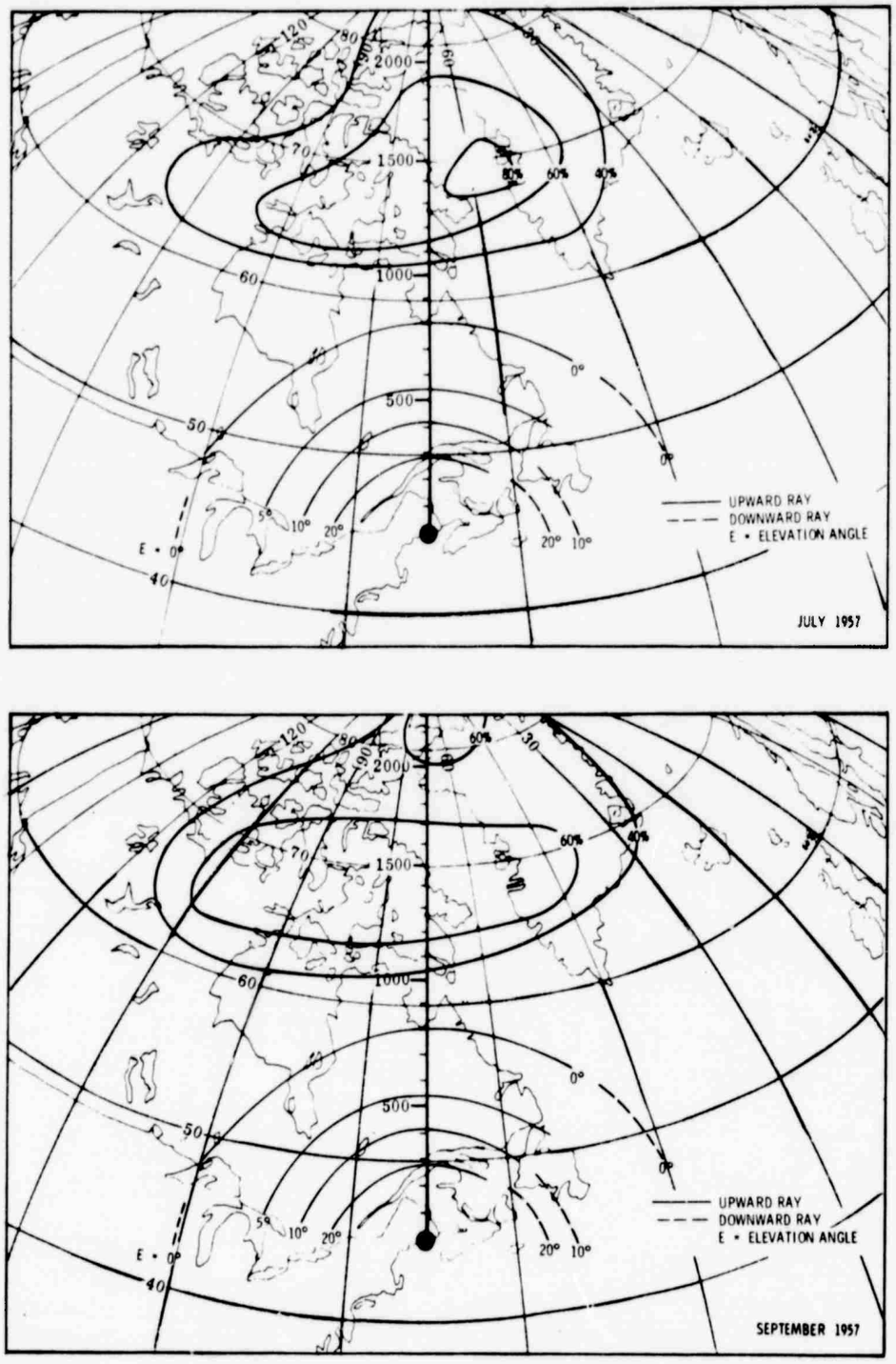

Figure 2-12. Contours of Zero-Degree Aspect Angle at 20 MHz and Penndorf's Probability of Occurrence of Spread-F as Viewed from a Mid-latitude Location, at 1300 Hours Local Time, Daytime Ionospheric Model A

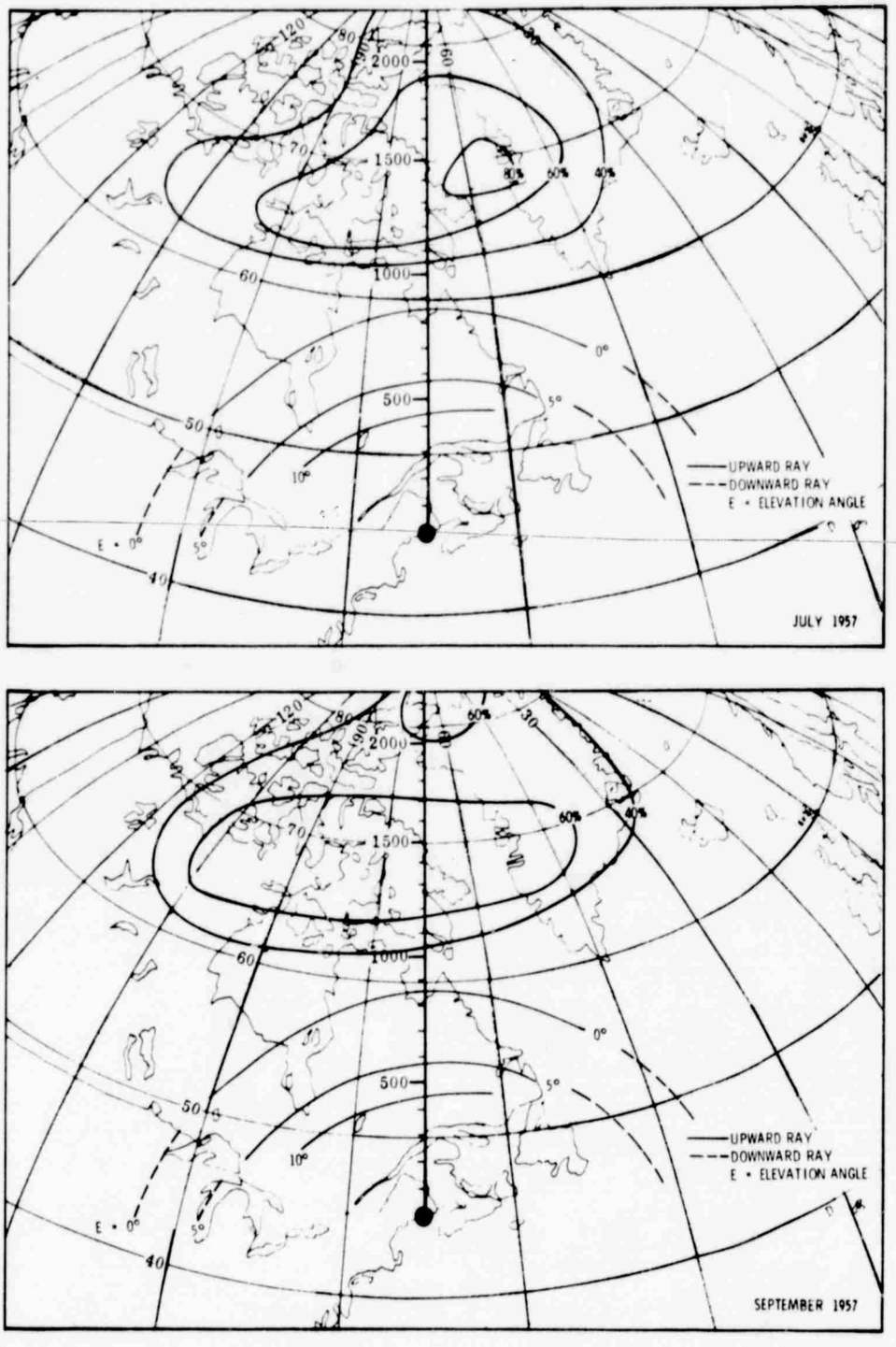

Figure 2-13. Contours of Zero-Degree Aspect Angle at 30 MHz and Penndorf's Probability of Occurrence of Spread-F as Viewed from a Mid-latitude Location, at 1300 Hours Local Time, Daytime Ionospheric Model A

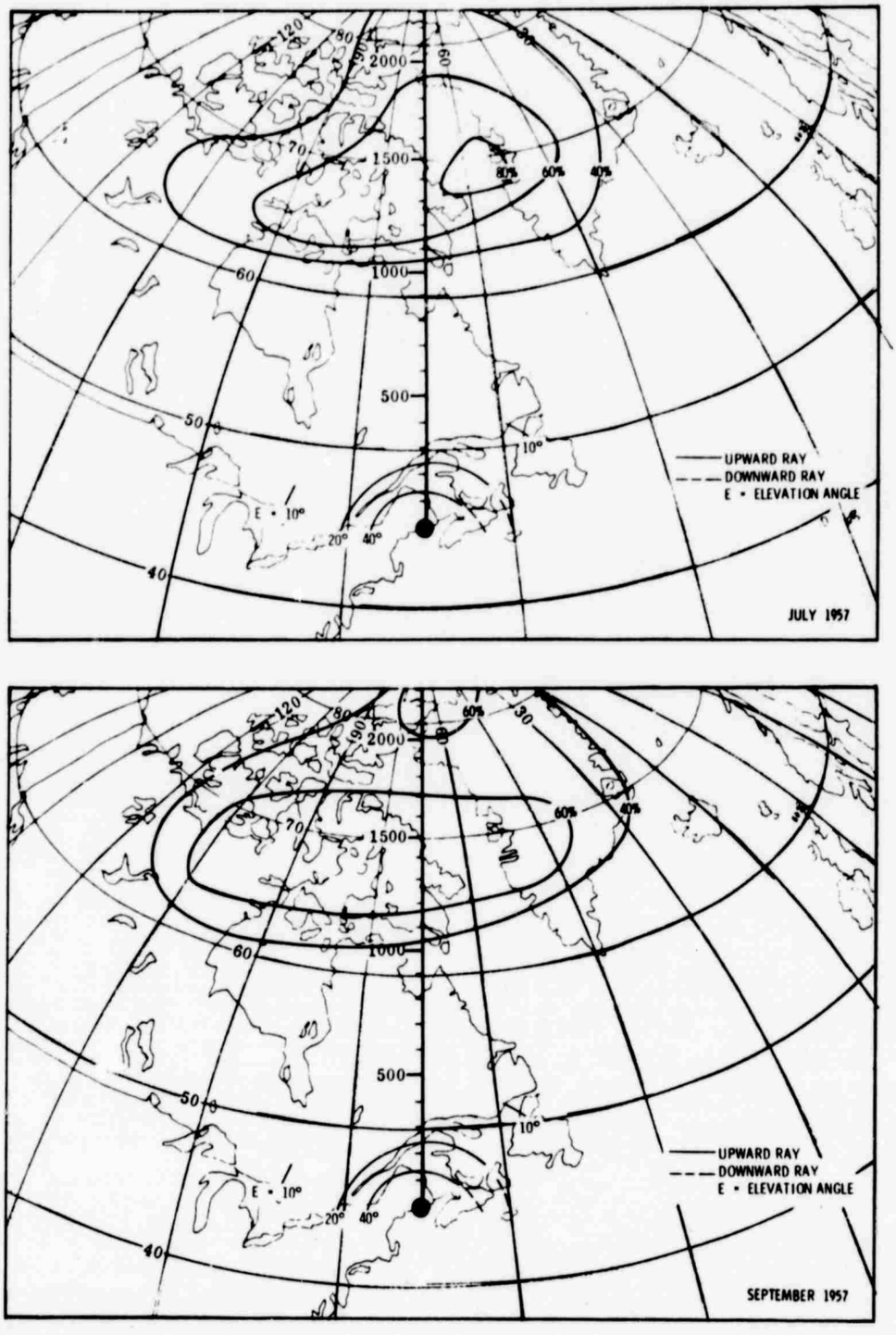

Figure 2-14. Contours of Zero-Degree Aspect Angle at 10 MHz and Penndorf's Probability of Occurrence of Spread-F as Viewed from a Mid-latitude Location, at 1300 Hours Local Time, Daytime Ionospheric Model B

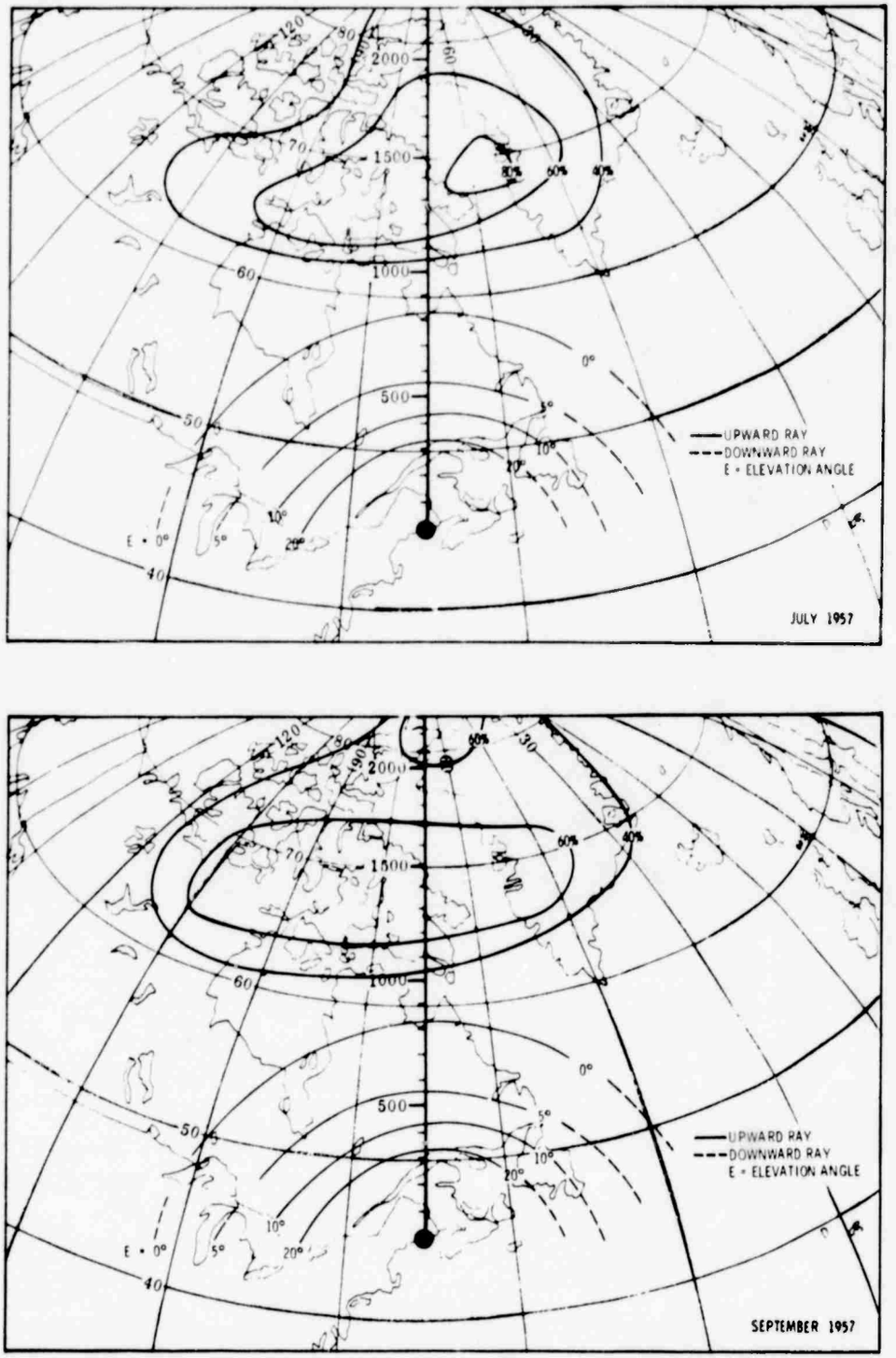

Figure 2-15. Contours of Zero-Degree Aspect Angle at 20 MHz and Penndorf's Probability of Occurrence of Spread-F as Viewed from a Mid-latitude Location, at 1300 Hours Local Time, Daytime Ionospheric Model B

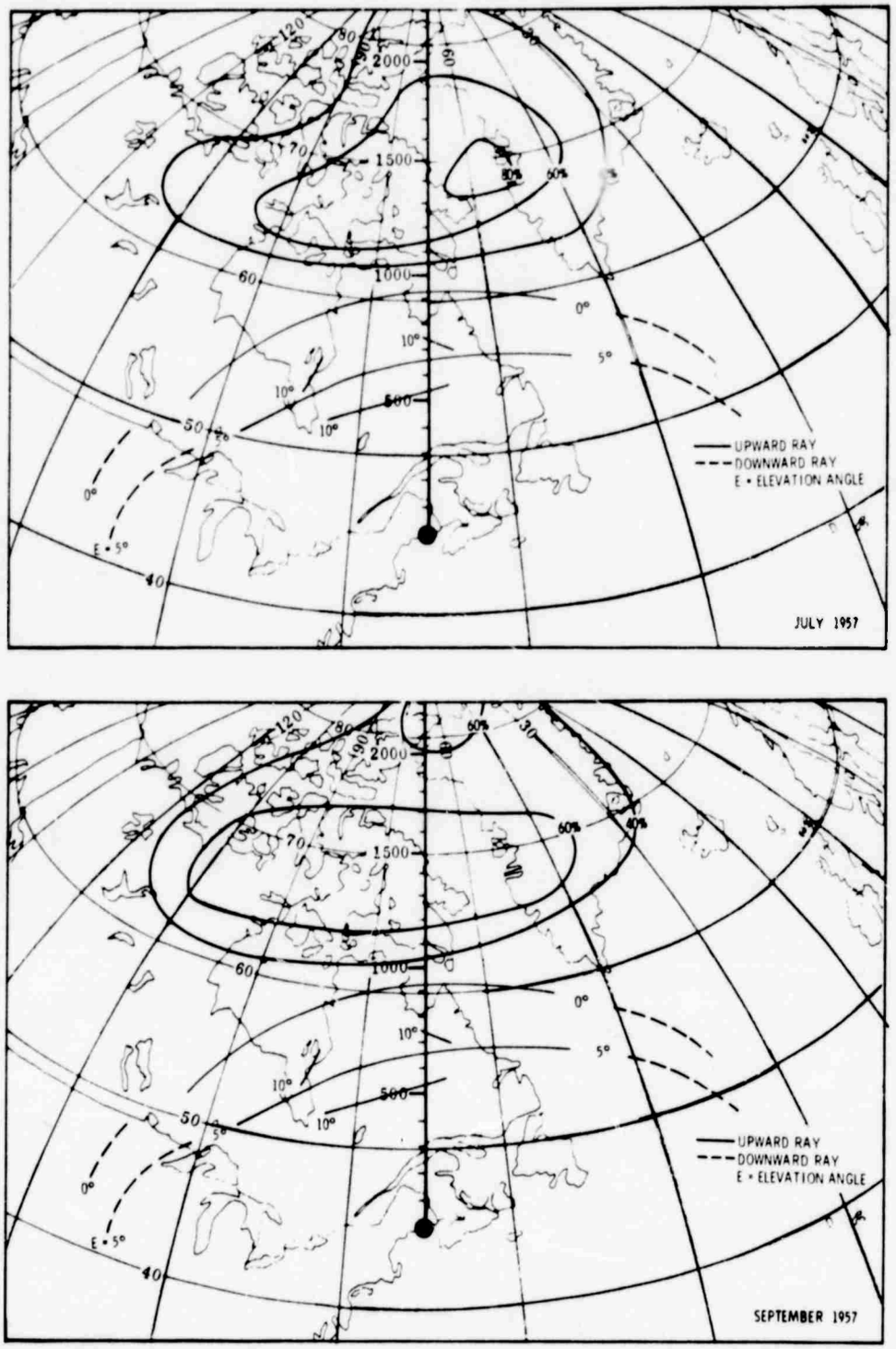

Figure 2-16. Contours of Zero-Degree Aspect Angle at 30 MHz and Penndorf's Probability of Occurrence of Spread-F as Viewed from a Mid-latitude Location, at 1300 Hours Local Time, Daytime Ionospheric Model B

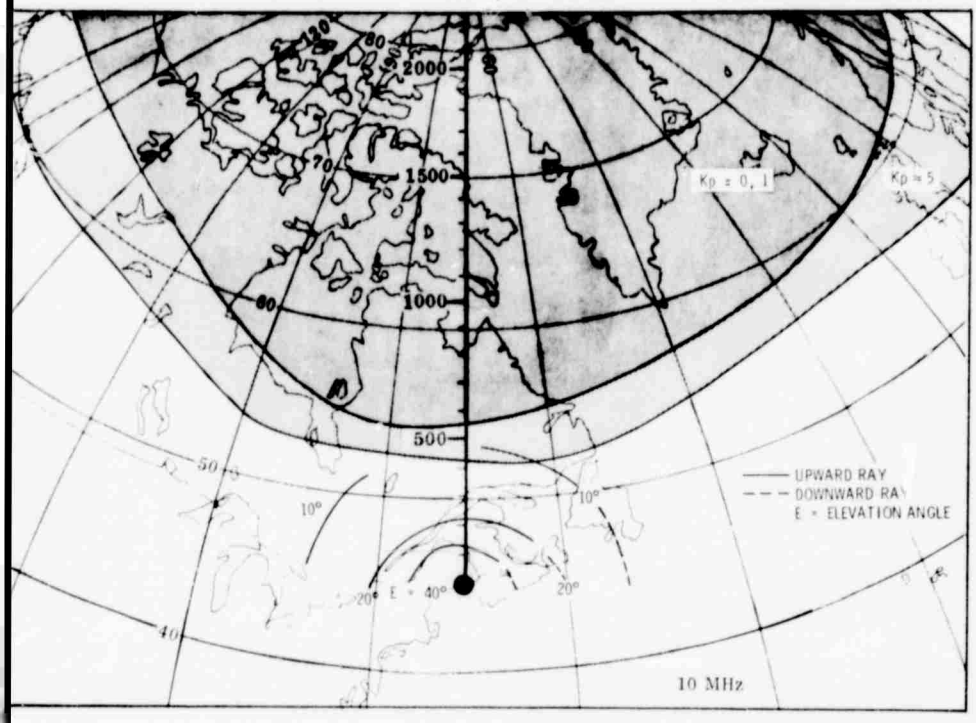

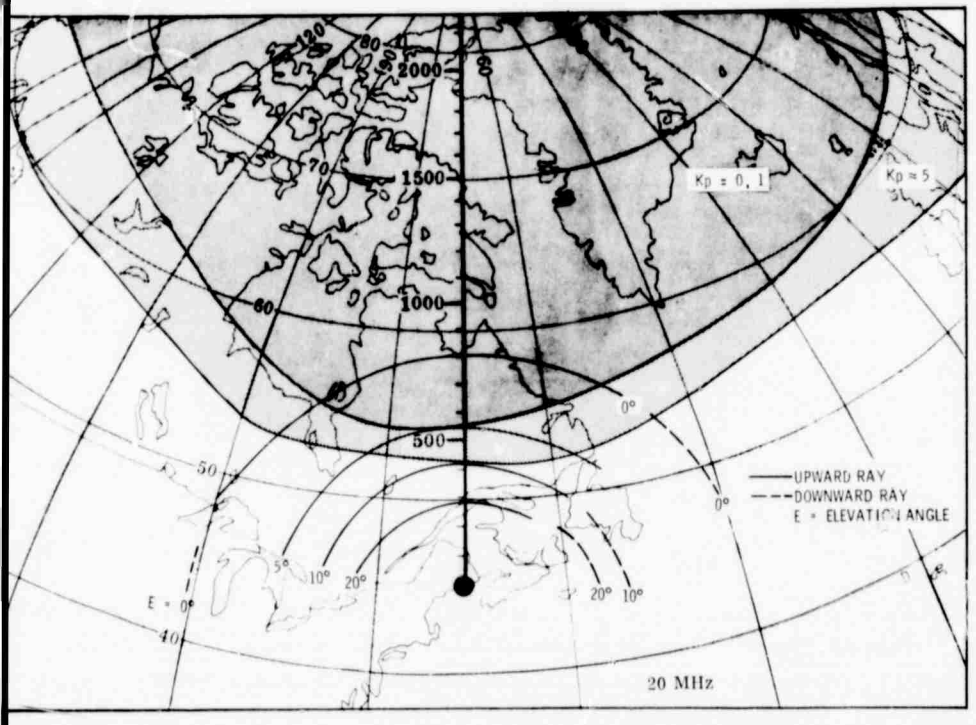

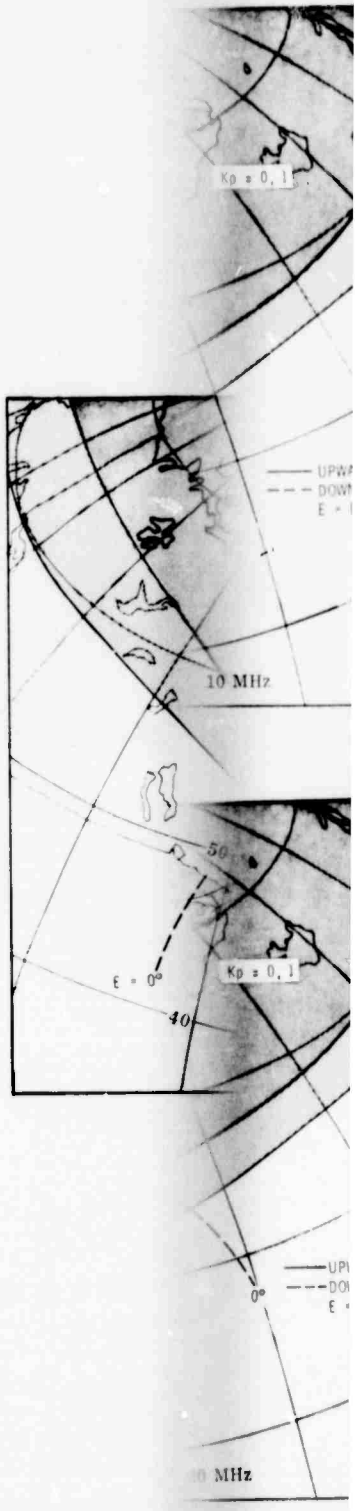

Figure 2-17. Contours of Ze
Irregularity Re
at 1200 Hours

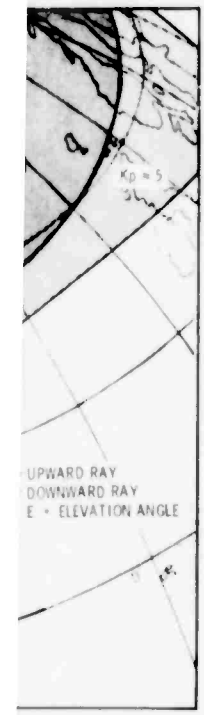

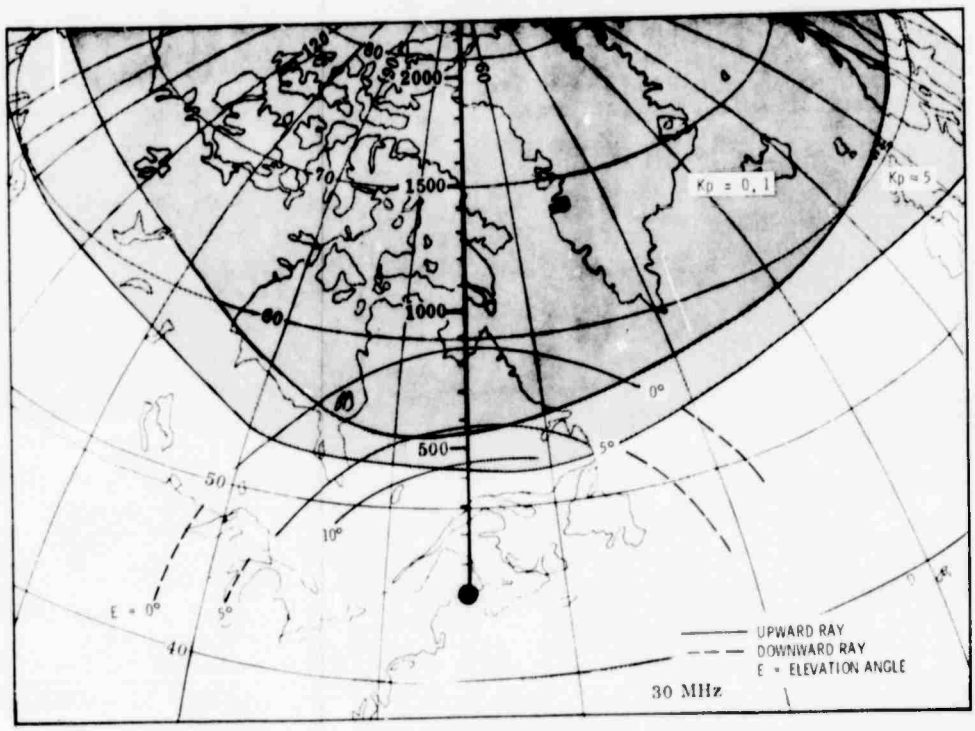

Figure 2-17. Contours of Zero Degree Aspect Angle and Aarons' F-Layer Irregularity Region as Viewed from a Midlatitude Location, at 1200 Hours Local Time, Daytime Ionospheric Model A

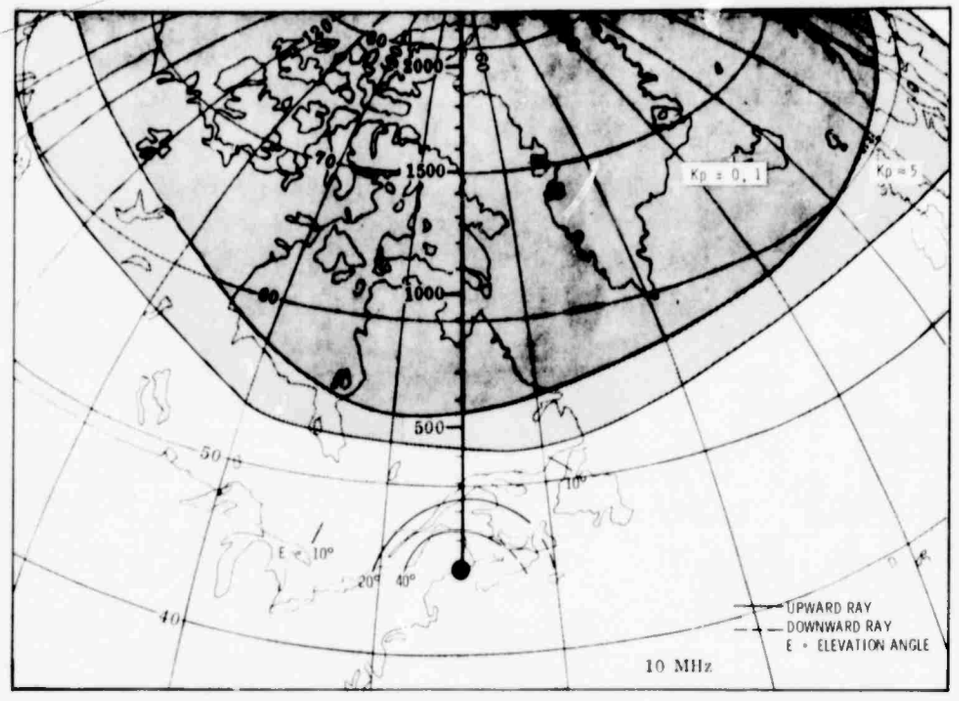

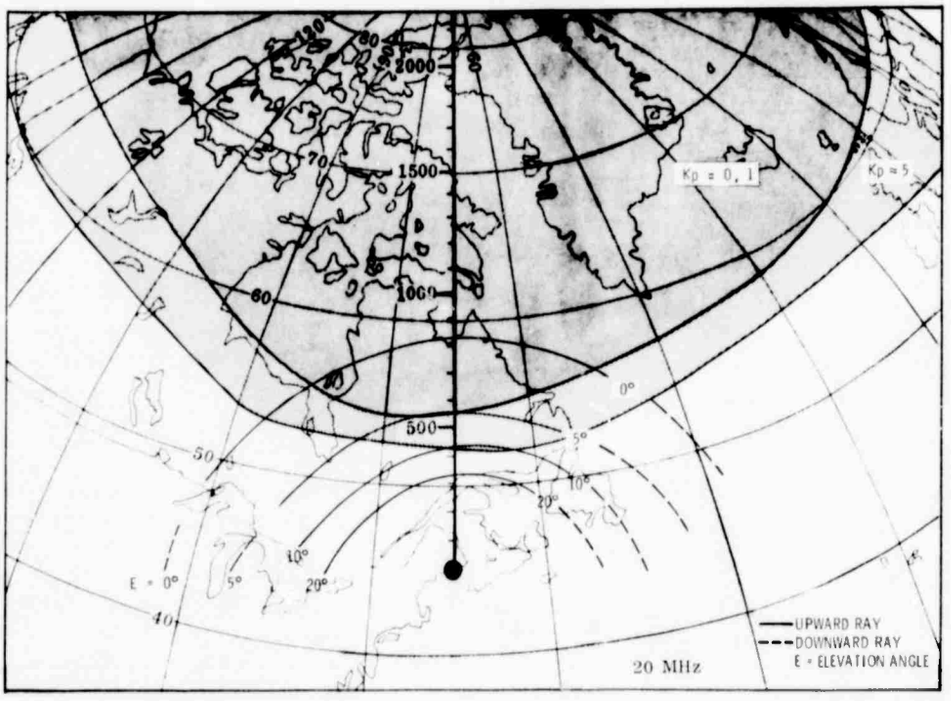

Figure 2-18. Contours of Zer
Irregularity Re
at 1200 Hours I

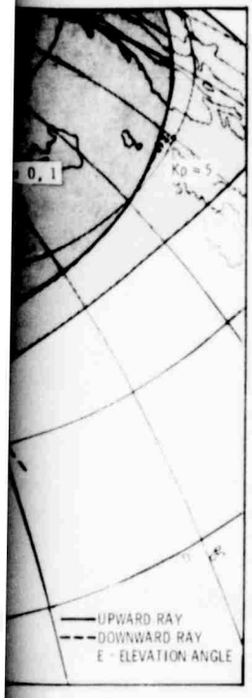

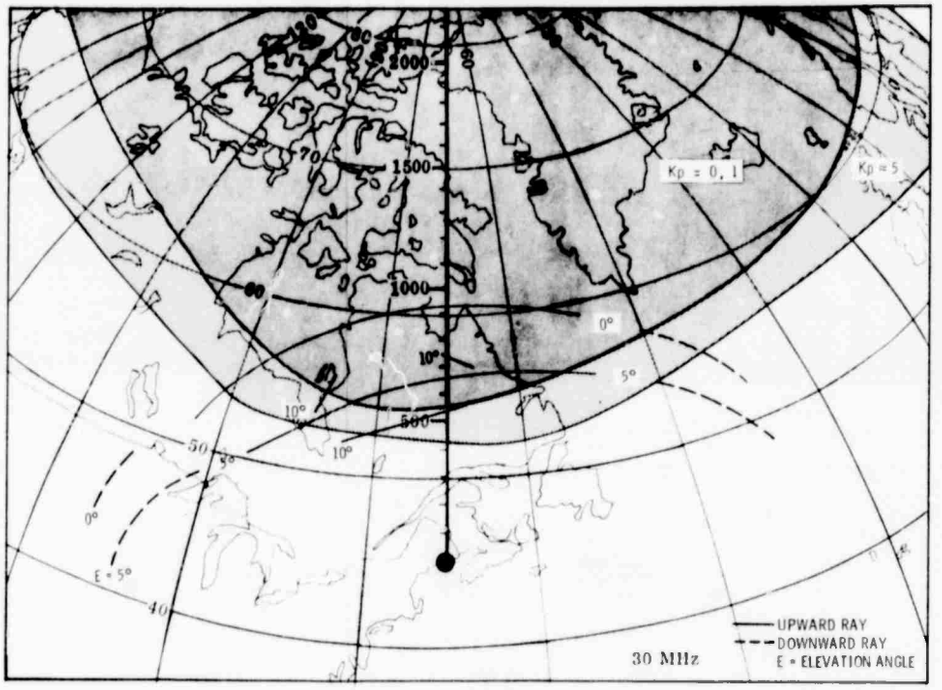

Figure 2-18. Contours of Zero-Degree Aspect Angle and Aarons' F-Layer Irregularity Region as Viewed from a Midlatitude Location, at 1200 Hours Local Time, Daytime Ionospheric Model B

Figures 2-19 and 2-20 are plots of the zero degree aspect angle at 10 MHz and Penndorf's (1962) spread-F probability contours at 0100 hour local time for both nighttime models. It is seen that the magnetic field orthogonality lines intersect the 80 percent probability contours. This would imply that echoes from field-aligned spread-F should be readily observed during the nighttime.

Figure 2-21 which depicts Aarons' (1973b) F-layer nighttime irregularity region with the zero degree aspect angle contours reveals that, even during low magnetic activity Kp = 0, 1), an HF radar should detect reflections from F-layer irregularities.

2.5 SUMMARY

Tables 2-2 and 2-3 summarize the regions (azimuth extent - ΔA, and range extent - ΔR) where field-aligned HF echoes are predicted for a midlatitude location.

It is seen that daytime E-layer auroral echoes should be nonexistent while, during the nighttime, for relatively quiet magnetic conditions (Q = 3), the echoes could appear within an azimuthal spread between -55° to +20° and range extent from 280 to 780 nmi.

Utilizing Penndorf's spread-F probability contours, spread-F echoes are predicted to be present only during the nighttime at the low frequencies (in the vicinity of 10 MHz). In terms of Aarons' irregularity region, however, both daytime and nighttime F-layer echoes can be expected.

It is emphasized that the regions in space where orthogonality with the magnetic field is attained is a function of the electron density along the ray paths. Thus, the estimates of the range and azimuth orientation of the field-aligned echoes, tabulated in Tables 2-2 and 2-3, will be modified depending on the ionization distribution in the ionosphere.

HF backscatter radar observations conducted at Caribou, Maine (geographic coordinates: 47°N, 68°W) revealed that radar reflections from E-layer irregularities could at times be observed over an entire 90° azimuthal coverage. The range extent of E-layer echoes attained a value as large as 500 km (Campbell et al., 1972). The angular extent of the backscatter from F-layer irregularities varied from 1° to about 30° while the range extent was found to be as great at 2000 km. The height interval over which the echoes existed could not be determined because of equipment limitations.

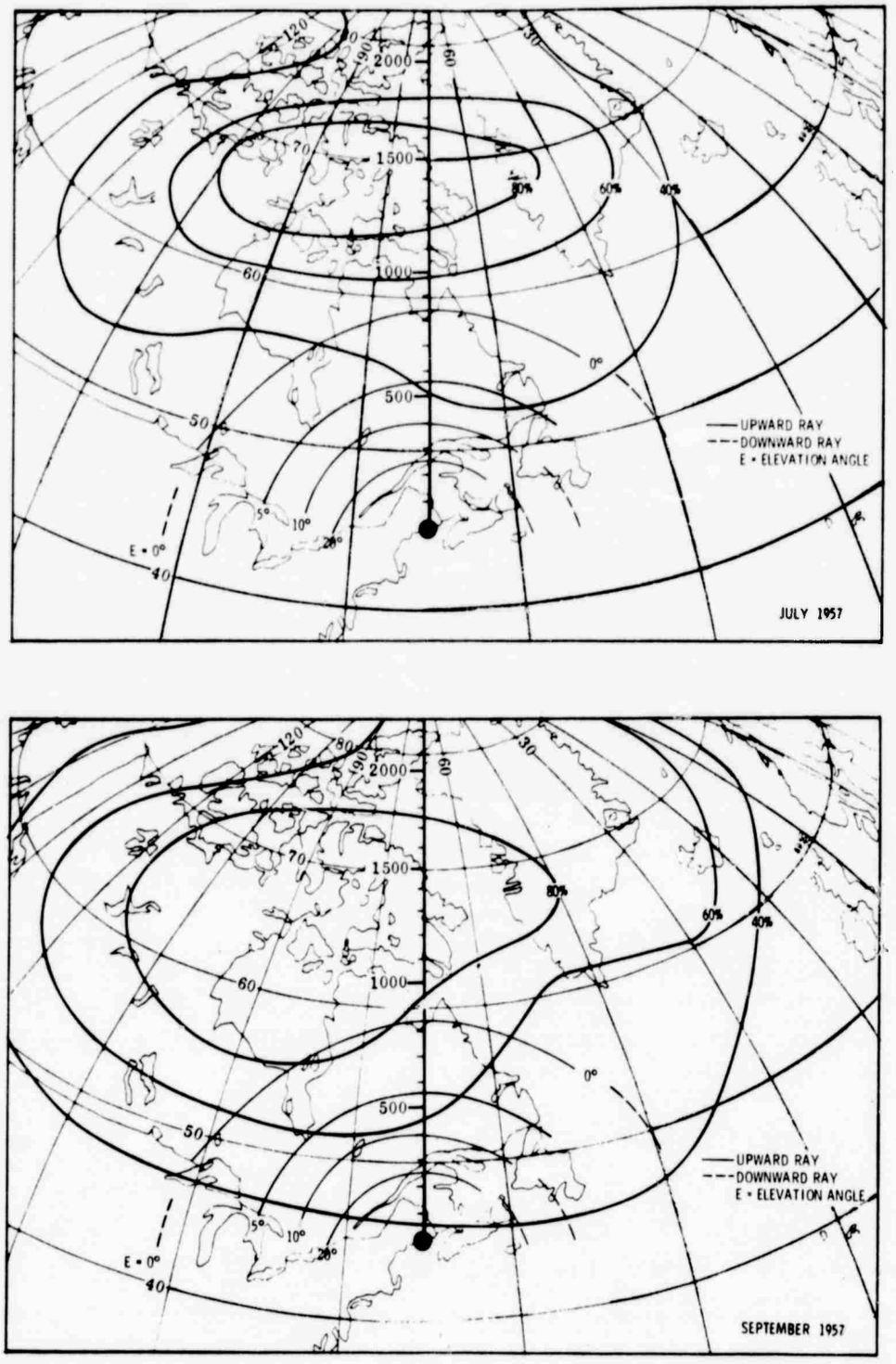

Figure 2-19. Contours of Zero-Degree Aspect Angle at 10 MHz and Penndorf's Probability of Occurrence of Spread-F as Viewed from a Mid-latitude Location, at 0100 Hours Local Time, Nighttime Ionospheric Model A

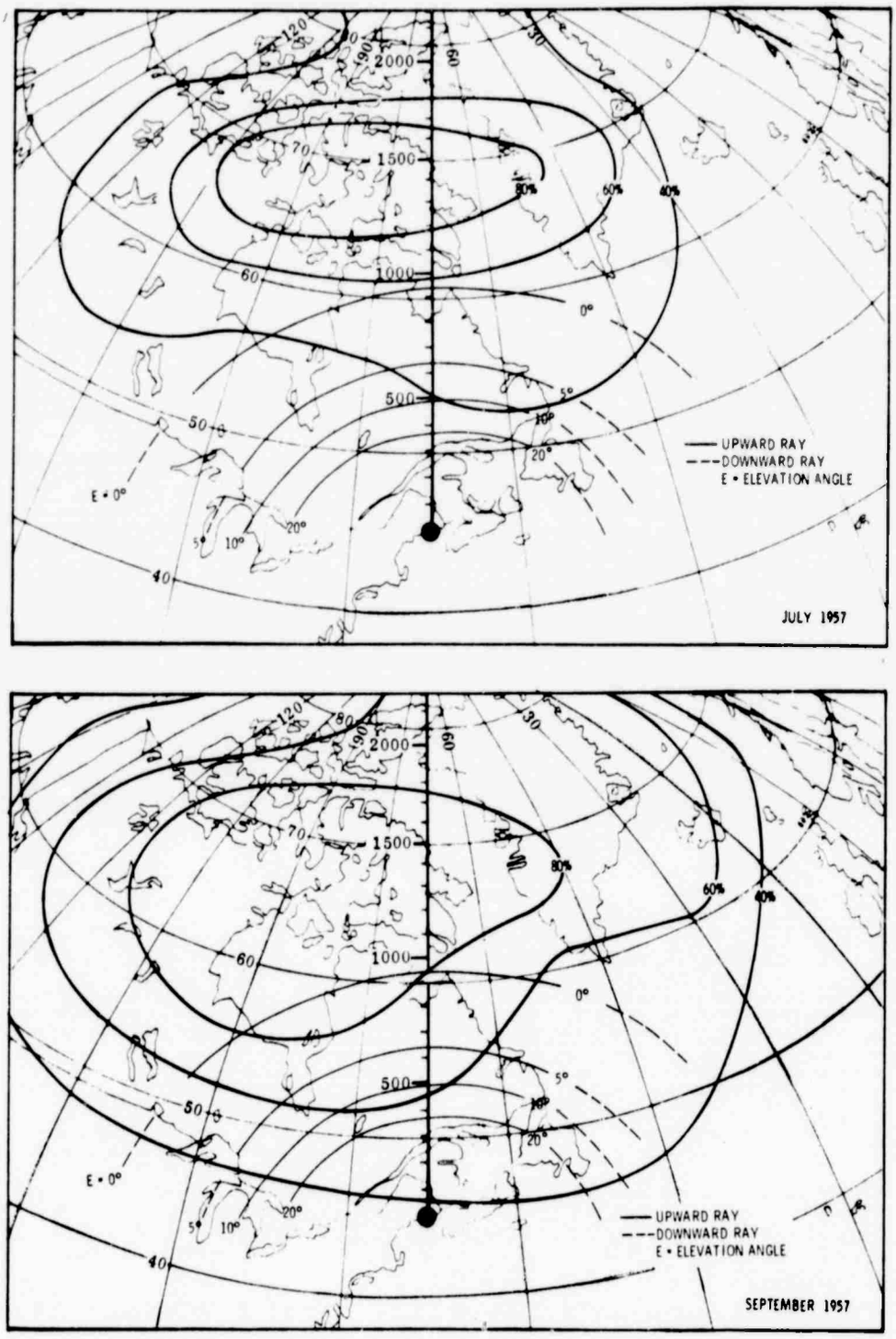

Figure 2-20. Contours of Zero-Degree Aspect Angle at 10 MHz and Penndorf's Probability of Occurrence of Spread-F as Viewed from a Mid-latitude Location, at 0100 Hours Local Time, Nighttime Ionospheric Model B

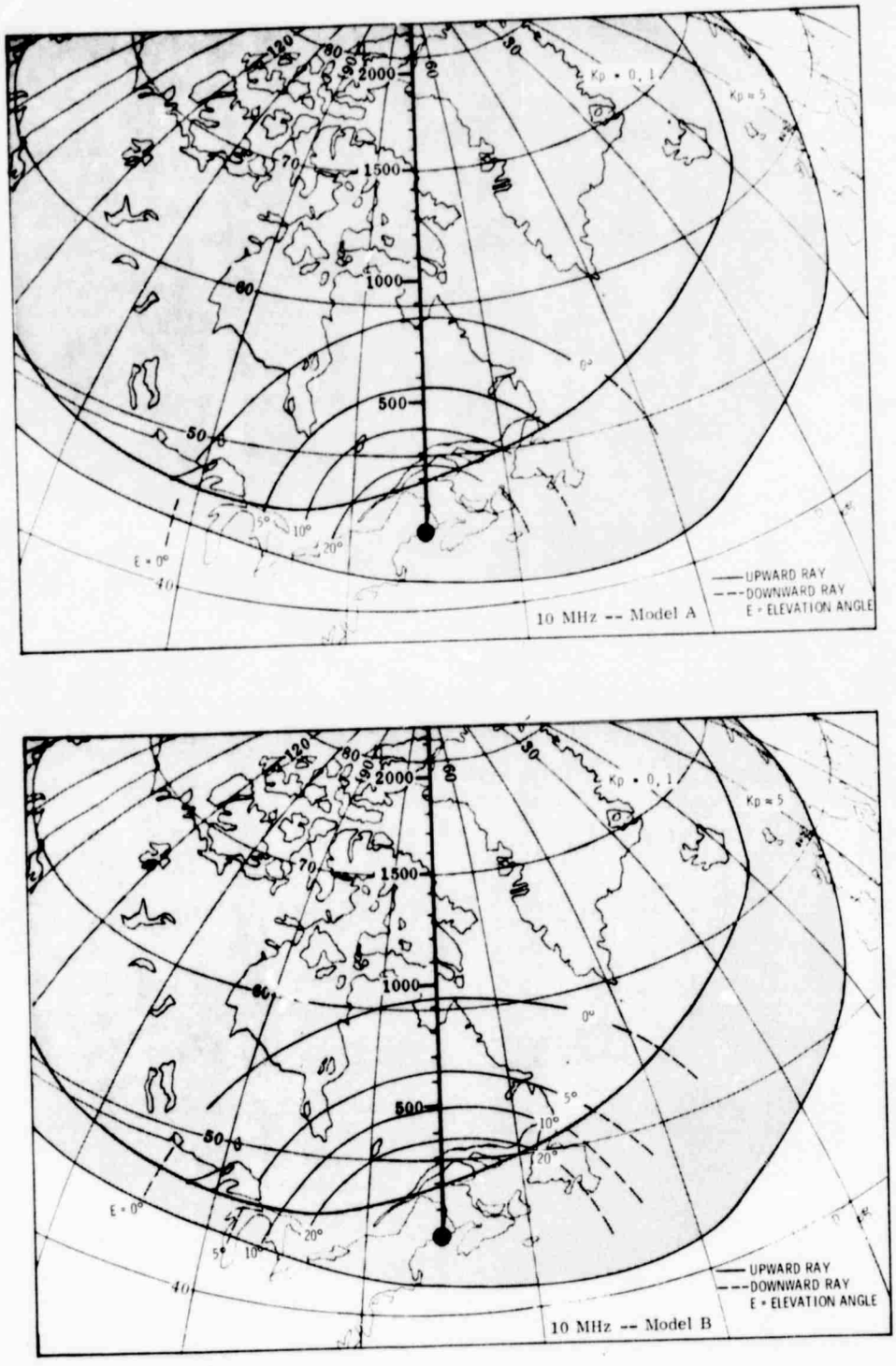

Figure 2-21. Contours of Zero-Degree Aspect Angle and Aarons' F-Layer Irregularity Region as Viewed from a Midlatitude Location, at 0000 Hours Local Time, Nighttime Ionospheric Models A and B

TABLE 2-2

ESTIMATED RANGE AND AZIMUTHAL EXTENT OF E-LAYER AURORAL ECHOES AS OBSERVED FROM A MIDLATITUDE LOCATION

Frequency (MHz)	Local Standard Time (h)	Magnetic Activity Index							
		Q = 1		Q = 3		Q = 5		Q = 7	
		ΔA (deg)	ΔR (nmi)	ΔA (deg)	ΔR (nmi)	ΔA (deg)	ΔR (nmi)	ΔA (deg)	ΔR (nmi)
10	0000	-39 to +19	560 to 780	-55 to +20	380 to 780	-55 to +20	320 to 780	-62 to +20	150 to 780
	1200	0	0	0	0	0	0	0	0
20	0000	-	-	-	-	-	-	-	-
	1200	0	0	0	0	0	0	0	0
30	0000	-	-	-	-	-	-	-	-
	1200	0	0	0	0	0	0	0	0

TABLE 2-3

ESTIMATED RANGE AND AZIMUTHAL EXTENT OF F-LAYER ECHOES AS OBSERVED FROM A MIDLATITUDE LOCATION

Frequency (MHz)	Local Standard Time (h)	Penndorf's Probability of Occurrence of Spread-F						Aarons' Irregularity Region			
		40% Probability		60% Probability		80% Probability		K_p = 0, 1		K_p = 5	
		ΔA (deg)	ΔR (nmi)	ΔA (deg)	ΔR (nmi)	ΔA (deg)	ΔR (nmi)	ΔA (deg)	ΔR (nmi)	ΔA (deg)	ΔR (nmi)
10	0000-0100	-75 to +82	50 to 1240	-58 to +25	450 to 1020	-44 to 0	780 to 1040	-80 to +53	180 to 1180	-90 to +90	0 to 1250
	1200-1300	0	0	0	0	0	0	0	0	+10 to +32	450 to 500
20	0000-0100	-	-	-	-	-	-	-	-	-	-
	1200-1300	0	0	0	0	0	0	-37 to +37	560 to 930	-52 to +51	430 to 930
30	0000-0100	-	-	-	-	-	-	-	-	-	-
	1200-1300	0	0	0	0	0	0	-39 to +43	560 to 1260	-52 to +52	440 to 1260

2.6 MAGNETIC ACTIVITY INDICES

It should be noted that the magnetic activity index, Q, used by Feldstein and Starkov (1967) is related to the geomagnetic planetary index, Kp. According to Valley (1965), a Q = 0 is comparable to a Kp = 0 or 1; Q = 1, Kp = 2; Q = 4, Kp = 5 or 6 and Q = 7, Kp = 8 or 9.

The geomagnetic planetary index, Kp, is a mean three-hour magnetic reading derived from observations located between 47° and 63° geomagnetic latitude. The scale of 0 to 9 is an arbitrary one where 0 refers to very quiet magnetic conditions and 9 to extremely disturbed magnetic conditions.

The magnetic activity index, Q (often referred to as the Polar Range Index), is a quarter-hourly index which is at times used to indicate the severity of magnetic conditions for high latitudes (above about 58° geomagnetic latitude). The index has not been widely employed in geophysical analysis because of the complexity involved in the data reduction of magnetic observations to obtain the parameter.

The cumulative distribution function of the occurrence of Kp is plotted in Figure 2-22 for the two extremes of solar activity and for the 1932-1970 period (Zawalick and Cage, 1971). In the period from April 1957 through December 1958, which encompasses the International Geophysical Year (IGY), the sunspot number was approximately 200 while, from January 1964 through October 1965, which was a period of quiet solar activity, the sunspot number was 10. It is seen that, during a time of minimum solar activity, the median and upper decile value of Kp is 1 and 3, respectively, while, during maximum solar activity, the corresponding values increase to approximately 2 and 4, respectively.

Figure 2-23 is a plot of the occurrence of the geomagnetic planetary index, Kp, from 1950 through 1971 (Aarons, 1973a) and the mean sunspot number. It is apparent that the occurrence of magnetic disturbed conditions is not correlated with solar activity. These results somewhat contradict the statistical data presented in Figure 2-22.

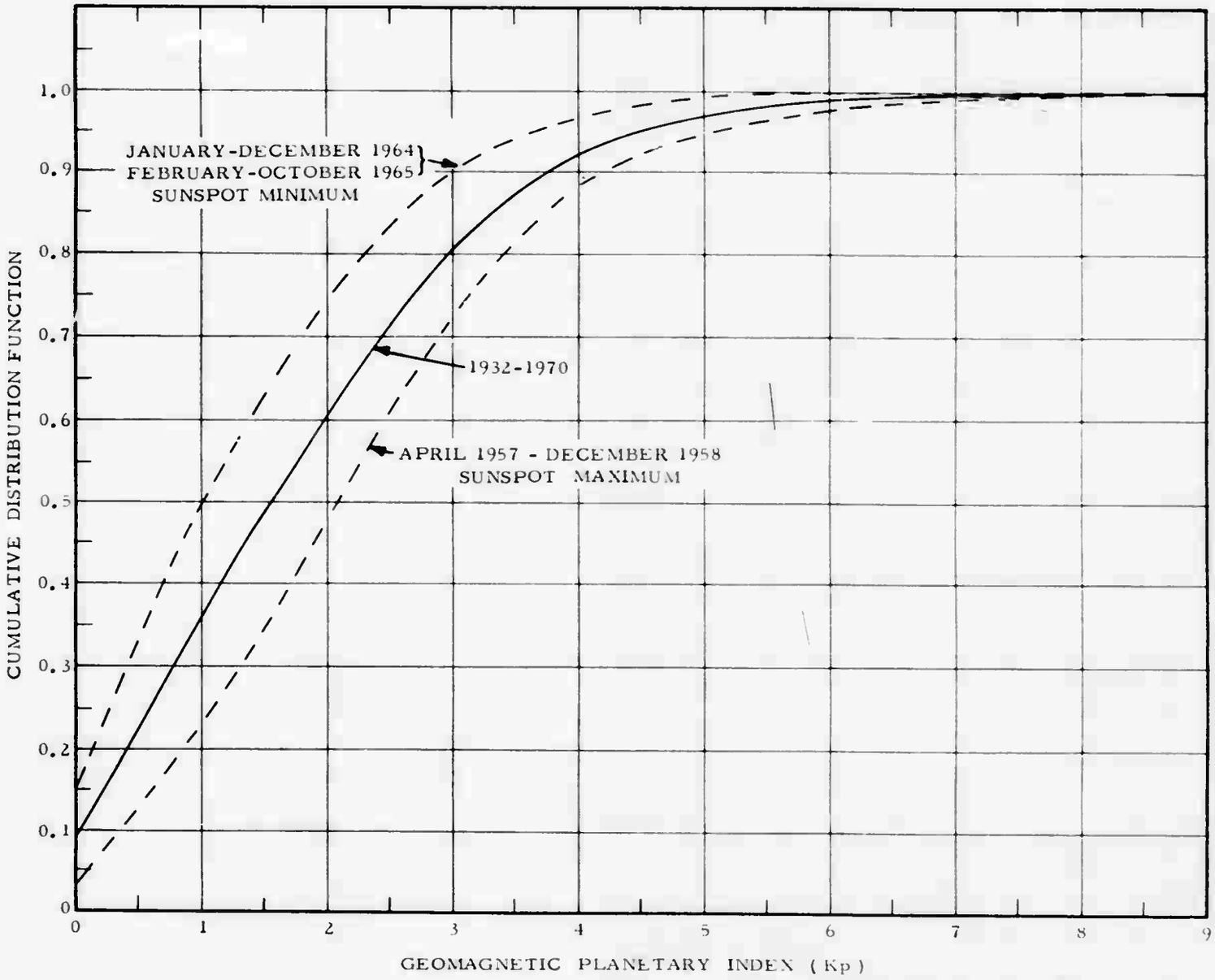

Figure 2-22. Cumulative Distribution Function of the Occurrence of the Geomagnetic Planetary Index, Kp

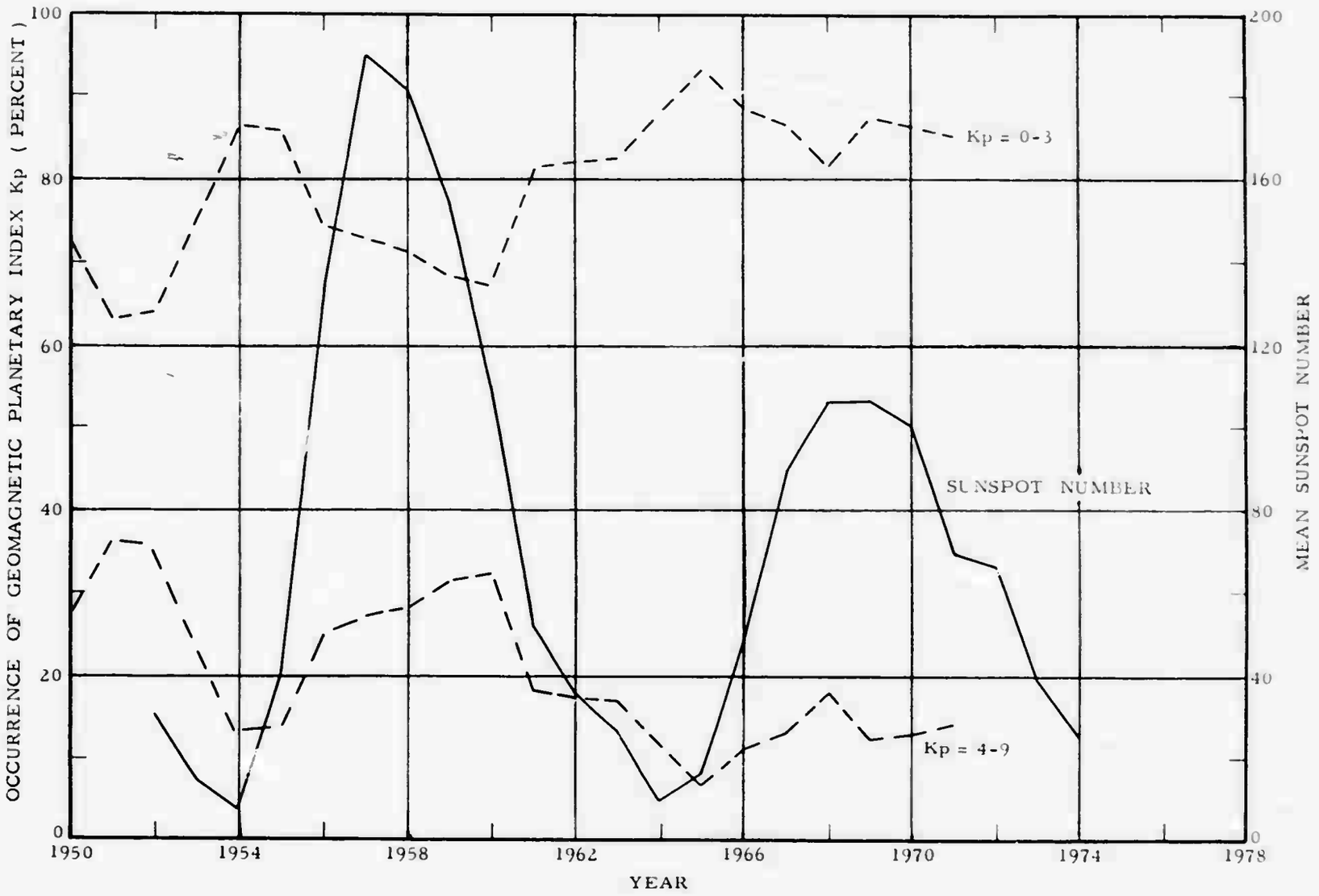

Figure 2-23. Correlation of Mean Sunspot Number with the Occurrence of Geomagnetic Planetary Index, Kp

SECTION III

SIGNAL AMPLITUDE AND CROSS SECTION STATISTICS OF IONOSPHERIC BACKSCATTER ECHOES

3.1 INTRODUCTION

In this section, an analysis is made of the statistical characteristics of the amplitude and cross-sectional area of HF ionospheric backscatter echoes that could be observed by an HF backscatter radar operating in the midlatitudes with a northerly oriented antenna beam. The echo data that are evaluated were obtained from measurements made by the Stanford Research Institude (SRI) (Leadabrand et al., 1965) and under the Polar Fox II program (Bradley et al., 1972; Herman and Vargas-Vila, 1973).

3.2 RADAR EQUATION

In order to interpret the SRI and Polar Fox II auroral data in terms of the corresponding effects on an HF backscatter radar, it is necessary to determine the relative sensitivities of the radars to the aurora. This is accomplished by comparing the various parameters which enter into the radar equation.

According to the radar equation, the signal-to-noise ratio (SNR) of the received signal is given by

$$\frac{P_r}{N} = \frac{P_t G_t G_r \lambda^2 \sigma}{(4\pi)^3 R^4 KTB\, \overline{NF}\, L_s\, L_p} \tag{3-1}$$

where P_t is the transmitted power, G_t is the gain of the transmitting antenna, G_r is the gain of the receiving antenna, λ is the wavelength, σ is the radar cross section of the target, R is the radar range, K is Boltzmann's constant (1.38×10^{-23} Ws/°K), T is the ambient temperature (288°K), B is the receiver noise bandwidth, $\overline{NF}$ is the receiver noise figure, L_s is the system loss and L_p is the two-way loss due to the propagation medium. This relationship is applicable to a point target, i.e., the antenna beamwidth is much larger than the dimensions of the target.

For aurora which partially fills the antenna beam, σ is replaced by the volume scattering coefficient, σ_v, i.e., radar cross section per unit volume, such that

$$\sigma = \sigma_v V \tag{3-2}$$

where V is the volume filled by the scatterers.

The volume of the aurora intersected by the antenna beam, shown in Figure 3-1, can be represented by

$$V = R \beta_H \Delta R \Delta h \tag{3-3}$$

where β_H is the horizontal beamwidth of the antenna, Δh is the thickness of the aurora in the vertical direction. The parameter, ΔR is the radar range resolution defined by

$$\Delta R = \frac{c\tau}{2} \tag{3-4}$$

where c is the free-space velocity and τ is the pulse length.

Substituting Equations (3-2), (3-3) and (3-4) in Equation (3-1), it follows that

$$\frac{P_r}{N} = \frac{P_t G_t G_r \lambda^2 \sigma_v c\tau \beta_H \Delta h}{2(4\pi)^3 R^3 KTB \overline{NF} L_s L_p} \tag{3-5}$$

It is seen that, for a partially filled beam, the SNR is inversely proportional to the range cubed.

When the scatterers completely fill the antenna beam, the scattering volume for a rectangular antenna can be described by

$$V = R^2 \beta_H \beta_V \Delta R \tag{3-6}$$

where β_V is the vertical antenna beamwidth.

Substituting Equations (3-2), (3-4) and (3-6) in Equation (3-1) results in

$$\frac{P_r}{N} = \frac{P_t G_t G_r \lambda^2 \sigma_v c\tau \beta_H \beta_V}{2(4\pi)^3 R^2 KTB \overline{NF} L_s L_p} \tag{3-7}$$

It is of interest to note that, for the filled beam case, the SNR is inversely proportional to the range squared.

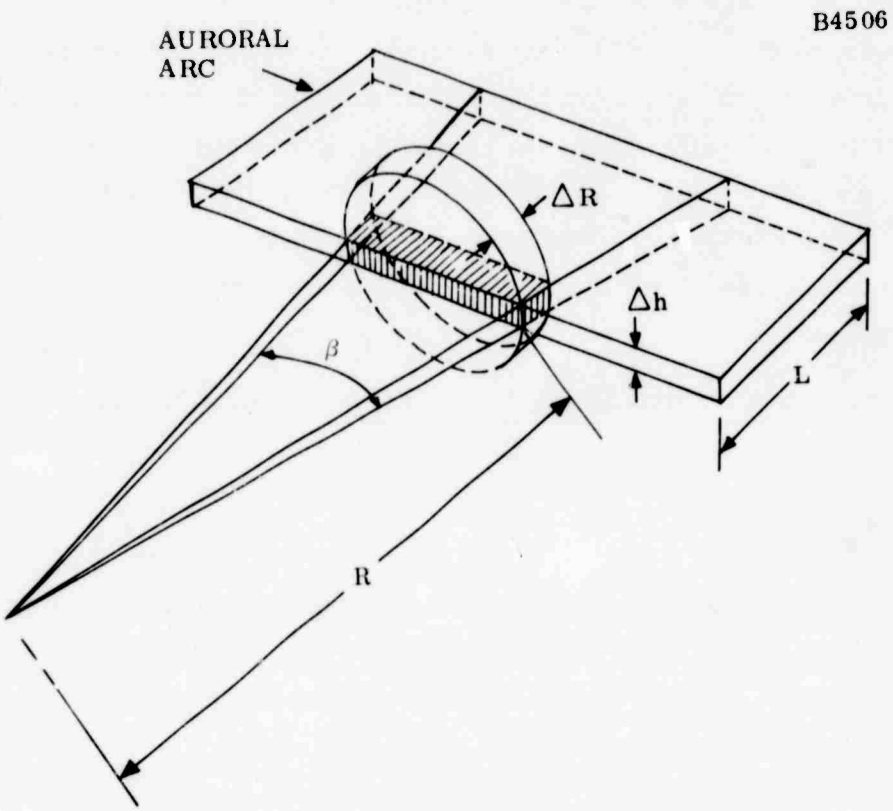

Figure 3-1. Intersection of Antenna Beam with Auroral Arc

3.3 SRI E-LAYER AURORAL DATA

During the 1959-60 period, SRI conducted an experimental program at Fraserburgh, Scotland, for the study of the characteristics of radar-auroral echoes (Leadabrand, et al., 1965). Radar measurements were made simultaneously at a frequency of 30, 401 and 800 MHz. The amplitude of the auroral echoes that could be encountered by a high-powered HF backscatter radar is obtained by extrapolation from the SRI data.

Figure 3-2 is a plot of the relative signal strengths of auroral echoes recorded at the three frequencies in April 1960. The region of uncertainty between 30 and 401 MHz results from the fact that there was no way to specify to what degree the auroral scatterers filled the 30-MHz antenna beam. At 401 and 800 MHz, the antenna beamwidth was 1.2° while, at 30 MHz, it was 15°. Thus, it was assumed that the scatterers completely filled the beam at the two higher frequencies. However, it was doubtful that the beam was completely filled at 30 MHz. The 1° x 1° aurora can be considered to be a point target in terms of the 30-MHz antenna.

It is noted that the data in Figure 3-2 are normalized with respect to 401 MHz. For a filled beam antenna, the relative signal strength of the 30-MHz echoes was 6 dB greater than those at 401 MHz, while for the point target case, there was a 28-dB difference between the 30- and 401-MHz data.

The absolute magnitude of the 30-MHz auroral echoes can be deduced by comparing the system sensitivities of the 30- and 401-MHz radars. According to Table 3-1, the 401-MHz radar was 48.9-dB more sensitive than the 30-MHz radar assuming that the aurora was a point target, and 26.9-dB more sensitive, assuming that the 30-MHz antenna beam was completely filled with scatterers. Thus, as indicated in Table 3-2, it follows that the magnitude of the 30-MHz radar auroral data was 20.9 dB less than that of the 401-MHz data.

The amplitude distribution of the 401-MHz radar-auroral echoes is presented in histogram form in Figure 3-3. It is noted that the system noise level was approximately -133 dBm and that the system saturated at -60 dBm which accounts for the large number of echoes at that amplitude.

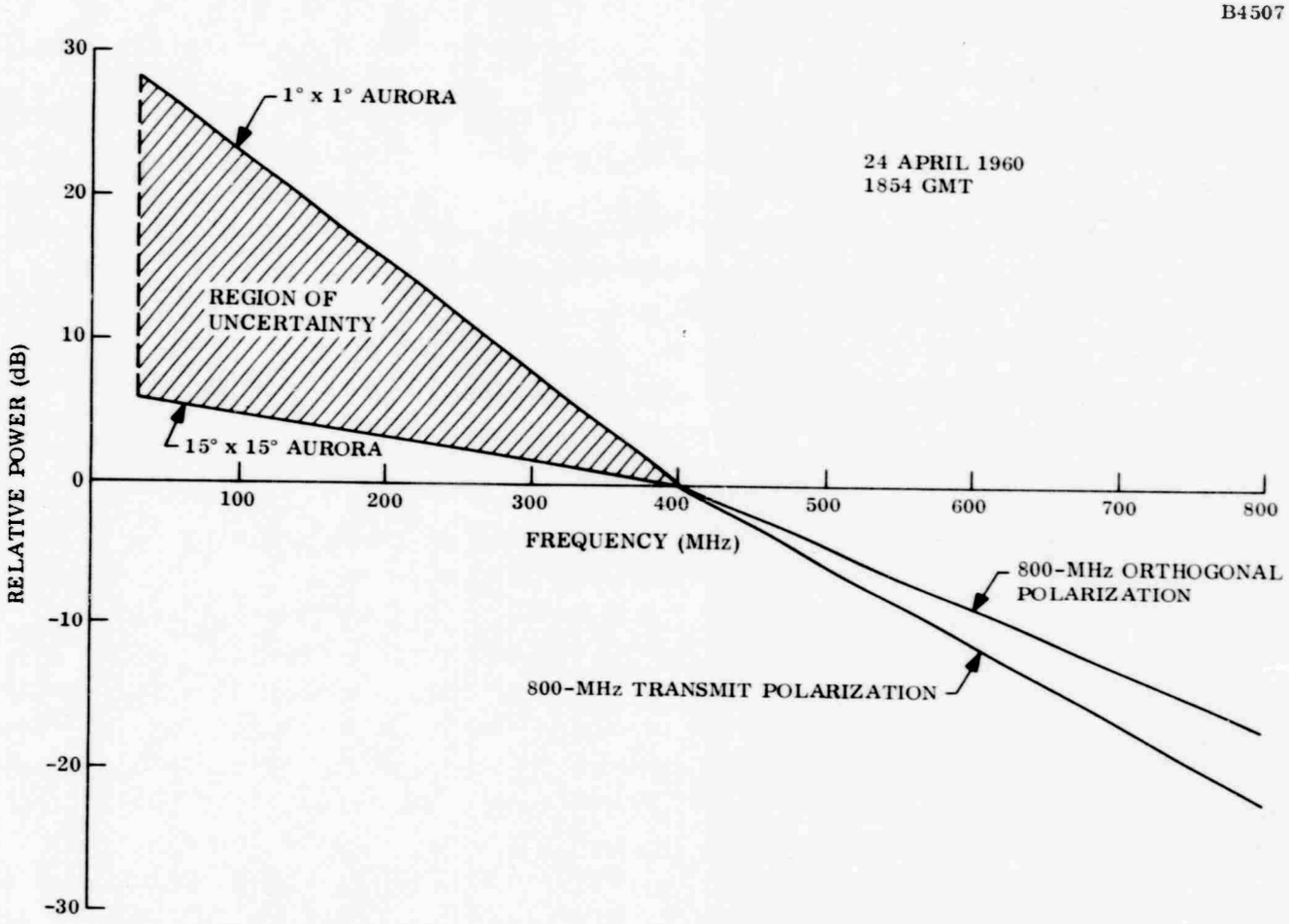

Figure 3-2. Relative Signal Strength of Auroral Echoes at 30-, 401- and 800-MHz Obtained by the SRI Radars at Scotland (After Leadabrand, et al., 1965)

TABLE 3-1

COMPARISON OF SRI-SCOTLAND 30-MHz AND 401-MHz RADAR SYSTEM SENSITIVITIES UTILIZED IN THE APRIL 1960 RADAR-AURORA L OBSERVATIONS

Parameter	30-MHz Radar	401-MHz Radar	Point Target (401 MHz/30 MHz) (dB)	Scatterers Fill Antenna Beam (401 MHz/30 MHz) (dB)
λ^2 (m^2)	$(10.0)^2$	$(0.748)^2$	-22.5	-22.5
P_t (MW)	0.0015	0.12	+19	+19
$G_t G_r$ (dB)	40	84	+44	+44
$(\overline{BW})_A$ (deg)	15	1.2	-	-11
$(\overline{BW})_E$ (deg)	15	1.2	-	-11
τ (μs)	300	300	0	0
B (kHz)	6	6	0	0
$\overline{NF}$ (dB)	9	4.5	+4.5	+4.5
L_s (dB)	7	3.1	+3.9	+3.9
			+48.9	+26.9

Note: $(\overline{BW})_A$ = Azimuth Beamwidth

$(\overline{BW})_E$ = Elevation Beamwidth

TABLE 3-2

ESTIMATE OF SRI 30-MHz RADAR-AURORAL SIGNAL MAGNITUDE RELATIVE TO 401-MHz RADAR DATA

Auroral Scatterers-Antenna Beam Configuration	Normalized Auroral Signal Magnitude (30 MHz/401 MHz) (dB)	Radar Sensitivities (401 MHz/30 MHz) (dB)	Auroral Signal Magnitude (30 MHz/401 MHz) (dB)
Point Target	+28	+48.9	-20.9
Filled Beam	+6	+26.9	-20.9

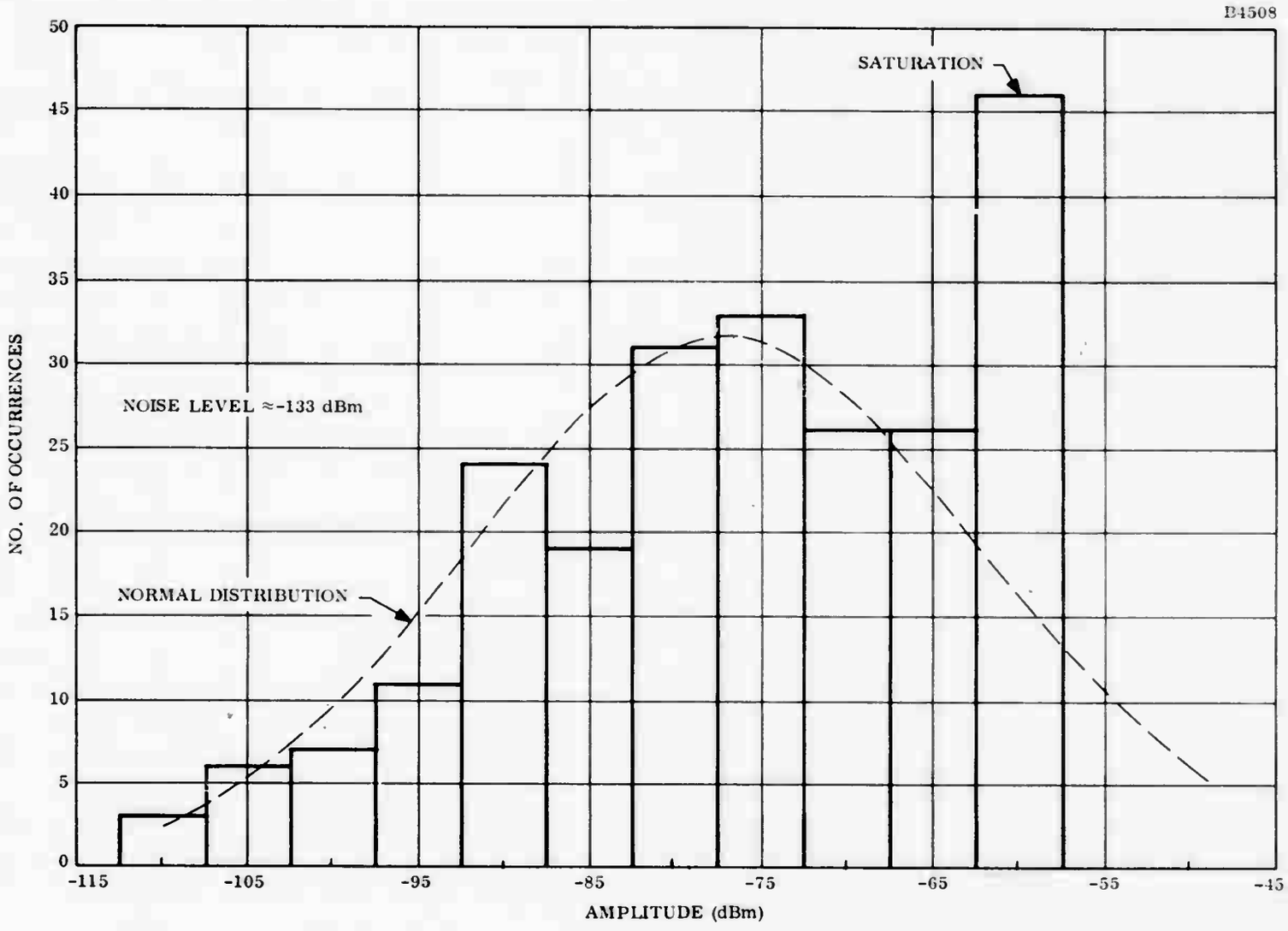

Figure 3-3. Amplitude Histogram of SRI 401-MHz Scotland Radar Aurora! Data (After Leadabrand, et al., 1965)

The histogram data, when replotted as a cumulative distribution on probability paper, shown in Figure 3-4, closely fit a straight line. This characteristic is indicative that the 401-MHz amplitudes are log-normally distributed. The theoretical normal distribution function plotted in Figure 3-3 was computed utilizing the value of -77.2 dBm for the mean as obtained from Figure 3-4.

It is assumed in this analysis that the 30-MHz amplitude data also followed a Gaussian distribution. Table 3-3 lists the statistical parameters of the 401-MHz distribution and the extrapolated 30-MHz distribution. The latter, which is also shown in Figure 3-4, was derived on the basis that the 30-MHz auroral echoes were 20.9 dB less than the 401-MHz results.

In estimating the magnitude of the auroral echoes that could be observed by an HF backscatter radar, it is necessary to compare the sensitivity of the HF backscatter radar to that of the SRI 30-MHz radar. According to Table 3-4, assuming a pulse length of 400 μs, the HF radar is 37.1 dB more sensitive than the SRI 30-MHz radar for the point target case and 33.5 dB more sensitive for the filled beam case. When the pulse length is decreased to 10 μs, the difference in sensitivities decreases to 21.1 dB and 1.5 dB for the point target and filled beam case, respectively.

The predicted HF backscatter radar-auroral clutter levels at 30 MHz are presented in Table 3-5. The calculations are based on combining the SRI 30 MHz radar-auroral data given in Table 3-3 with radar sensitivities in Table 3-4.

In deducing the radar-auroral signal levels at other frequencies in the HF band, it is assumed that the auroral echo power is frequency dependent according to the law

$$P = kf^{-n} \tag{3-8}$$

where k and n are constants. Utilizing the data in Figure 3-2, it can be shown that, for this power law, n = 2.5 for a point target and n = 0.5 for the filled beam case. However, an examination of other radar-auroral data taken by SRI at Scotland indicated a value of n = 6.8 for a point target and n = 2.7 for a filled beam (Leadabrand, et al., 1965).

An analysis of auroral echoes from simultaneous multiple frequency observations in Alaska by Leadabrand et al. (1967) revealed that n = 2 for frequencies between 50 and 850 MHz and n = 5 between 850 and 3000 MHz.

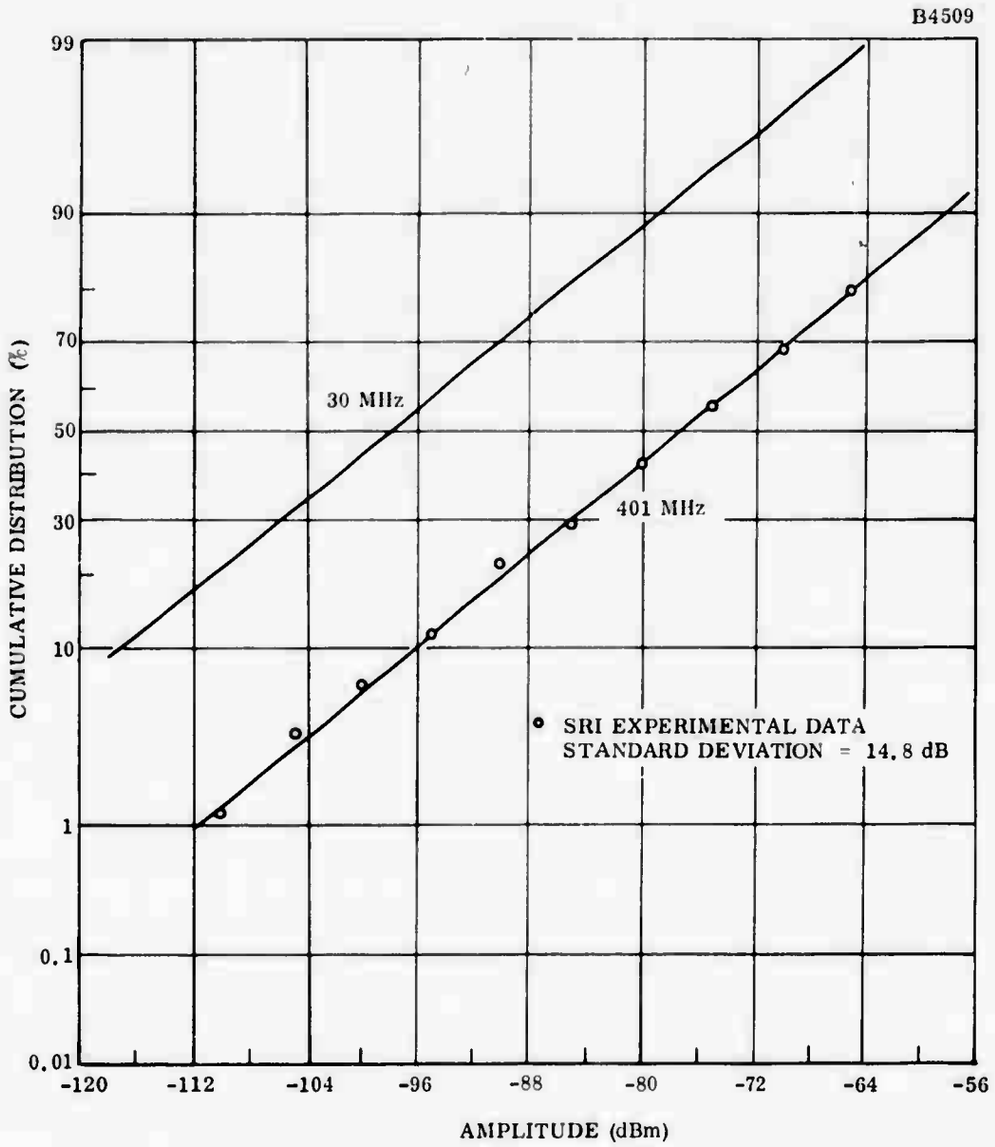

Figure 3-4. Cumulative Distribution Function of SRI Scotland Radar-Auroral Data

TABLE 3-3

STATISTICAL PARAMETERS OF SRI RADAR-AURORAL DATA

Statistical Parameter	401-MHz Data (dBm)	30-MHz Data (dBm)
Upper Decile	-58.2	-79.1
Upper Quartile	-67.2	-88.1
Median	-77.2	-98.1
Lower Quartile	-87.2	-108.1
Lower Decile	-96.2	-117.1
Standard Deviation	14.8	14.8

TABLE 3-4

COMPARISON OF HF BACKSCATTER RADAR SYSTEM SENSITIVITY TO THAT OF THE SRI-SCOTLAND 30-MHz RADAR

Parameter	HF Backscatter Radar	SRI-Scotland Radar	Point Target (HF Radar/SRI) (dB)	Scatterers Fill Antenna Beam (HF Radar/SRI) (dB)
λ^2 (m^2)	$(10.0)^2$	$(10.0)^2$	0	0
P_t (MW)	0.4	0.0015	+24.3	+ 4.3
$G_t G_r$ (dB)	45	40	+5	+5
$(\overline{BW})_A$ (deg)	5	15	-	-4.8
$(\overline{BW})_E$ (deg)	15	15	-	0
τ (μs)	400 10	300	-	+1.2 -14.8
B (kHz)	2.5 100	6	+3.8 -12.2	+3.8 -12.2
$\overline{NF}$ (dB)	9	9	0	0
L_s (dB)	3	7	+4	+4
			———	———
		(τ = 400 μs)	+37.1 dB	+33.5 dB
		(τ = 10 μs)	+21.1 dB	+1.5 dB

TABLE 3-5

ESTIMATE OF HF BACKSCATTER RADAR-AURORAL SIGNAL LEVELS AT 30 MHz BASED ON SRI DATA

Statistical Parameter	Point Target		Scatterers Fill Antenna Beam	
	τ = 400 μs (dBm)	τ = 10 μs (dBm)	τ = 400 μs (dBm)	τ = 10 μs (dBm)
Upper Decile	-42.0	-58.0	-45.6	-77.6
Upper Quartile	-51.0	-67.0	-54.6	-86.6
Median	-61.0	-77.0	-64.6	-96.6
Lower Quartile	-71.0	-87.0	-74.6	-106.6
Lower Decile	-80.0	-96.0	-83.6	-115.6
Standard Deviation	14.8	14.8	14.8	14.8

Radar backscatter measurements of artificial electron clouds in the E-region of the ionosphere by Gallagher and Barnes (1963) yielded a constant, n, of 4 for frequencies between approximately 20 and 50 MHz and -4 between 5 and 20 MHz. At times, however, it was found that the amplitude returns were insensitive to frequency in approximately the 10- to 20-MHz range.

From simultaneous auroral echo measurements at a frequency of 49.7, 143.5 and 226 MHz, Flood (1965) has deduced a value of n = 3.5 to 3.7 between 49.7 and 143.5 MHz and n = 6.5 ± 1.3 between 143.5 and 226 MHz. During periods of intense auroral reflections, there were instances when n = 12.9 ± 1.2 between 143.5 and 226 MHz.

Since there is wide discrepancy in the experimental measurements of the frequency dependence of auroral backscatter, which could be due to the characteristics of the auroral ionization, i.e., inhomogeneous distribution of auroral electrons, varying scale sizes of ionization irregularities and different scattering altitudes, a value of 4 for the exponent in Equation (3-8) is assumed in this analysis.

The estimated median auroral-echo amplitudes that could confront an HF backscatter radar in the 5- to 30-MHz band are plotted in Figure 3-5. The external noise level of a rural environment also shown in Figure 3-5 is the average median value in a 1-Hz bandwidth as predicted for a location in Maine for all seasons, all times of day and a sunspot number of 70. The more precise values of the external noise levels are given in Table 3-6. It is seen that the auroral echo amplitude increases with decreasing frequency and increasing pulse length and that the amplitude of the point target case is greater than that of the filled beam case.

Figure 3-6 is a replot of the data in Figure 3-5 in terms of the auroral SNR assuming a 1-Hz bandwidth. It is of interest to note that the SNR maximizes in the vicinity of 10 MHz. This is due to the fact that the external noise level increases with decreasing frequency.

The statistical estimates of the auroral SNR are listed in Table 3-7. It is seen that the quartile values are ±10 dB with respect to the median level while the decile values are ±19 dB. In other words, there is a 20-dB difference in the auroral clutter-to-noise ratio between the upper and lower quartiles and 38-dB difference between the upper and lower deciles.

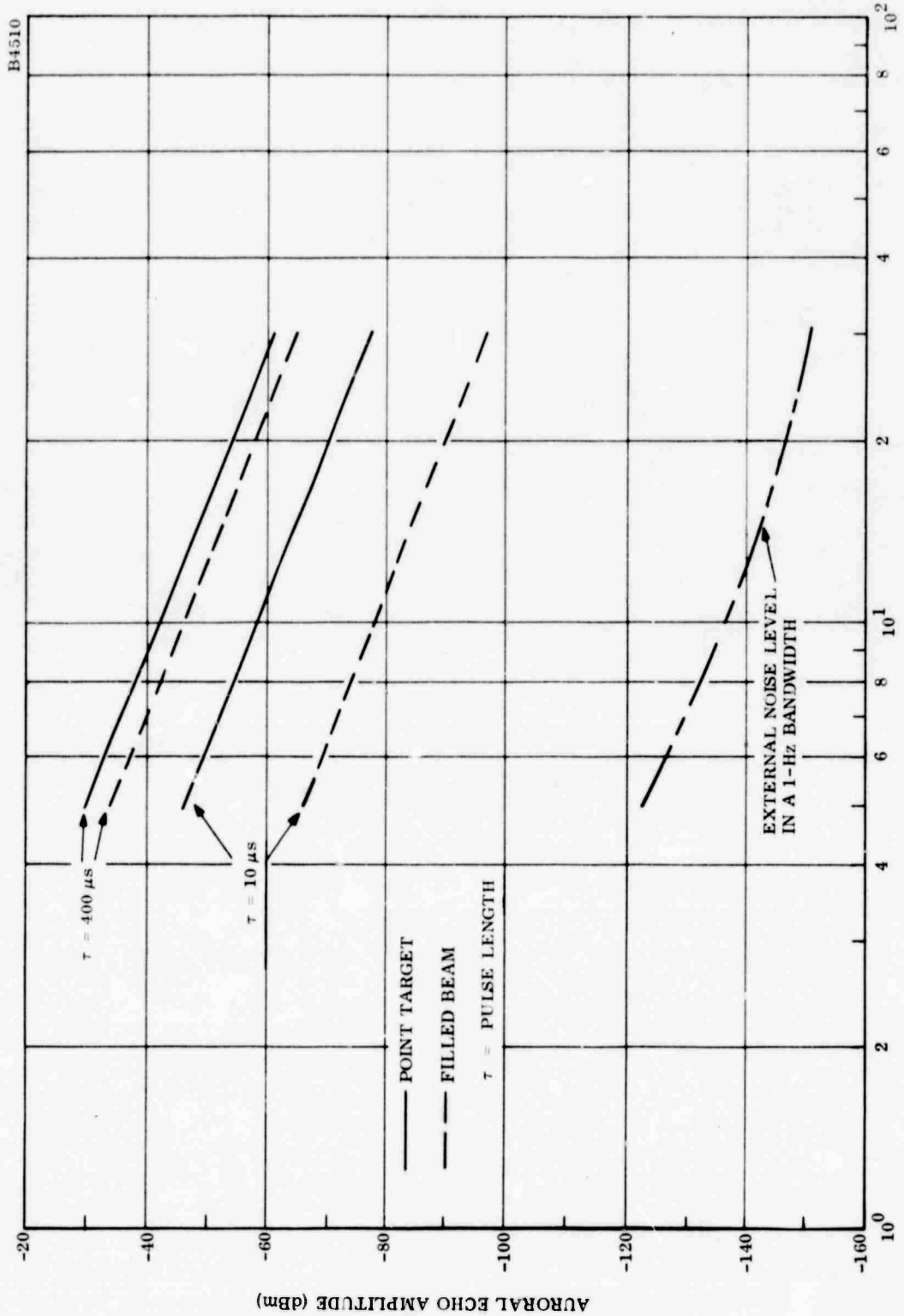

Figure 3-5. Estimated Median Radar-Auroral Signal Amplitude for an HF Backscatter Radar Based on SRI Scotland Radar Data

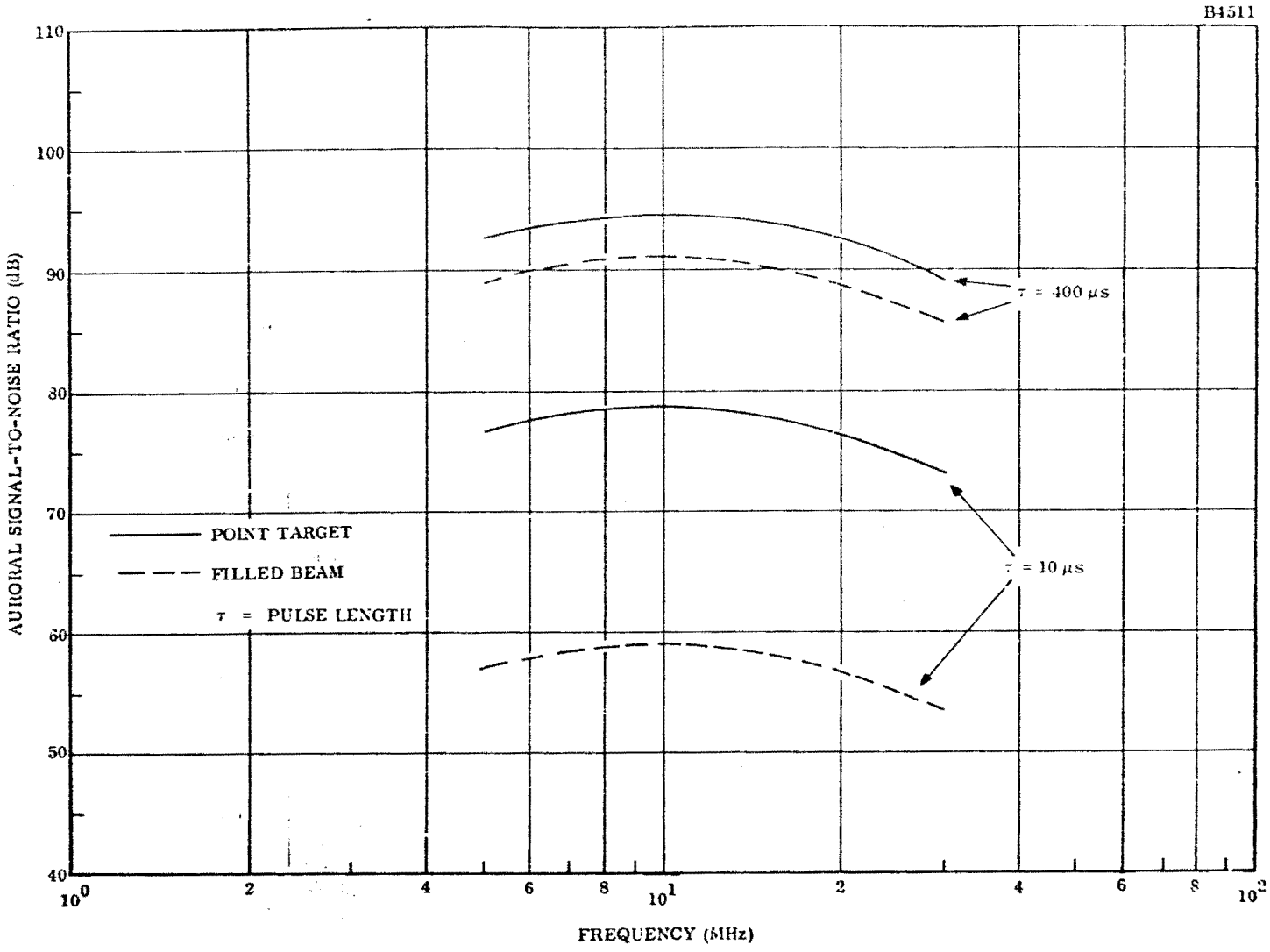

Figure 3-6. Estimated Median Radar-Auroral Signal-to-Noise Ratio for an HF Backscatter Radar Based on SRI Scotland Radar Data

TABLE 3-6

AVERAGE MEDIAN VALUES OF EXTERNAL NOISE (RURAL ENVIRONMENT) AS A FUNCTION OF MEDIAN MAXIMUM USABLE FREQUENCY AS PREDICTED FOR MAINE FOR ALL SEASONS, TIMES OF DAY AND SSN OF 70

Maximum Usable Frequency (MHz)	Median Noise (dBm/Hz)
5	-122.6
10	-136.8
15	-142.6
20	-146.5
25	-148.5
30	-150.3

TABLE 3-7

ESTIMATE OF HF BACKSCATTER RADAR E-LAYER AURORAL SNR
BASED ON SRI DATA

Freq (MHz)	Target Configuration	Pulse Length (μs)	Upper Decile (dB)	Upper Quartile (dB)	Median (dB)	Lower Quartile (dB)	Lower Decile (dB)
5	PT	400	111.7	102.7	92.7	82.7	73.7
		10	95.7	86.7	76.7	66.7	57.7
	FB	400	108.1	99.1	89.1	79.1	70.1
		10	76.1	67.1	57.1	47.1	38.1
10	PT	400	113.9	104.9	94.9	84.9	75.9
		10	97.9	88.9	78.9	68.9	59.9
	FB	400	110.3	101.3	91.3	81.3	72.3
		10	78.3	69.3	59.3	49.3	40.3
15	PT	400	112.6	103.6	93.6	83.6	74.6
		10	96.6	87.6	77.6	67.6	58.6
	FB	400	109.0	100.0	90.0	80.0	71.0
		10	77.0	68.0	58.0	48.0	39.0
20	PT	400	111.5	102.5	92.5	82.5	73.5
		10	95.5	86.5	76.5	66.5	57.5
	FB	400	107.9	98.9	88.9	78.9	69.9
		10	75.9	66.9	56.9	46.9	37.9
25	PT	400	109.7	100.7	90.7	80.7	71.7
		10	93.7	84.7	74.7	64.7	55.7
	FB	400	106.1	97.1	87.1	77.1	68.1
		10	74.1	65.1	55.1	45.1	36.1
30	PT	400	108.3	99.3	89.3	79.3	70.3
		10	92.3	83.3	73.3	63.3	54.3
	FB	400	104.7	95.7	85.7	75.7	66.7
		10	72.7	63.7	53.7	43.7	34.7

PT = Point Target
FB = Filled Beam

Standard Deviation = 14.8 dB

The auroral SNR's presented in Table 3-8 are the averages of the filled beam and the point target echo data of Table 3-7. The interesting point to note in Table 3-8 is that the averaging manipulation does not alter the value of the differences between the magnitudes of the statistical parameters.

It should be noted that the height distribution of the auroral echoes observed by SRI in Scotland were peaked at about 100 to 120 km, i.e., in the E-region, although heights as great as 200 km were observed. Thus, the estimates given in Tables 3-7 and 3-8 can be considered to apply only to E-region reflections.

An additional item which should be mentioned is that the amplitude distribution of the 401-MHz auroral echoes, shown in Figure 3-3, which was used as a basis of extrapolation to the HF backscatter radar, was applicable to data obtained when the direction of propagation at the reflection point was perpendicular to the magnetic field lines. When the angle between the directions of propagation and magnetic field lines are not orthogonal, the auroral clutter amplitude should decrease.

Bates and Albee (1969) report that, if a simple model of auroral backscatter from the E-region that includes ionospheric refraction effects is assumed, a lower limit of 6 dB/deg in the 15- to 50-MHz range was observed for the aspect-sensitive decrease in backscatter cross section with off-perpendicular angle from the geomagnetic field.

The aspect-sensitive decrease of the cross section of F-layer backscatter echoes was found by Bates and Albee (1970) to be on the order of 5 dB/deg of off-perpendicularity from the magnetic field in the 6- to 15-MHz band.

The results of aspect sensitivity measurements made in the frequency range from HF to UHF are summarized in Table 3-9.

3.4 POLAR FOX II E-LAYER AURORAL AND F-LAYER DATA

An objective of the Polar Fox II program was to investigate the characteristics of HF ionospheric backscatter echoes. The experimental measurements were conducted at Caribou, Maine, during the period between December 1971 and November 1972. Ionospheric observations were made at five frequencies in the HF band. However, in this analysis, only the echo data recorded at 8.125 and 14.875 MHz in January 1972 (Bradley, et al., 1972) and in July 1972 (Herman and Vargas-Vila, 1973) are examined.

TABLE 3-8

ESTIMATE OF HF BACKSCATTER RADAR-AVERAGE E-LAYER AURORAL SNR BASED ON SRI DATA

Frequency (MHz)	Pulse Length (μs)	Upper Decile (dB)	Upper Quartile (dB)	Median (dB)	Lower Quartile (dB)	Lower Decile (dB)
5	400	111.0	102.0	92.0	82.0	73.0
	10	95.0	86.0	76.0	66.0	57.0
10	400	113.2	104.2	94.2	84.2	75.2
	10	97.2	88.2	78.2	68.2	59.2
15	400	111.9	102.9	92.9	82.9	73.9
	10	95.9	86.9	76.9	66.9	57.9
20	400	110.8	101.8	91.8	81.8	72.8
	10	94.8	85.8	75.8	65.8	56.8
25	400	109.0	100.0	90.0	80.0	71.0
	10	93.0	84.0	74.0	64.0	55.0
30	400	107.6	98.6	88.6	78.6	69.6
	10	91.6	82.6	72.6	62.6	53.6

TABLE 3-9

ASPECT SENSITIVITY MEASUREMENTS

Frequency (MHz)	Aspect Sensitivity (dB/deg)	Aspect Angle Interval (deg)	Location	Investigator
6-15	5	$0 \leq \Delta\theta \leq 5$	College, Alaska	Bates and Albee, 1970
15-50	>6	$0 \leq \Delta\theta \leq 4$	College, Alaska	Bates and Albee, 1969
30	2	$0 \leq \Delta\theta \leq 7$	Fraserburgh, Scotland	Leadabrand et al., 1965
401, 800	10	$0 \leq \Delta\theta \leq 7$		
48	2	$4.5 \leq \Delta\theta \leq 19.5$	Baker Lake and Saskatoon, Canada	McDiarmid, 1972
48.5	1	$1° \leq \Delta\theta \leq 19°$	Baker Lake, Ottawa, Resolute and Saskatoon, Canada	McNamara, 1972
50, 139, 398, 850, 1210, 3000	10	$0 \leq \Delta\theta \leq 2$	Homer, Alaska	Chesnut et al., 1968
448	5	$4.5 \leq \Delta\theta \leq 7.5$	Prince Albert, Canada	Jaye et al., 1967
501	10	$0 \leq \Delta\theta \leq 2$	Manchester, England	Barber et al., 1962

Figures 3-7 and 3-8 are plots of the diurnal variation of the area scattering coefficient of E-layer and F-layer echoes, respectively. The latter can be considered to originate at an altitude of approximately 300 km while the former at an altitude of about 100 km. The data are averaged over the azimuthal extent of the radar, i.e., -30° to +60° measured with respect to geographic north. For simplicity in data analysis, the azimuthal spread was divided into 5 zones of -30° to -12° (zone 1), -12° to +6° (zone 2), +6° to +24° (zone 3), +24° to +42° (zone 4) and +42° to +60° (zone 5).

It should be noted that the data in Figures 3-7 and 3-8 describe the median and the lower and upper quartile values and that the propagation losses, L_p, have not been removed from the calculation of the area scattering coefficient, σ_A. In other words, the vertical axis is, in reality, the term, σ_A/L_p.

It is apparent that the signals from both E- and F-layer irregularities show a slight decrease in the median value of the scattering coefficient during the nighttime hours. However, in the case of the 8.125-MHz F-layer clutter, the median scattering coefficient remains relatively constant at approximately -30 dBsm/m^2 during the nighttime and decreases to about -40 dBsm/m^2 during the early hours of the morning. In addition, it is seen that, at a given time, the median value of scattering coeficient at 14.875 MHz is less than that at 8.125 MHz irrespective of the altitude of the scattering irregularities.

The zonal variation of the area scattering coefficient of the E- and F-layer irregularities are presented in Tables 3-10 and 3-11, respectively. It is seen that, for all the statistical parameters, the 8.125-MHz data are from 12 to 21 dB greater than the 14.875-MHz results. The most interesting feature of the data is the lack of influence of the geographic locations of the scatterers on the magnitude of the scattering coefficient. By intuition, it would seem that the scattering coefficient would be greater in zone 1 or 2 than in zone 4 or 5, since the former are the regions encompassed by the auroral belt (Feldstein and Starkov, 1967).

Table 3-12 illustrates the difference between the F-layer scattering coefficient, $(\sigma_A)_F$, and the E-layer coefficient, $(\sigma_A)_E$, shown in Tables 3-10 and 3-11, respectively. It is interesting to note that, except for 8.125-MHz upper quartile results, the F-layer area scattering coefficient is on the order of 17 to 20 dB greater than the E-layer coefficient, irrespective of the transmission frequency.

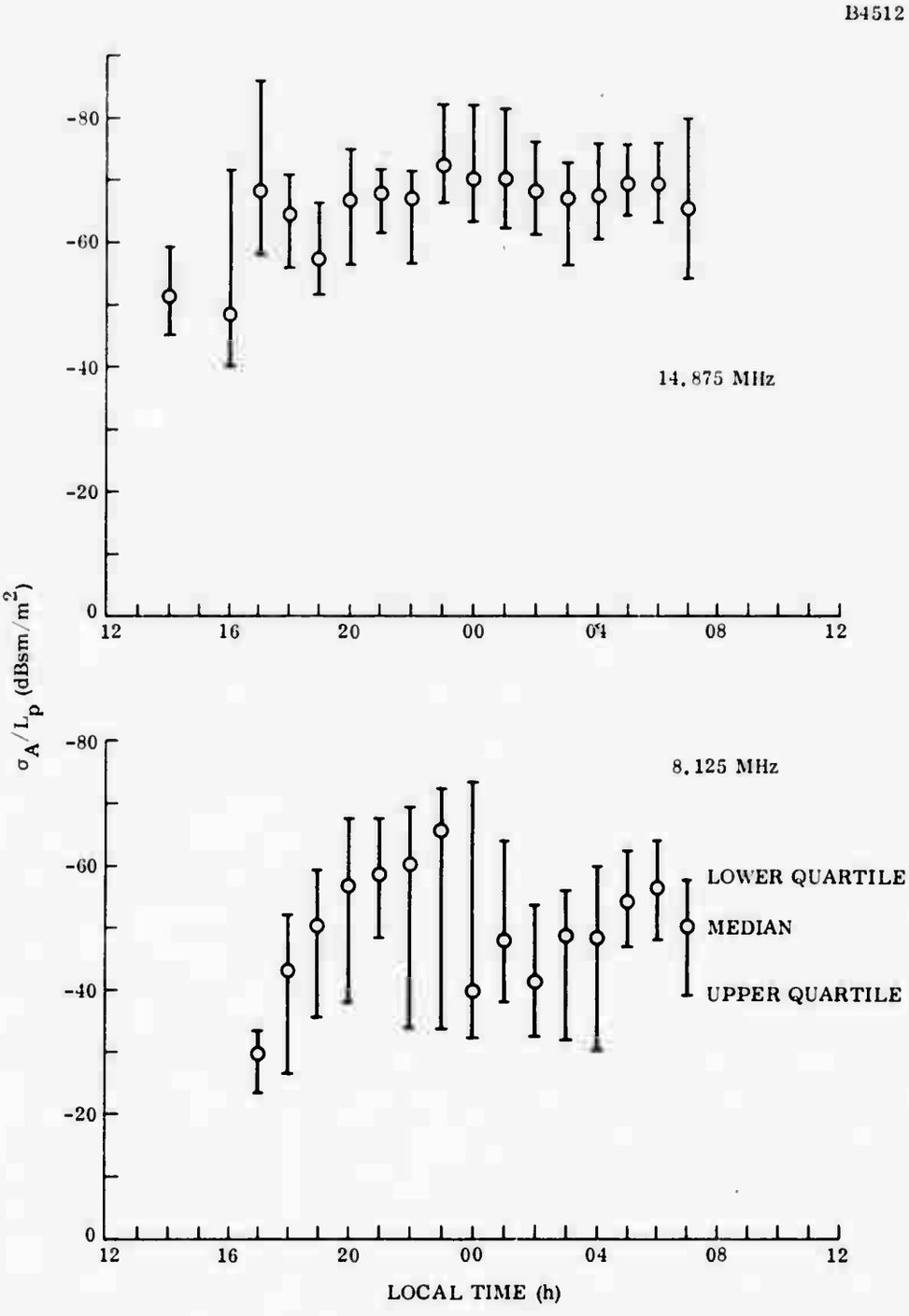

Figure 3-7. Diurnal Variation of Area Scattering Coefficient of Polar Fox II E-Layer Irregularities Averaged over Five Zones at a Frequency of 8.125 and 14.875 MHz, January 1972 (after Bradley et al., 1972)

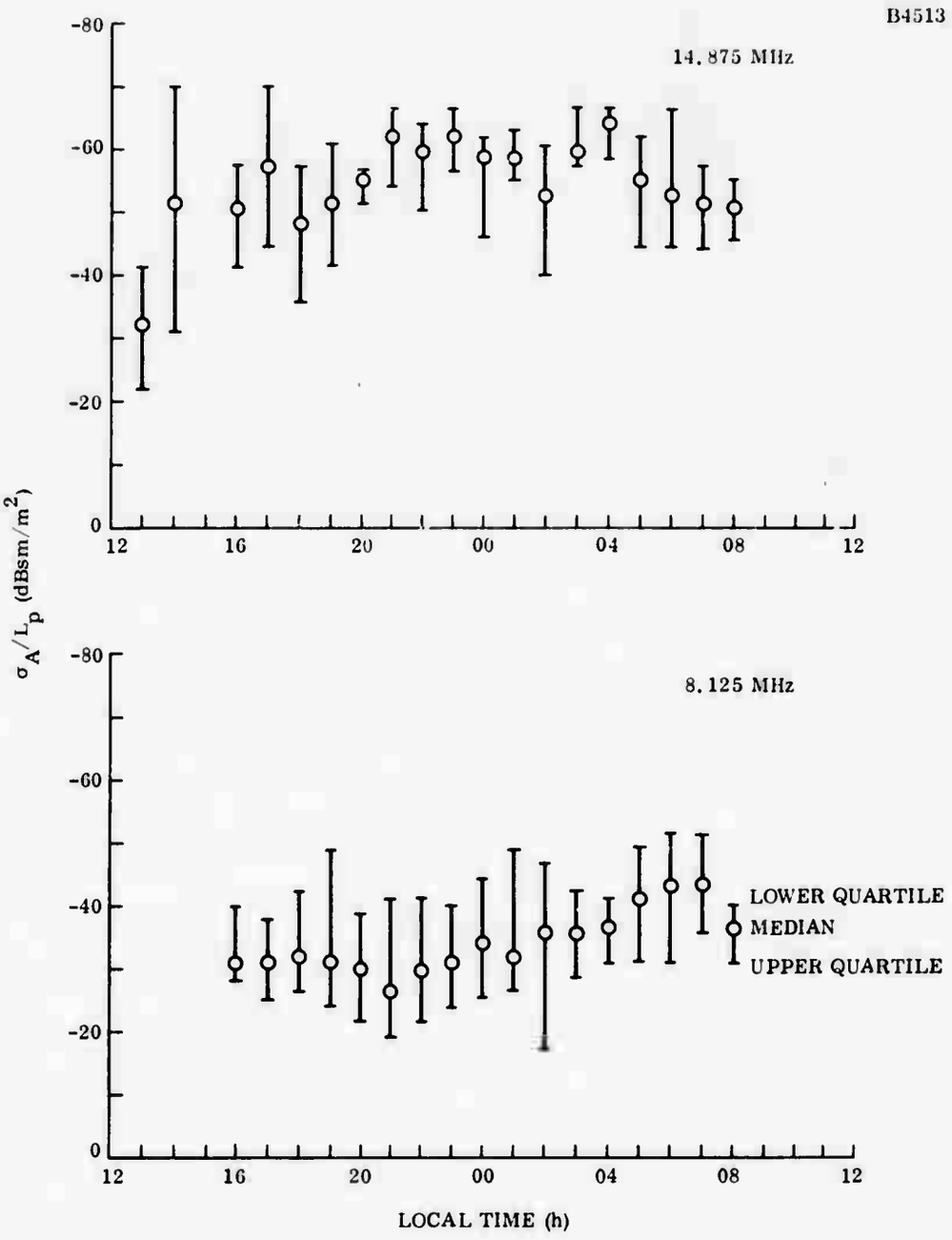

Figure 3-8. Diurnal Variation of Area Scattering Coefficient of Polar Fox II F-Layer Irregularities Averaged over Five Zones at a Frequency of 8.125 and 14.875 MHz, January 1972 (after Bradley et al., 1972)

TABLE 3-10

ZONAL VARIATION OF AREA SCATTERING COEFFICIENT OF E-LAYER IRREGULARITIES AVERAGED OVER TIME AT A FREQUENCY OF 8.125 AND 14.875 MHz, JANUARY 1972

Frequency (MHz)	Statistical Parameter	Area Scattering Coefficient ($dBsm/m^2$)					
		Zone					
		1	2	3	4	5	Average
8.125	Upper Quartile	-36.9	-35.8	-37.5	-38.2	-32.5	-34.2
	Median	-48.2	-48.2	-51.6	-52.6	-46.0	-47.6
	Lower Quartile	-63.0	-58.8	-62.9	-62.9	-56.9	-58.6
14.875	Upper Quartile	-59.2	-58.4	-57.0	-59.1	-54.9	-56.5
	Median	-65.0	-66.2	-66.2	-68.1	-62.2	-63.9
	Lower Quartile	-75.4	-72.6	-74.2	-76.6	-74.3	-74.0

Note: Propagation losses not removed from area scattering coefficient.

TABLE 3-11

ZONAL VARIATION OF AREA SCATTERING COEFFICIENT OF F-LAYER IRREGULARITIES AVERAGED OVER TIME AT A FREQUENCY OF 8.125 AND 14.875 MHz, JANUARY 1972

Frequency (MHz)	Statistical Parameter	Area Scattering Coefficient ($dBsm/m^2$)					
		Zone					
		1	2	3	4	5	Average
8.125	Upper Quartile	-28.4	-25.8	-26.8	-28.3	-30.0	-27.2
	Median	-33.5	-32.2	-33.2	-34.8	-36.6	-33.6
	Lower Quartile	-42.9	-40.5	-42.1	-45.7	-46.2	-42.0
14.875	Upper Quartile	-41.3	-39.3	-42.8	-40.8	-35.3	-37.1
	Median	-49.7	-50.2	-53.4	-50.1	-45.4	-47.2
	Lower Quartile	-56.7	-59.8	-62.2	-63.0	-52.5	-54.3

Note: Propagation losses not removed from area scattering coefficient.

TABLE 3-12

DIFFERENCE BETWEEN AREA SCATTERING COEFFICIENTS OF F-LAYER AND E-LAYER IRREGULARITIES AT A FREQUENCY OF 8.125 MHz AND 14.875 MHz, JANUARY 1972

Frequency (MHz)	Statistical Parameter	$(\sigma_A)_F - (\sigma_A)_E$ (dB)					
		Zone					
		1	2	3	4	5	Average
8.125	Upper Quartile	8.5	10.0	10.7	9.9	2.5	9.6
	Median	14.7	16.0	18.4	17.8	9.4	17.1
	Lower Quartile	20.1	18.3	20.8	17.2	10.7	19.5
14.875	Upper Quartile	17.9	19.1	14.2	18.3	19.6	18.5
	Median	15.3	16.0	12.8	18.0	16.8	16.6
	Lower Quartile	18.7	12.8	12.0	13.6	21.8	20.1

Note: Propagation losses not removed from area scattering coefficients.

The conversion of the area scattering coefficient into a radar cross section can be accomplished utilizing Equations (3-2), (3-3) and (3-4). It is evident that the radar cross section, σ, is related to the volume scattering coefficient, σ_v, by

$$\sigma = \sigma_v R \beta_H \frac{c\tau}{2} \Delta h \tag{3-9}$$

Since the thickness of the scatterers in the vertical direction, Δh, was an unknown factor in the Polar Fox II experiment, it was assumed to be unity (1 m). Thus, Equation (3-9) can be described in terms of the area scattering coefficient, σ_A, by

$$\sigma = \sigma_A A = \sigma_A R \beta_H \frac{c\tau}{2} \tag{3-10}$$

where A is the area containing the scatterers.

The scattering area of the HF backscatter radar is depicted in Figure 3-9 as a function of range for the two pulse lengths.

The cross sections of ionospheric backscatter echoes that could be observed by the HF backscatter radar are presented in Table 3-13. The calculations are derived utilizing the data in Tables 3-4, 3-11 and 3-12 and assuming a radar range of 700 km for the E-layer irregularities and 1500 km for the F-layer irregularities. These ranges correspond to a ray path oriented at an elevation angle of 5° and intersecting the ionosphere at an altitude of approximately 100 and 300 km, respectively. For this configuration, the E-layer scattering area evaluates to a 95.6 dBsm and 79.6 dBsm for a pulse length of 400 and 10 μs, respectively. For the corresponding pulse lengths, the F-layer scattering area is 99.0 dBsm and 82.9 dBsm. It is seen that, except for the upper quartile 8.125-MHz results, the F-layer cross section is about 17 to 20 dB greater than the E-layer at 8.125 MHz and 20 to 23 dB at 14.875 MHz. The difference between the F-layer and E-layer cross sections are most likely due to the fact that the F-layer scatterers cover a wider spatial extent than the E-layer scatterers.

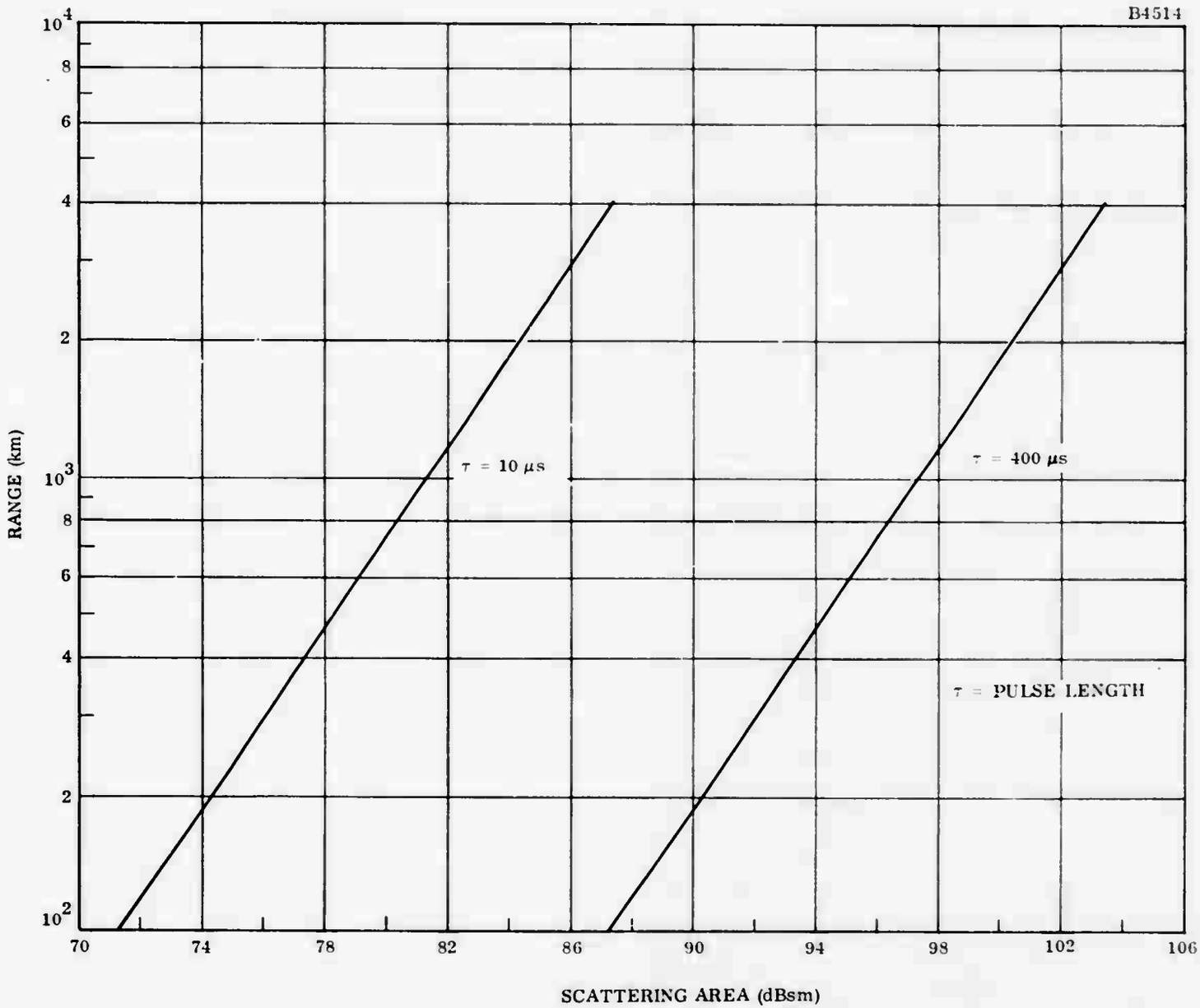

Figure 3-9. HF Backscatter Radar-Auroral Scattering Area as a Function of Range

TABLE 3-13

HF BACKSCATTER RADAR - ESTIMATED AVERAGE CROSS-SECTION OF E-LAYER AND F-LAYER IRREGULARITIES BASED ON POLAR FOX II DATA, JANUARY 1972

Frequency (MHz	Pulse Length (μs)	Statistical Parameter	Average Cross Section (dBsm)		Cross Section Ratio (dB) F-Layer/E-Layer
			E-Layer	F-Layer	
8.125	400	Upper Quartile	61.2	71.8	10.6
		Median	48.0	65.4	17.4
		Lower Quartile	37.0	57.0	20.0
	10	Upper Quartile	45.4	55.7	10.3
		Median	32.0	49.3	17.3
		Lower Quartile	21.0	40.9	19.9
14.875	400	Upper Quartile	39.1	61.9	22.8
		Median	31.7	51.8	20.1
		Lower Quartile	21.6	44.7	23.1
	10	Upper Quartile	23.1	45.8	22.7
		Median	15.7	35.7	20.0
		Lower Quartile	5.6	28.6	23.0

Note: Propagation losses not removed from average cross section.

Figures 3-10 and 3-11 are histograms of the mean cross section per Hz Doppler bandwidth of ionospheric backscatter echoes deduced from Polar Fox II measurements made at a frequency of 8.125 and 14.875 MHz, respectively, in July 1972 between 2000 and 0300 hours local time. The data which were supplied by the Lincoln Laboratory for incorporation in a report by Herman and Vargas-Vila (1973) are based on the assumption that the echoes originated from a point source. It should be noted that the ionospheric loss term has not been removed from the calculations. The data are applicable to reflections obtained in the azimuth interval from -30° to 7° and range interval from 624 to 2199 km. In addition, the data contain various modes of propagation such as slant-F, direct-F, 1-hop F-layer plus slant and direct F, direct-E and single-hop E-layer returns.

The theoretical normal distribution curve also plotted in Figures 3-10 and 3-11 were derived utilizing the statistical parameters of the experimental data as specified by Herman and Vargas-Vila (1973). At 8.125 MHz, the mean of the distribution, μ = 63.3 dBsm/Hz and the standard deviation, σ = 10.0 dBsm/Hz while, at 14.875 MHz, μ = 36.7 dBsm/Hz and σ = 15.0 dBsm/Hz.

Evidence that the 8.125- and 14.875-MHz cross section data are approximately log-normally distributed is presented in Figures 3-12 and 3-13. As illustrated in Figure 3-4, a similar distribution is obtained for the amplitudes of the 401-MHz E-layer reflections observed by SRI in Scotland.

According to Pollon (1970), no satisfactory physical mechanism for the occurrence of log-normally distributed scattering has as yet been found.

The statistical parameters of the radar cross section listed in Table 3-14 are obtained from the cumulative distribution functions presented in Figures 3-12 and 3-13. The difference between the median and the standard deviation deduced by this analysis and by Herman and Vargas-Vila (1973) is due to the fact that the exact values of Herman's and Vargas-Vila's experimentally derived radar cross sections, shown in Figures 3-10 and 3-11, were not available.

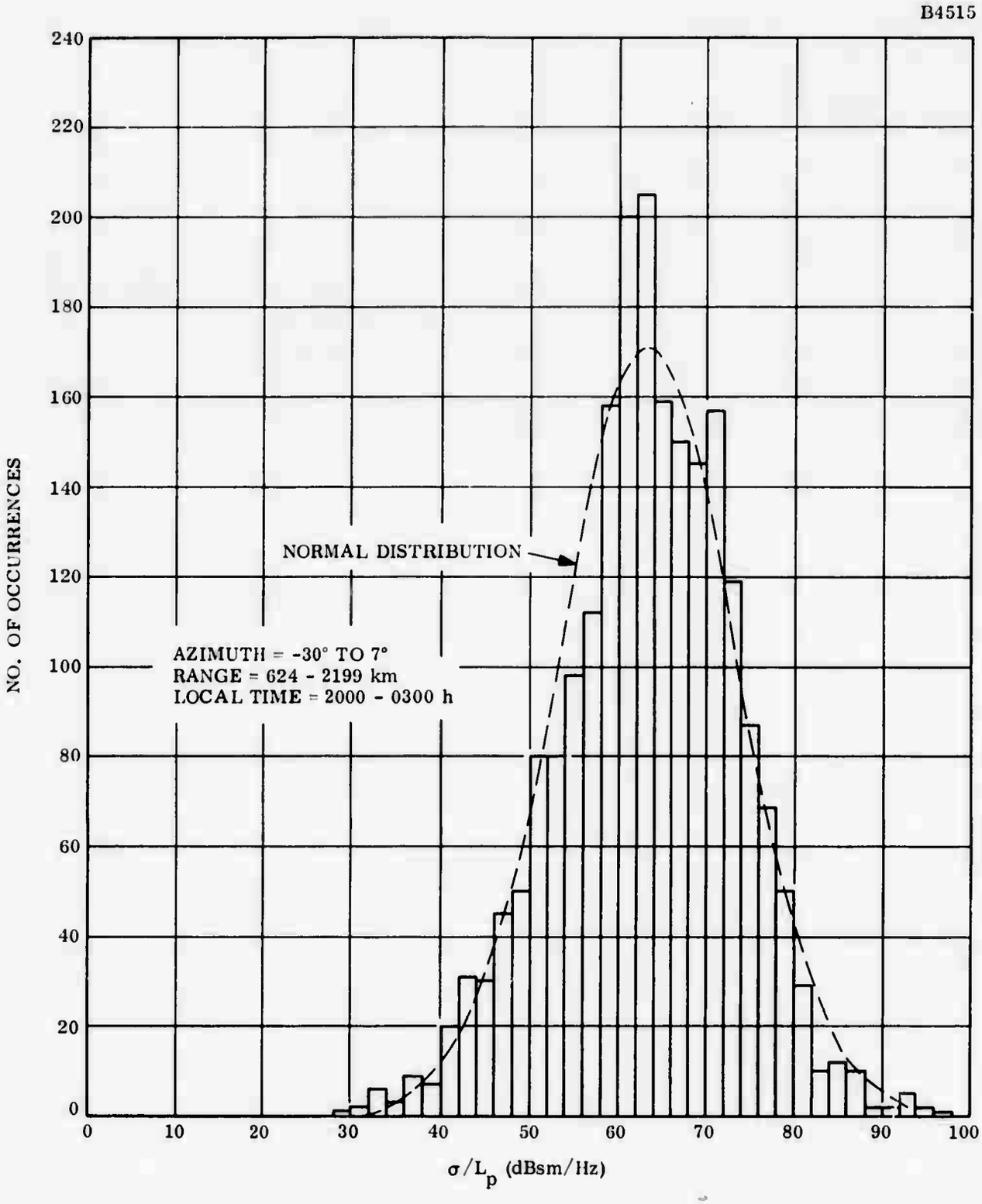

Figure 3-10. Radar Cross Section of Polar Fox II Ionospheric Echoes Recorded at a Frequency of 8.125 MHz, July 1972 (after Herman and Vargas-Vila, 1973)

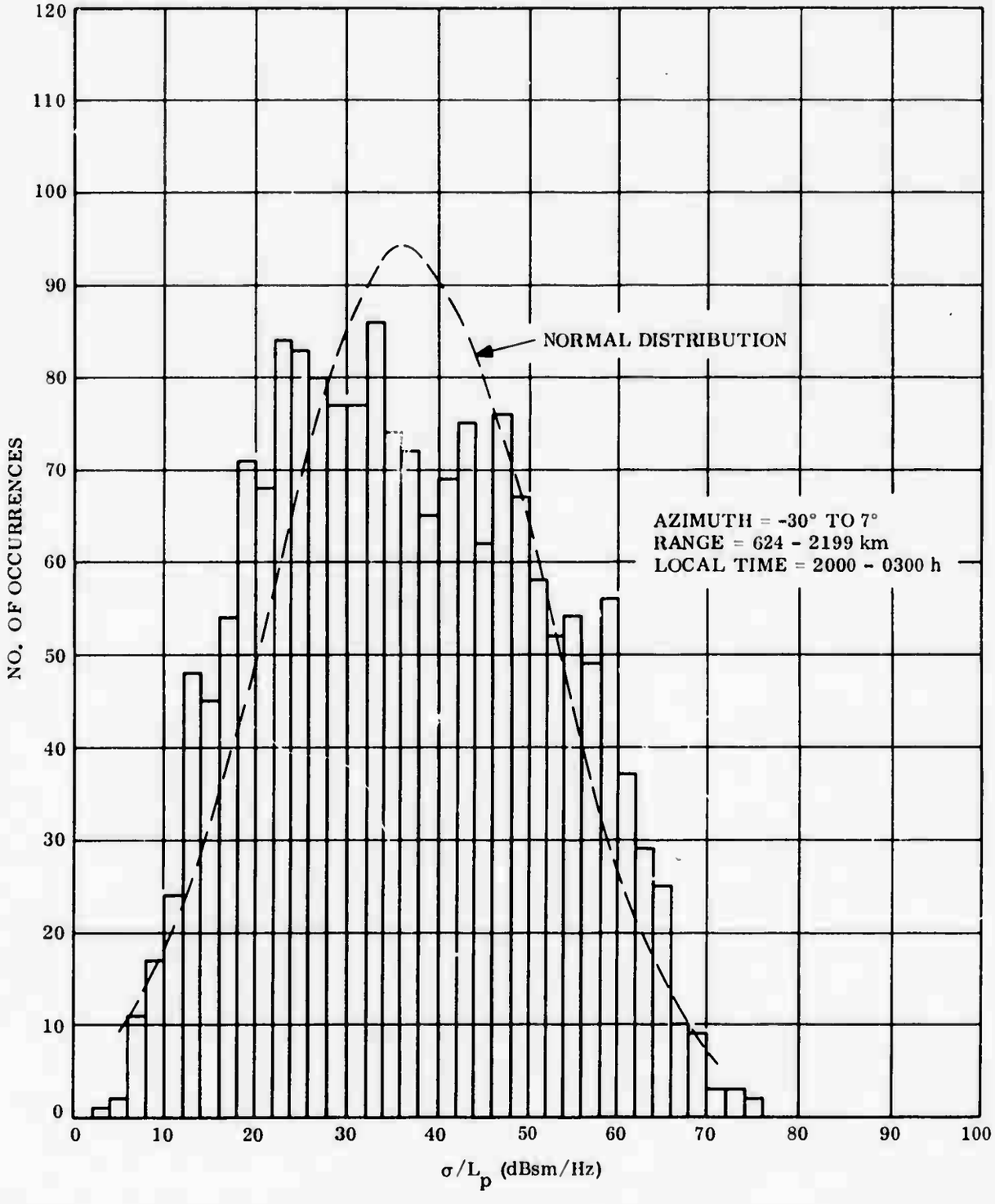

Figure 3-11. Radar Cross Section of Polar Fox II Ionospheric Echoes Recorded at a Frequency of 14.875 MHz, July 1972 (after Herman and Vargas-Vila, 1973)

TABLE 3-14

RADAR CROSS SECTION OF FIELD-ALIGNED IONIZATION FOR THE AZIMUTH INTERVAL FROM -30° TO 7° AND RANGE INTERVAL FROM 624 TO 2199 km, JULY 1972, 2000 TO 0300 HOURS LOCAL TIME

Statistical Parameter	Radar Cross Section (dBsm/Hz)			
	8.125 MHz		14.875 MHz	
	GE Analysis	Herman and Vargas-Vila Analysis	GE Analysis	Herman and Vargas-Vila Analysis
Upper Decile	74.5	-	56.9	-
Upper Quartile	69.2	-	47.3	-
Median	62.3	63.4	34.6	35.6
Lower Quartile	56.4	-	23.5	-
Lower Decile	49.3	-	16.1	-
Standard Deviation	9.8	10.0	16.8	15.0
Mean	-	63.3	-	36.7

Note: Propagation losses not removed from radar cross section.

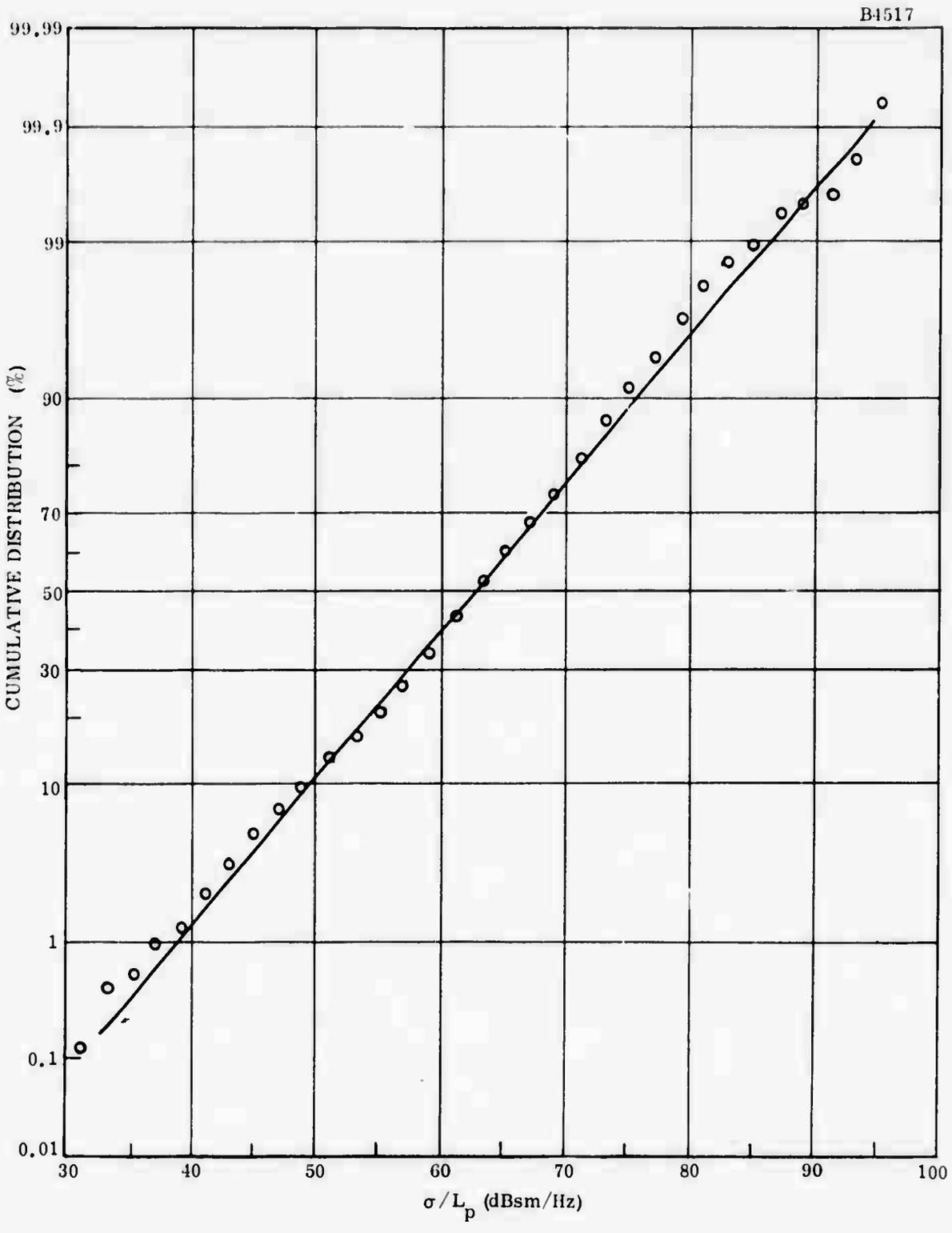

Figure 3-12. Cumulative Distribution Function of Radar Cross Section of Polar Fox II Ionospheric Echoes Recorded at a Frequency of 8.125 MHz, July 1972

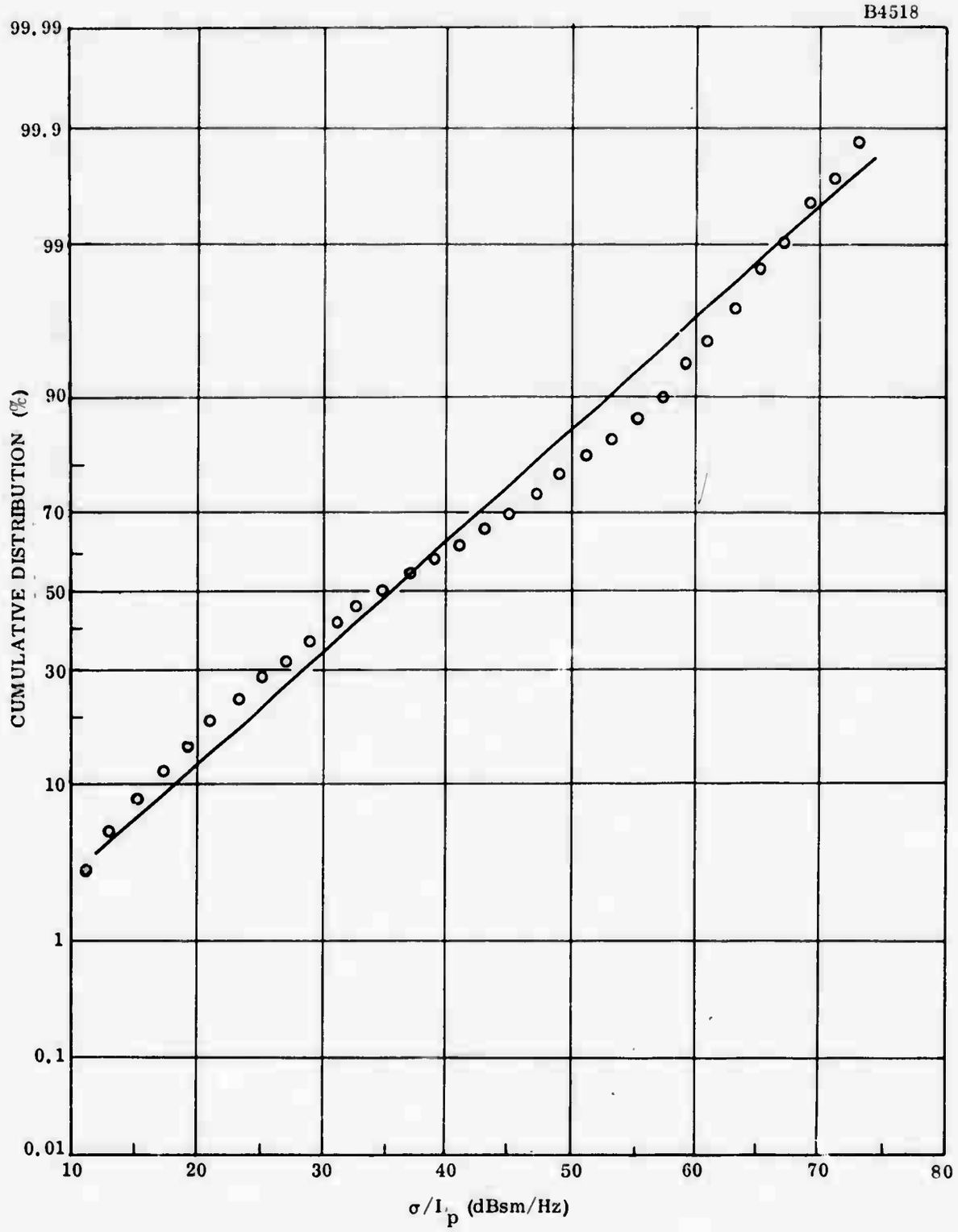

Figure 3-13. Cumulative Distribution Function of Radar Cross Section of Polar Fox II Ionospheric Echoes Recorded at a Frequency of 14.375 MHz, July 1972

It is of interest to note the independency of radar cross section with azimuthal orientation and range was found to exist in the July 1972 ionospheric echo data (Herman and Vargas-Vila, 1973). As shown in Tables 3-10 and 3-11, the January 1972 data also disclosed the azimuthal independency.

It is reiterated that the Polar Fox II estimates of the E- and F-layer scattering coefficients, Tables 3-10 and 3-11, and radar cross sections, Table 3-14, contain the propagation loss terms, i.e., the ionospheric propagation losses have not been removed from the calculations. Because of this, it is not possible to use the Polar Fox II ionospheric backscatter echo data for extrapolation to other frequencies in the HF band.

SECTION IV

DOPPLER FREQUENCY SPECTRUM OF IONOSPHERIC BACKSCATTER ECHOES

The Doppler spectrum of radar pulses reflected from the aurora differs from that of the original pulse. The changes that can take place are: (1) the center frequency can be shifted; and (2) the spectral width can be increased.

The shift in the center frequency corresponds to a drift motion of the auroral ionization. Radar-auroral data indicate an east-west drift before magnetic midnight and a west-east drift after magnetic midnight (Leadabrand, et al., 1965). Drift velocities of the order of 500 m/s are typical. According to the analysis of E-layer radar-auroral echoes recorded in Scotland at a frequency of 401 MHz, the maximum Doppler shift is normally ±2.15 kHz (Larson and Hodges, 1967).

The spread in the Doppler spectrum is due to the random, turbulent motion of the irregularities of electron density in the auroral ionization. Figure 4-1 which is the Doppler frequency spectrum obtained by averaging over 17 consecutive pulses (Leadabrand, et al., 1965) gives evidence that the auroral spectrum is significantly broadened compared to the transmitted pulse spectrum. According to Larson and Hodges (1967), the maximum Doppler frequency spread at 401 MHz is on the order of 1.90 kHz at -6 dB below the peak, 4.00 kHz at -12 dB and 4.75 kHz at -18 dB.

The expected (one standard deviation) of Doppler frequency shift and spread at HF are presented in Figure 4-2. The estimates are based on the fact that the Doppler frequency variations are directly proportional to frequency and on the assumption that shifts and spreads are normally distributed. Thus, the maximum shift and spread are equivalent to the 3-sigma (standard deviation) value of the distribution. At 10 MHz, the Doppler frequency shift evaluates to ±18 Hz and the Doppler frequency spread becomes 16 Hz at the -6 dB level, 33 Hz at -12 dB and 40 Hz at -18 dB.

The estimates of E-layer HF radar-auroral total Doppler frequency deviation are plotted in Figure 4-3. At 10 MHz, it is possible that the 1-sigma value of the total Doppler deviation could be on the order of ±26 Hz at the -6 dB level, ±35 Hz at -12 dB and ±38 Hz at -18 dB.

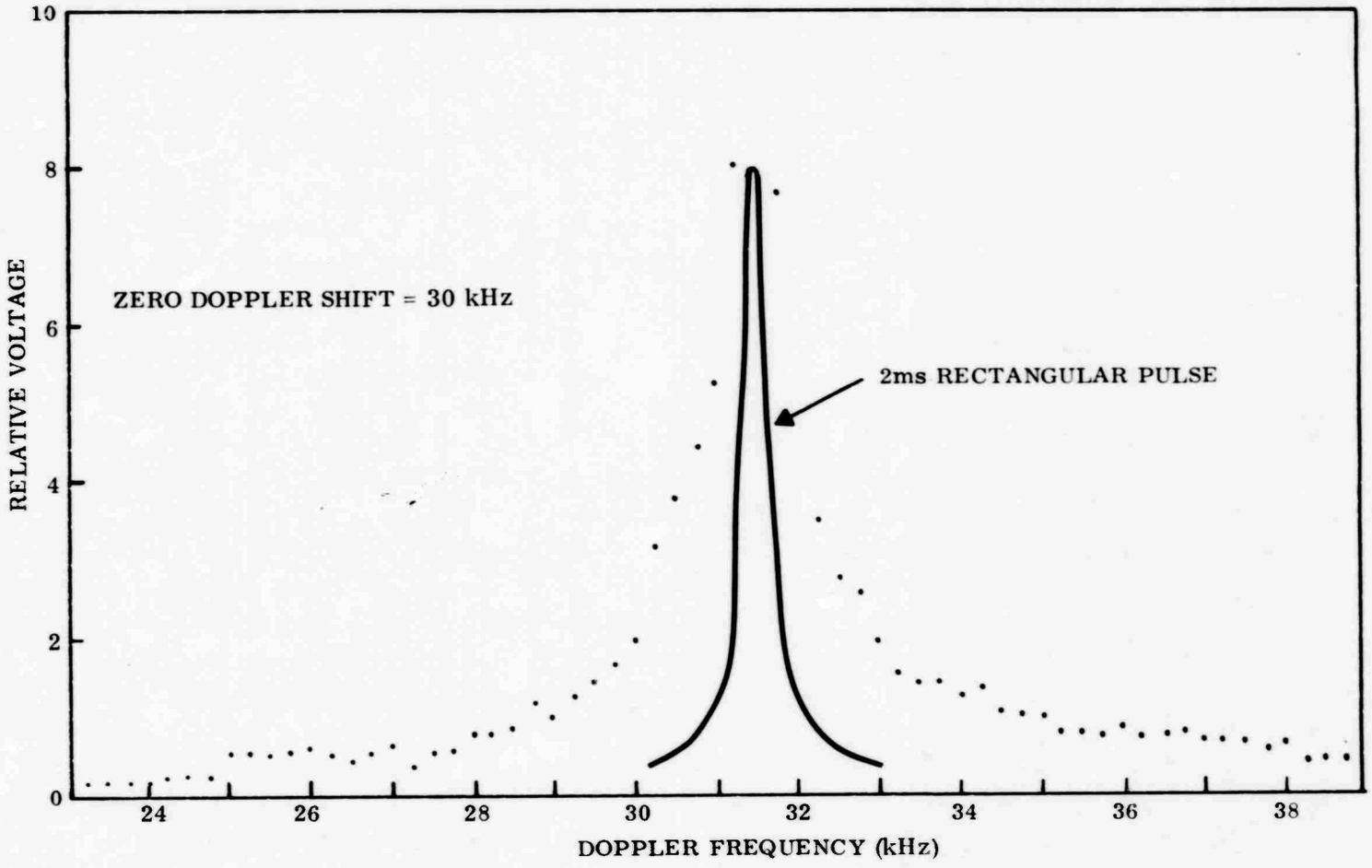

Figure 4-1. Average Spectrum of 17 Pulses from SRI-Scotland 401-MHz Radar Data (after Leadabrand, et al., 1965)

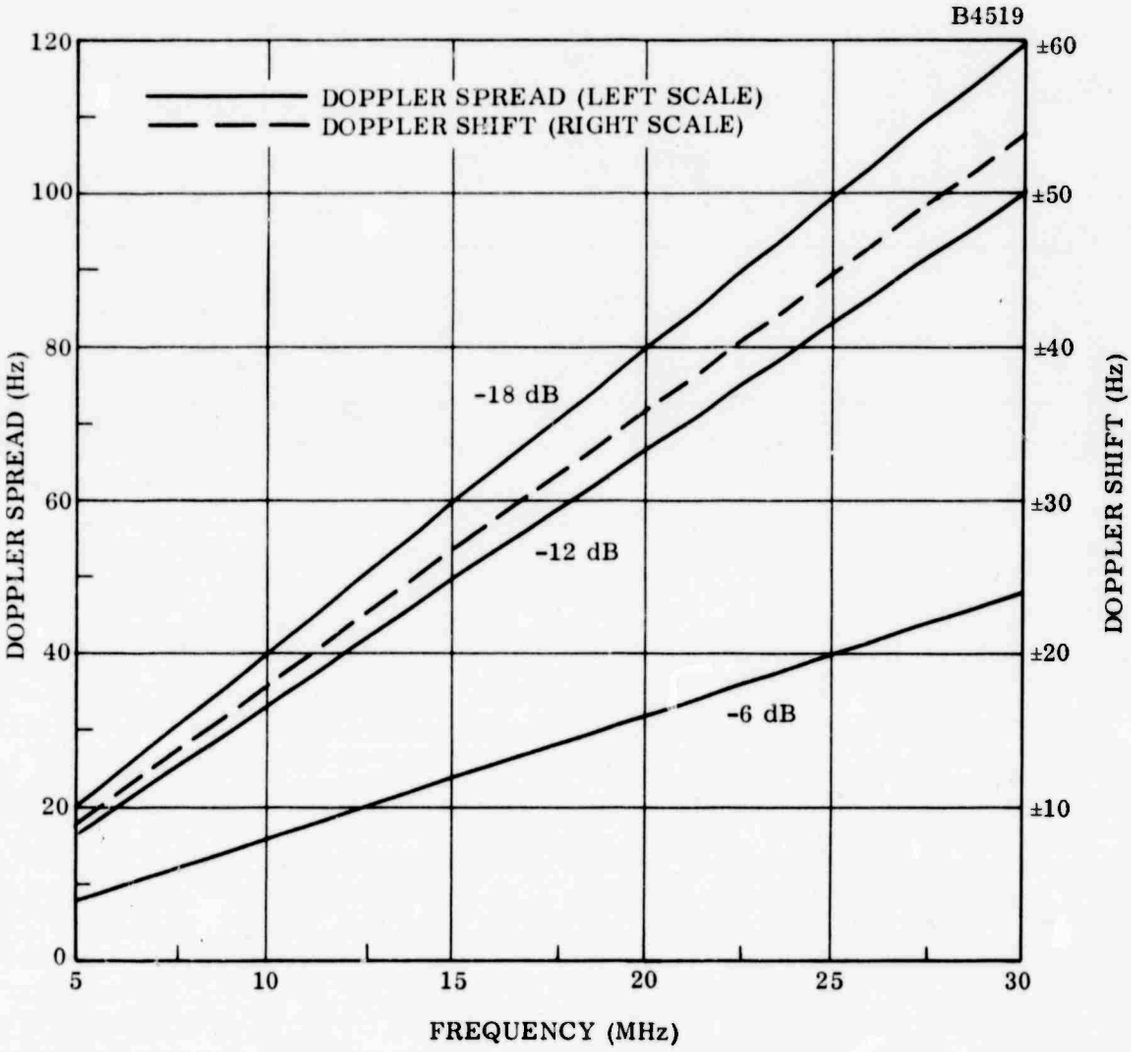

Figure 4-2. Estimate of E-Layer HF Radar-Auroral Doppler Frequency Spread and Shift Based on SRI-Scotland Measurements at 401 MHz

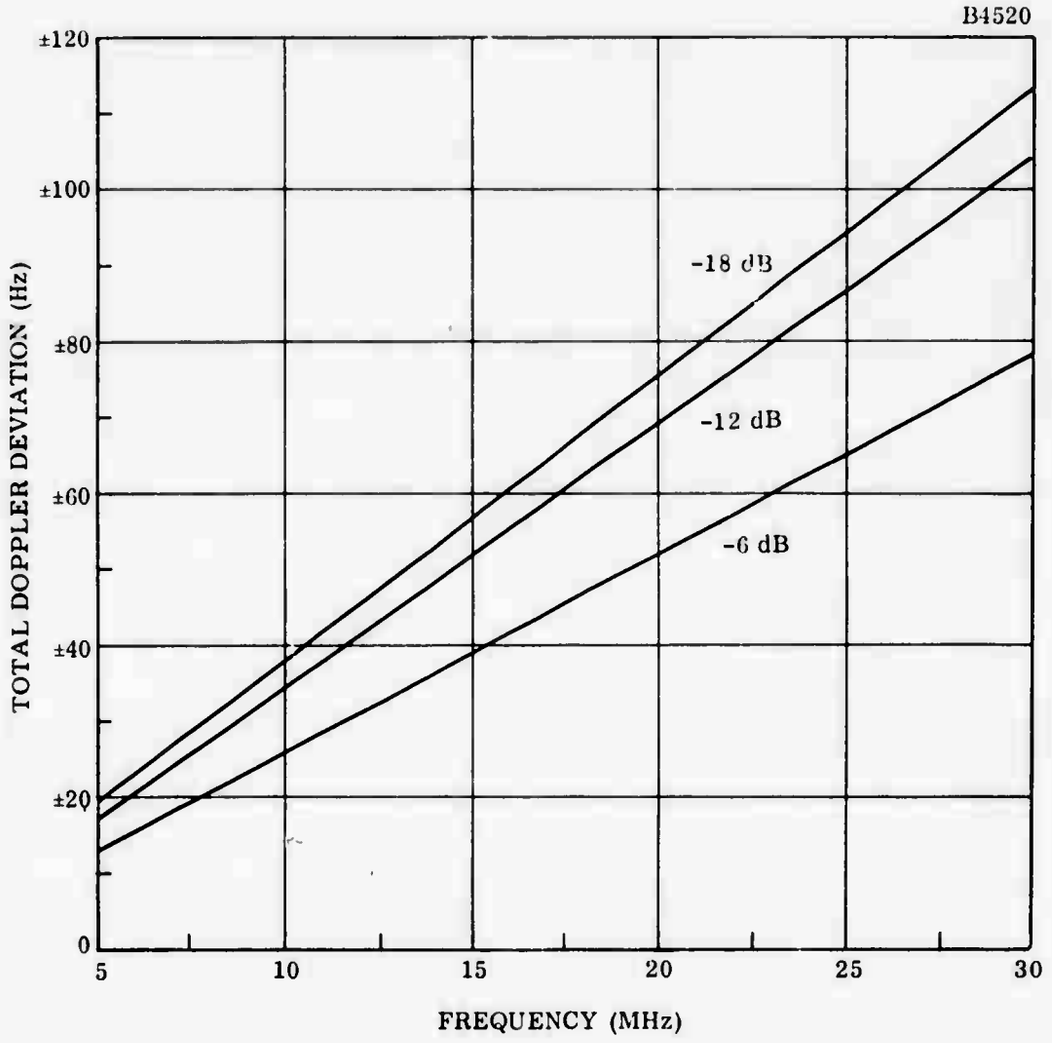

Figure 4-3. Estimate of E-Layer HF Radar-Auroral Total Doppler Frequency Deviation Based on SRI-Scotland Measurements at 401 MHz

E-layer radar-auroral echoes, having radial velocities as high as 1450 m/s, have been observed at 17 MHz by Brooks (1966). This corresponds to a Doppler frequency shift (f_d) of 164.3 Hz which is derived from the expression

$$f_d = -\frac{2V}{\lambda} \tag{4-1}$$

where V is the radial velocity and λ is transmitted wavelength.

The measurements of the spectral characteristics of F-layer irregularities made under the Polar Fox II program reveal that the spectrum is somewhat flat over the ±15 Hz Doppler bandwidth at frequencies up to and including 19.25 MHz (Campbell, et al., 1972).

The maximum radial velocity of F-region field-aligned irregularities detected at 17.3 MHz (Baggaley, 1970) was found to be on the order of 165 m/s with a mean of 65 m/s. In terms of the Doppler frequency shift, these velocities evaluate to 19.0 and 7.5 Hz, respectively.

SECTION V

FREQUENCY OF OCCURRENCE OF IONOSPHERIC BACKSCATTER ECHOES AND CORRELATION WITH SOLAR-GEOPHYSICAL CONDITIONS

The experimental observations of field-aligned echoes at 19.4 MHz conducted over a three-year period (1961-1963) at a site located in the vicinity of Boston disclosed that the echoes were present for as long as 11 h/day (Malik and Aarons, 1964). Although a seasonal pattern was clearly defined, there appeared to be a tendency for the reflections to occur on a greater number of days during the summer than during the winter. The correlation of echo activity with sunspot number was found to exist. For example, in 1961 when the sunspot number was 53, echoes appeared on 73% of the days at an average of 3.0 h/day. In 1963 when the sunspot number was 28, 55% of the echoes appeared at an average of 1.5 h/day. Maximum echo activity occurred between 1800 and 2000 h local time.

A more thorough analysis of the 19.4 MHz field-aligned echoes recorded over a period from 1961 through 1965 has been performed by the Air Force Cambridge Research Laboratories (AFCRL) (Basu et al., 1973, 1974). It was found that, under quiet magnetic conditions, field-aligned E-layer echoes showed a summer evening maximum and appeared to be associated with the ground-backscatter echoes from sporadic E (Basu, et al., 1973). A weak secondary maximum existed in the winter with no detectable field-aligned echoes during the daytime. During disturbed magnetic conditions, the field-aligned E-layer echoes increased with magnetic activity and appeared during the daytime with a corresponding decrease in sporadic E. The data did not reveal a seasonal dependence.

Under quiet magnetic conditions, the field-aligned F-layer echoes were found to be a sunset phenomenon and correlated with the sunspot cycle (Basu, et al., 1974). In general, the echoes occurred in the range interval from 1050 to 1500 km. However, during the daytime, long range echoes, at times, were observed at ranges of 3000 to 3300 km. An interesting disclosure was the fact that the occurrence of the F-layer field-aligned echoes increased directly with the increase in magnetic activity until the level K_{Fr} (Fredericksburg, Maryland, three-hourly K index) attained a value of four. Beyond this level, there was a decrease in the occurrence of the F-layer echoes with no echoes being observed when $K_{Fr} \geq 7$. Radar auroral measurements made at Stanford University at a frequency of 17.3 MHz reveal that maximum auroral activity occurred between 1900 and 0400 hours local time (Peterson et al., 1955).

According to the HF radar echo observations conducted at 12 and 18 MHz at Pullman, Washington, there was a pronounced peak in the frequency of occurrence of the echoes from field-aligned irregularities near the time of local sunset (Hower, et al., 1966). The characteristics of the echoes detected at sunset were different from those occurring at night. It was found that the local sunset echoes appeared at ranges of about 2000 km and were generally spread in range (diffuse). The occurrence of the sunset echoes was relatively independent of magnetic activity. The nighttime echoes, on the other hand, appeared at ranges of about 1000 km and tended to display little spread in range (discrete). The occurrence of nighttime echoes was highly dependent on magnetic activity.

Hower, et al., (1966) noted a decreasing echo activity with solar cycle, the maximum percentage occurrences during the nighttime being approximately 80% in December 1958, 37% in December 1963 and 35% in March 1964. The (Zurich) relative sunspot number during the corresponding period was 185.2, 11.8 and 14.5, respectively.

Hower and Makhijani (1969) have concluded that HF F-layer backscatter echoes arise from the same general irregularity regions in which spread-F is detected.

Sprenger and Glöde (1964) have reported that the diurnal variation of the frequency of occurrence of radar-auroral echoes recorded from late 1958 to mid 1962 at 33 MHz at Kuhlungsborn (geographic coordinates: 54°N, 12°E; geomagnetic latitude: 54°N) showed a double-maximum at approximately 0100 and 1700 hours local time. The probability of occurrence of E-layer auroral echoes was found to be a function of magnetic activity. No auroral echoes were observed at a magnetic index, $Kp < 5$ and 100% occurrence at $Kp = 9$. With regard to the correlation of auroral echo activity with sunspot cycle, Sprenger and Glöde (1964) have concluded that the maximum of auroral activity occurred in 1960 about two years after the sunspot maximum and that the activity decreased to zero within a period of only one and a half years.

Brooks' (1965, 1966) investigation of radar-auroral echoes at 17 MHz conducted in the 1959-1960 period indicated that, for the discrete echoes, the maximum number appeared between 0000-0300 hours local time and, for the diffuse echoes, between 1900-2100 hours local time.

A maximum of occurrence of backscatter echoes at 13.866 MHz from the F-region on 75% of the nights for March 1958 was reported by Weaver (1965). A minimum number of echoes were observed in June, the data being collected during 1957 and 1958 at Ithaca, New York, with the antenna beam oriented in a northward direction.

Backscatter observations of F-region field-aligned irregularities made at 17 MHz near Sheffield, England (geographic coordinates: 53.43°N, 1.58°W; geomagnetic latitude: 56.4°N) between mid-October, 1964, and mid-January, 1966, (Baggaley, 1970) which was a period of low sunspot activity, showed that, on the average, the echoes were present on 23.3% of the days while only 1.5% of the total observing time was occupied by the echoes. A summer maximum and a winter minimum were found to exist. This seasonal variation correlates with Malik's and Aarons' (1964) results.

With regard to the temporal variation, Baggaley (1970) noted that there was a correlation between the onset of F-layer echoes and the solar zenith angle at the reflection point in the F-layer (assuming a height of 300 km). That is, a maximum number of echoes occurred at a solar zenith angle of 90-95°, and a minimum at angles less than 85° and greater than 125°. In addition, no correlation was found to exist between F-layer echo occurrence and magnetic activity. Of the total time for which F-layer echo activity was present, only 11% was associated with magnetic index $Kp \geq 4$.

Field-aligned echoes from the F-region observed at Brisbane, Australia, at 16 MHz occurred preferentially during geomagnetic disturbances and correlated strongly with spread-F and radio star scintillations occurring in the same region of the ionosphere (Swenson, 1972).

An analysis of 29-MHz backscatter measurements carried out in Northern (West) Germany and Scandanavia (geomagnetic latitudes of 55-77°N) by Czechowsky, et al. (1974) confirmed the close correlation between radio-auroral occurrence and geomagnetic activity. Most of the radio auroras appeared in the afternoon and evening hours.

The Polar Fox II HF-ionospheric backscatter measurements revealed that, in the summertime, the echoes appeared most often at night and at the shorter ranges. During the wintertime, the long range echoes appeared most often during the daytime while the short range echoes were equally present during the day and night. The maximum number of echoes appeared in the northerly direction. The echoes would appear at a given range at one frequency and not at another (Edwards, et al., 1973).

Table 5-1 summarizes the experimental results of the characteristics of HF ionospheric backscatter echoes and their correlation with solar-geophysical conditions.

TABLE 5-1

EXPERIMENTAL OBSERVATIONS OF HF IONOSPHERIC BACKSCATTER ECHOES

Frequency (MHz)	Max. Backscatter Activity	Solar Cycle Correlation			Magnetic Activity Correlation	Location	Investigator
8-19	Night - Summer Day and Night - Winter					Caribou, Maine (47°N, 68°W)	Edwards et al. (1973)
12, 18	Local Sunset	Date	SSN	Nights With Echoes	Sunset Echoes (Diffuse) - Not Correlated Nighttime Echoes (Discrete) - Correlated	Pullman, Washington (Geomagnetic, 53.5°N)	Hower et al. (1966)
		12/58 12/63 3/64	185.2 11.8 14.5	80% 37% 35%			
13.9	Max. - 3/58 (Night) Min - 6/58					Ithaca, New York (42.4°N, 76.5°W)	Weaver (1965)
16					F-layer Echoes - Correlated	Brisbane, Australia (27.53°S, 152.92°E) (Geomagnetic, 35.8°S)	Swenson (1972)
17	0000-0300 LT (Discrete) 1900-2100 LT (Diffuse)					Sheffield, England (53.43°N, 1.58°W) (Geomagnetic, 56.4°N)	Brooks (1965, 1966)
17	Max. - Summer Min - Winter	Days - 23.3% With Echoes (1.5% Observing Time)			F-layer Echoes - Not Correlated	Sheffield, England	Baggaley (1970)
17.3	1900-0400 LT					Stanford, California (Geomagnetic, 43.7°N)	Peterson et al. (1955)
19.4	1800-2000 LT	Date	SSN	Days With Echoes	Correlation Evident	Plum Island, Mass. (42.63°N, 70.32°W) (Geomagnetic, 54°N)	Malik and Aarons (1964)
		1961 1963	53 28	73% 55%			
19.4	2000-0300 LT (Summer)				E-layer Echoes - Correlated	Plum Island, Mass.	Basu et al. (1973)
19.4	Local Sunset				Sunset F-layer Echoes (Diffuse) - Not Correlated Nighttime F-layer Echoes (Discrete) - Correlated	Plum Island, Mass.	Basu et al. (1974)
29	Afternoon and Evening				Correlation Evident	Scandanavia and West Germany (Geomagnetic, 55°-70°N)	Czechowsky et al. (1974)
33	0100 and 1700 LT	E-layer Auroral Activity Max. - 1960 Min - 1961-1962			No E-layer Echoes, Kp < 5 100% Occurrence, Kp = 9	Kühlungsborn, East Germany (54°N, 12°E) (Geomagnetic, 54°N)	Sprenger and Glöde (1964)

LT = Local Time

SECTION VI

CONCLUSIONS

The spatial distribution of HF radar-ionospheric backscatter echoes can be readily determined utilizing the concept that the reflections originate in regions of space where the direction of propagation is near perpendicular to the direction of the lines of force of the earth's magnetic field, and where high auroral activity and ionospheric irregularities are encountered.

It is estimated that, for a midlatitude location, HF E-layer auroral echoes should be nonexistent during the daytime while, during the evening for quiet magnetic conditions (Q = 1), E-layer echoes could appear between the azimuths of -39° and +19° and between the ranges of 560 and 780 nmi. Under severe magnetic conditions (Q = 7), the azimuthal and range extents could increase to -62° to +20° and 150 to 780 nmi, respectively.

F-layer echoes can be expected to be observed, during both the daytime and nighttime, out to ranges on the order of 1250 nmi, while the azimuthal extent of the F-layer reflections could cover the entire region between -90° to +90°.

In the frequency range between 5-30 MHz, the median E-layer radar-auroral SNR deduced from UHF radar-auroral data acquired by SRI at Scotland, could vary between 88-94 dB and 72-78 dB for a pulse length of 400 and 10 μs, respectively, with the maximum occurring at 10 MHz. The quartile values of the E-layer SNR are ±10 dB with respect to the median level while the decile values are ±19 dB.

An analysis of the HF ionospheric backscatter data obtained in Maine under the Polar Fox II program reveals that, except for the upper quartile 8.125-MHz results, the F-layer cross section could be 17-20 dB greater than the E-layer cross section at 8.125 MHz and 20-23 dB at 14.875 MHz.

It is found that the amplitude of E-layer auroral echoes and the cross section of E- and F-layer reflections are log-normally distributed.

Extrapolating from the SRI-Scotland UHF radar-auroral data, it found that, for 5 MHz radar transmissions reflected from E-layer auroral ionization, the 1-sigma value of the total Doppler frequency deviation, i.e., Doppler frequency shift and spread, could be on the order of ±13 Hz at the -6 dB normalized signal level, ±17 Hz at -12 dB and ±19 Hz at -18 dB. At 30 MHz, the 1-sigma Doppler deviation should increase to approximately ±78 Hz, ±105 Hz and ±114 Hz, respectively.

Based on the Polar Fox II HF ionospheric measurements, the Doppler frequency spectrum of field-aligned F-layer backscatter appears to be flat over the ±15 Hz bandwidth up to a frequency of 19.25 MHz.

The frequency of occurrence of HF field-aligned backscatter echoes maximizes, for the most part, near local sunset. However, experimental observations have shown, at times, peak activity near the midnight hours.

There is a strong correlation of backscatter echoes with the solar cycle. That is, the percentage of days displaying backscatter reflections decrease with decreasing sunspot number.

The characteristics of sunset echoes are found to be different from those occurring during the night. The sunset echoes are generally of the diffuse type and are independent of magnetic activity which the nighttime echoes are discrete and correlate with magnetic activity.

SECTION VII

REFERENCES

Aarons, J., "Total Electron Contact and Scintillation Studies of the Ionosphere," AGARDograph No. 166, pp 83-84, March 1973a.

Aarons, J., "A Descriptive Model of F-Layer High-Latitude Irregularities as Shown by Scintillation Observations," Journal of Geophysical Research, Vol. 78, pp 7441-7450, November 1, 1973b.

Abel, W. G. and R. E. Newell, "Measurements of the Afternoon Radio Aurora at 1295 MHz," Journal of Geophysical Research, Vol. 74, pp 231-245, January 1, 1969.

Au, W. W. L. and G. L. Hower, "Multi-Station Observations of Long-Range Backscatter from Field-Aligned Irregularities in the F-Layer," Journal of Atmospheric and Terrestrial Physics, Vol. 32, pp 1577-1589, 1970.

Baggaley, W. J. "Backscatter Observations of F-region Field-Aligned Irregularities During the I.Q.S.Y.," Journal of Geophysical Research, Vol. 75, pp 152-158, January 1, 1970.

Barber, D., H. K. Sutcliffe and C. D. Watkins, "Some Radar Observations of Meteors and Aurorae at 300 and 500 Mc/s Using a Large Radio Telescope-II," Journal of Atmospheric and Terrestrial Physics, Vol. 24, pp 599-607, 1962.

Basu, S., R. L. Vesprini and J. Aarons, "Field-Aligned Ionospheric E-Region Irregularities and Sporadic E," Radio Science, Vol. 8, pp 235-246, March 1973.

Basu, S., R. L. Vesprini and J. Aarons, "F-Layer Irregularities as Determined by Backscatter Studies at 19 MHz over Half of a Solar Cycle," Radio Science, Vol. 9, pp 355-371, March 1974.

Bates, H. F., "HF Propagation Characteristics through Auroral Ionosphere," Stanford Research Institute, Final Report, General Electric Contract No. 211-000480-T1926, May 1969.

Bates, H. F., "HF Propagation through the Auroral Curtain," Journal of Geophysical Research, Vol. 75, pp 143-151, January 1, 1970.

Bates, H. F. and P. R. Albee, "Aspect Sensitivity of HF Auroral Echoes," Journal of Geophysical Research, Vol. 74, pp 1164-1168, March 1, 1969.

Bates, H. F. and P. R. Albee, "Aspect Sensitivity of F-Layer HF Backscatter Echoes," Journal of Geophysical Research, Vol. 75, pp 165-170, January 1, 1970.

Bates, H. F., A. E. Belon, G. J. Romick and W. J. Stringer, "On the Correlation of Optical and Radio Auroras," Journal of Atmospherie and Terrestrial Physics, Vol, 28, pp 439-446, 1966.

Bates, H. F., R. D. Sharp, A. E. Belon and J. S. Boyd, "Spatial Relationships Between HF Radar Aurora, Optical Aurora and Electron Precipitation," Planetary Space Science, Vol. 17, pp 1164-1168, 1969.

Booker, H. G., C. W. Gartlein and B. Nichols, "Interpretation of Radio Reflections from the Aurora," Journal of Geophysical Research, Vol. 60, pp 1-22, March 1955.

Booker, H. G., "Radio Studies of the Aurora," in Physics of the Upper Atmosphere, Academic Press, pp 355-375, 1960.

Bradley, A. M., L. W. Campbell, S. K. Jones, J. P. Kates, A. H. Katz and D. E. Patton, "Polar Fox II - Experimental Phase, Spring Data," Raytheon Company, Interim Technical Report No. RADC-TR-73-2, September 1972.

Brooks, D., "Observations of Radio Auroral Echoes and Simultaneous Magnetic Disturbances," Journal of Atmospheric and Terrestrial Physics, Vol. 27, pp 1151-1158, 1965.

Brooks, D., "Observations of Auroral Echoes Following Worldwide Storm Sudden Commencements," Journal of Atmospheric and Terrestrial Physics, Vol. 28, pp 103-109, 1966.

Cain, J.C., and R. E. Sweeney, "Magnetic Field Mapping of the Inner Magnetosphere," Journal of Geophysical Research, Vol. 75, pp 4360-4362, August 1, 1970.

Campbell, L. W., S. K. Jones, J. P. Kates, A. H. Katz and D. E. Patton, "Polar Fox II - Experimental Phase, Winter Data," Raytheon Company, Technical Report No. RADC-TR-72-189, June 1972.

Chapman, S., "The Earth's Magnetism," Methuen and Co., 1951.

Chapman, S., and J. Bartels, "Geomagnetism," Vols. I and II, Oxford University Press, 1940.

Chesnut, W. G., J. C. Hodges and R. L. Leadabrand, "Auroral Backscatter Wavelength Dependence Studies," Stanford Research Institute, Final Report, Contract AF 30(602)-3734, June 1968.

Czechowsky, P., W. Dieminger and H. Kochan, "Backscatter Results from Lindau-I. Observations of Radio-Auroras," Journal of Atmospheric and Terrestrial Physics, Vol. 36, pp 955-966, 1974.

Davies, K., "Ionospheric Radio Propagation," National Bureau of Standards Monograph 80, U.S. Government Printing Office, 1965.

Edwards, L. C., A. H. Katz, D. E. Patton and L. W. Campbell, "Polar Fox II - Experimental Phase; Executive Summary," Raytheon Company, Final Technical Report No. RADC-TR-73-203, Vol. II, May 1973.

Feldstein, Y. I. and G. V. Starkov, "Dynamics of Auroral Belt and Polar Geomagnetic Disturbances," Planetary Space Science, Vol. 15, pp 209-229, 1967.

Flood, W. A., "Part I: Some Evidence for the Occurrence of High Electron Densities in the Auroral D and E Region; Part II: An Analysis of the Statistics of Simultaneous Auroral Echoes," Cornell Aeronautical Laboratory Report No. CN-1677-p-1 (Report No. AFCRL-65-451), 1965.

Fouguere, P. F., "Spherical Harmonic Analysis, 2. A New Model Derived from Magnetic Observatory Data for Epoch 1960.0," Journal of Geophysical Research, Vol. 70, pp 2171-2179, May 1, 1965.

Gallagher, P. B. and R. A. Barnes, "Radio-Frequency Backscatter of Artificial Electron Clouds," Journal of Geophysical Research, Vol. 68, pp 2987-3010, May 15, 1963.

Hendricks, S. J., and J. C. Cain, "Magnetic Field Data for Trapped-Particle Evaluations," Journal of Geophysical Research, Vol. 71, pp 346-347, January 1, 1966.

Herman, J. R. and R. Vargas-Vila, "Analysis of Selected Polar Fox II Observations in Light of Auroral Ionospheric Characteristics," Analytical Systems Engineering Corporation, Report No. ESD-TR-73-188, June 1973.

Hower, G. L., and A. B. Makhijani, "Further Comparison of Spread-F and Backscatter Sounder Measurements," Journal of Geophysical Research, Vol. 74, pp 3723-3725, July 1, 1969.

Hower, G. L., D. M. Ranz and C. L. Allison, "Comparison of HF Radar Echoes and High-Latitude Spread-F Measurements," Journal of Geophysical Research, Vol. 71, pp 3215-3221, July 1, 1966.

Hurwitz, L., D. G. Knapp, J. H. Nelson, and D. E. Watson, "Mathematical Model of the Geomagnetic Field for 1965," Journal of Geophysical Research, Vol. 71, pp 2373-2383, May 1, 1966.

IAGA Commission 2 Working Group 4, Analysis of the Geomagnetic Field, "International Geomagnetic Reference Field 1965.0," Journal of Geophysical Research, Vol. 74, pp 4407-4408, August 15, 1969.

Jaye, W. E., W. G. Chesnut and B. Craig, "Analysis of Auroral Data from the Prince Albert Radar Laboratory," Stanford Research Institute, Final Report, Contract DA-30-069-AMC-333(Y), September 1969.

Jensen, D. C. and J. C. Cain, "An Interim Geomagnetic Field," Journal of Geophysical Research, Vol. 67, pp 3568-3569, August 1962.

Larson, A. C. and J. C. Hodges, "VHF/UHF Auroral Radar Measurements," Stanford Research Institute, Final Report, prepared for the General Electric Company under Contract DA 30-039 AMC-333(Y), June 1967.

Leadabrand, R. L., "Some Characteristics of VHF and UHF Auroral Reflections," Stanford Research Institute, Final Report, Upper Atmosphere Clutter Research, Part XI, Contract AF30(602)-1762, March 1960.

Leadabrand, R. L., A. G. Larson and J. C. Hodges, "Preliminary Results on the Wavelength Dependence and Aspect Sensitivity of Radar Auroral Echoes between 50 and 3000 MHz," Journal of Geophysical Research, Vol. 72, pp 3877-3887, August 1, 1967.

Leadabrand, R. L., J. C. Schlobohm and M. J. Baron, "Simultaneous Very High Frequency and Ultra High Frequency Observations of the Aurora at Fraserburgh, Scotland," Journal of Geophysical Research, Vol. 70, pp 4235-4284, September 1965.

Lyon, G. F. and P. A. Forsyth, "Radio-Auroral Reflection Mechanisms," Canadian Journal of Physics, Vol. 40, pp 749-760, 1962.

Malik, C. and J. Aarons, "A Study of Auroral Echoes at 19.4 Megacycles per Second," Journal of Geophysical Research, Vol. 69, pp 2731-2736, July 1, 1964.

McDiarmid, D. R., "On the Aspect Sensitivity of Radio Aurora," Canadian Journal of Physics, Vol. 50, pp 2557-2564, November 1, 1972.

McNamara, A. G., "The Occurrence of Radio Aurora at High Altitudes: the IGY Period, 1957-1959," Geofysiske Publikasjoner, Vol. 29, pp 135-149, 1972.

Millman, G. H., "The Geometry of Radar-Auroral Reflections," General Electric Technical Information Series Report No. R58EMH3, March 1958a.

Millman, G. H., "Atmospheric Effects on VHF and UHF Propagation," Proceedings IRE, Vol. 46, pp 1492-1501, August 1958b.

Millman, G. H., "The Geometry of the Earth's Magnetic Field at Ionospheric Heights," Journal of Geophysical Research, Vol. 64, pp 717-726, July 1959.

Millman, G. H., "Atmospheric and Extraterrestrial Effects on Radio Wave Propagation," General Electric Technical information Series Report No. R61EMH29, June 1961.

Millman, G. H., "Field-Aligned Ionization Scatter Geometry," Journal of Geophysical Research, Vol. 74, pp 900-905, February 1, 1969.

Millman, G. H., "Ionospheric Refraction Effect on the Geometry of Field-Aligned Ionization," Radar Propagation in the Arctic, AGARD Conference Proceedings No. 97, pp (31-1) - (31-15), 1972.

Millman, G. H., "Refraction Effects on Magnetic Field Geometry and HF Propagation," Journal of Atmospheric and Terrestrial Physics, Vol. 37, pp 751-760, May 1975.

Moorcroft, D. R., "Models of Auroral Ionization: Part I. Auroral Ionization Models and Their Radio-Reflection Characteristics," Canadian Journal of Physics, Vol. 39, pp 677-694, 1961a.

Moorcroft, D. R., "Models of Auroral Ionization: Part II. Applications to Radio Observations of Aurora," Canadian Journal of Physics, Vol. 39, pp 695-715, 1961b.

Penndorf, R., "Geographic Distribution of Spread-F in the Arctic," Journal of Geophysical Research, Vol. 67, pp 2274-2288, June 1962.

Peterson, A. M., O. G. Villard, R. L. Leadabrand and P. B. Gallagher, "Regularly Observable Aspect-Sensitive Radio Reflections from Ionization Aligned with the Earth's Magnetic Field and Located within the Ionosphere Layer at Middle Latitudes," Journal of Geophysical Research, Vol. 60, pp 497-512, December 1955.

Pollon, G. E., "Statistical Parameters for Scattering from Randomly Oriented Arrays, Cylinders and Plates," IEEE Transactions on Antennas and Propagation, Vol. AP-18, pp 68-75, January 1970.

Presnell, R. I., R. L. Leadabrand, R. B. Dyce, J. C. Schlobohm and M. C. Berg, "VHF and UHF Auroral Investigations at College, Alaska," Stanford Research Institute, Final Report, Upper Atmosphere Clutter Research, Part I, Contract AF30(602)-1762, April 1959.

Schlobohm, J. C., R. L. Leadabrand, R. B. Dyce, L. T. Dolphin, and M. R. Berg, "High-Altitude 106.1-Mc Radio Echoes from Auroral Ionization Detected at a Geomagnetic Latitude of 43°," Journal of Geophysical Research, Vol. 64, pp 1191-1196, September 1959.

Sprenger, K., and P. Glöde, "Some Properties of Radio Aurorae in Medium Latitudes," Journal of Atmospheric and Terrestrial Physics, Vol. 26, pp 193-198, 1964.

Swenson, E. M., "Aspect-Sensitive Reflections from Ionization Irregularities in the F-Region," Journal of Atmospheric and Terrestrial Physics, Vol. 34, pp 1469-1476, 1972.

Unwin, R. S., "Studies of the Upper Atmosphere from Invercargill, New Zealand; Part 1, Characteristics of Auroral Radar Echoes at 55 Mc/sec," Annales de Geophysique, Vol. 15, pp 377-394, July-September 1959.

Valley, S. L., "Handbook of Geophysics and Space Environment," McGraw-Hill Book Co., New York, 1965.

Vestine, E. H., "The Geographic Incidence of Aurora and Magnetic Disturbance, Northern Hemisphere," Terrestrial Magnetism and Atmospheric Electricity, Vol. 49, pp 77-102, June 1944.

Vestine, E. H., L. LaPorte, I. Lange and W. E. Scott, "The Geomagnetic Field, Its Description and Analysis," Carnegie Institution of Washington Publication 580, 1947.

Watkins, C. D. and H. K. Sutcliffe, "Radar Observations of Weak Field-Aligned Ionization at a Frequency of 300 Mc/s," Journal of Atmospheric and Terrestrial Physics, Vol. 27, pp 309-320, 1965.

Weaver, P. F., "Backscatter Echoes from Field-Aligned Irregularities in the F-Region," Journal of Geophysical Research, Vol. 70, pp 5425-5432, November 1, 1965.

Whalen, J. A., "Auroral Oral Plotter and Nomograph for Determining Corrected Geomagnetic Local Time, Latitude, and Longitude for High Latitudes in the Northern Hemisphere," Air Force Cambridge Research Laboratories, Environmental Research Papers No. 327, AFCRL-70-0422, July 1970.

Zawalick, E. J. and A. L. Cage, "Frequency Tables of the Geomagnetic Index Kp, 1932-1970," Journal of Geophysical Research, Vol. 76, pp 7009-7012, October 1, 1971.

APPENDIX A

RADAR-AURORAL CLUTTER (RAC) COMPUTER PROGRAM

The radar-auroral clutter (RAC) computer program provides a means for determining: (1) the magnetic field geometry necessary for radar-auroral backscatter reflections to take place, i.e., angular orientation (aspect angle) of the direction of propagation with respect to the direction of the lines of force of the earth's magnetic field, and (2) the locations on the earth's surface for the reception of magnetic field-forward scatter from a given transmitter location.

The detailed mathematical developments of the backscatter and forward scatter magnetic field geometries have been published; thus they will not be discussed in this report (Millman, 1958a, 1959, 1969). In the case of radar-auroral backscatter, the magnetic field-aspect angle, θ, can be expressed by the function

$$\theta = f(\phi, \lambda, A, E, h, I, D, n_t, N_e)$$

where ϕ and λ are the geographic latitude and longitude of the radar site, respectively, A and E are the azimuth and elevation angles of the antenna beam, respectively, h is the altitude above the earth's surface of the reflection point, I and D are the magnetic indication and declination angles, respectively, n_t is the index of refraction in the troposphere and N_e is the electron density in the ionosphere. A more complete discussion of this function is given in Appendix B.

The RAC computer program has the capability of determining the orientation of the lines of force of the earth's magnetic field (angle θ) for any geographic location, antenna azimuth angle, elevation angle and radar range or altitude above the earth's surface.

An option is provided in the program to employ one of the following three models of the earth's magnetic field:

1. Graphical model
2. Dipole model
3. Spherical harmonic model

In the graphical model, the parameters I and D have been scaled in 2.5° and 5° latitude and longitude increments over the whole earth's surface from the epoch 1955 isogonic and isoclinic maps issued by the U.S. Navy Hydrographic Office and the Canadian Department of Mines and Technical Surveys. The ground observed magnetic data obtained from these maps are stored in matrix form in the H635 digital computer. Linear interpolation is used for determining the values of the magnetic field elements at other geographic locations. For propagation through the ionosphere, the angles I and D at the subionospheric point are assumed to be invariant at all altitudes. According to the 1955 magnetic charts, the geographic positions of the north and south dip-poles, which are dependent upon local surface anomalies and irregularities, are approximately 73.5°N, 101.1°W and 67.6°S, 144.0°E, respectively.

In the dipole model, it is assumed that the earth's magnetic field can be approximated by a magnetic dipole located at the earth's center having geomagnetic poles at 78.6°N, 70.1°W, and 78.6°S, 109.9°E (Vestine, et al., 1947). For the magnetic dipole approximation, the inclination and declination angles are invariant with altitude.

The spherical harmonic model assumes that the earth's main field, i.e., the magnetic field that excludes such phenomena as magnetic disturbances and diurnal variations, can be represented by a regular or dipole field and an irregular field. A series of spherical harmonics expresses the magnetic potential function for the main field over the earth's surface, the spherical harmonic coefficients being input parameters in the RAC program. For the spherical harmonic model, the angles I and D are altitude dependent. The mathematical formulation of the dipole and spherical harmonic models are contained in Appendix B.

The calculation of the angle θ is performed for either

1. An unrefracted ray which is applicable for line-of-sight radars operating at a frequency of approximately 400 MHz and above (Millman, 1972, 1975) and with the antenna beam elevated at angles greater than about 5° (Millman, 1975) or

2. A refracted ray which takes into account the deflection introduced by the troposphere and/or ionosphere.

The refractive bending in the troposphere is small compared to the ionospheric effect at HF (Millman, 1975) and thus, as a first approximation, is neglected in the magnetic field computations appropriate to HF radars.

The basic assumption used in the refraction computation is that the troposphere and ionosphere can be considered to be stratified into spherical layers of constant refractive index. The computational procedure has already appeared in the literature (Millman, 1958b) and therefore will not be discussed in this report. The accuracy of this method, which is dependent upon the number of stratified layers, can be greatly improved by merely increasing the numbers of stratified layer, i.e., decreasing the thickness of each individual layer element (Millman, 1961).

The computer program incorporates the option for single or multiple ionospheric "hops", i.e., ionospheric reflection points, with a different ionospheric electron density profile for each individual "hop". The magnetic field aspect angle is computed along both the upward ray and the downward ray at every "hop".

An option is available in the program for determining, in the unrefracted ray case, the azimuth angle corresponding to a specified preset aspect angle θ for a set of values of elevation angles and radar ranges or ionospheric altitudes. For the refracted case, this option provides a means for obtaining, along any ray path, the altitude at which a specified aspect angle is attained.

The probability of observing radar reflections from the aurora is, in addition to the geometric and height restriction, dependent upon the frequency of occurrence of auroral activity in the region of interest. Auroral reflections can be expected to exist in regions where both the conditions of near-perpendicularity at ionospheric heights and high auroral activity are satisfied. The fulfillment of only one requirement is not sufficient to warrant a radar-auroral return. The auroral activity model of Vestine (1944), shown in Figure A-1, is presently an integral part of the RAC program. The contour plots, which are stored in matrix form in the program, give the estimated frequency of days with occurrence of visual aurora, on clear, dark nights in the northern hemisphere. The probability of auroral occurrence is computed along the ray paths for both the unrefracted and refracted rays. It is realized that Vestine's model is quite restricted since it applies only to the midnight hours and does not take into account the effect of magnetic activity. A more appropriate model to use for this application is the Feldstein's and Starkov's (1967) auroral belt model, presented in Figure A-2, mainly because the spatial orientation of the auroral activity region is both time- and geomagnetic activity dependent.

Figure A-3 is a logic diagram of the RAC computer program. The dashed line around the Feldstein-Starkov auroral belt model signifies that this function is not presently incorporated in the RAC program.

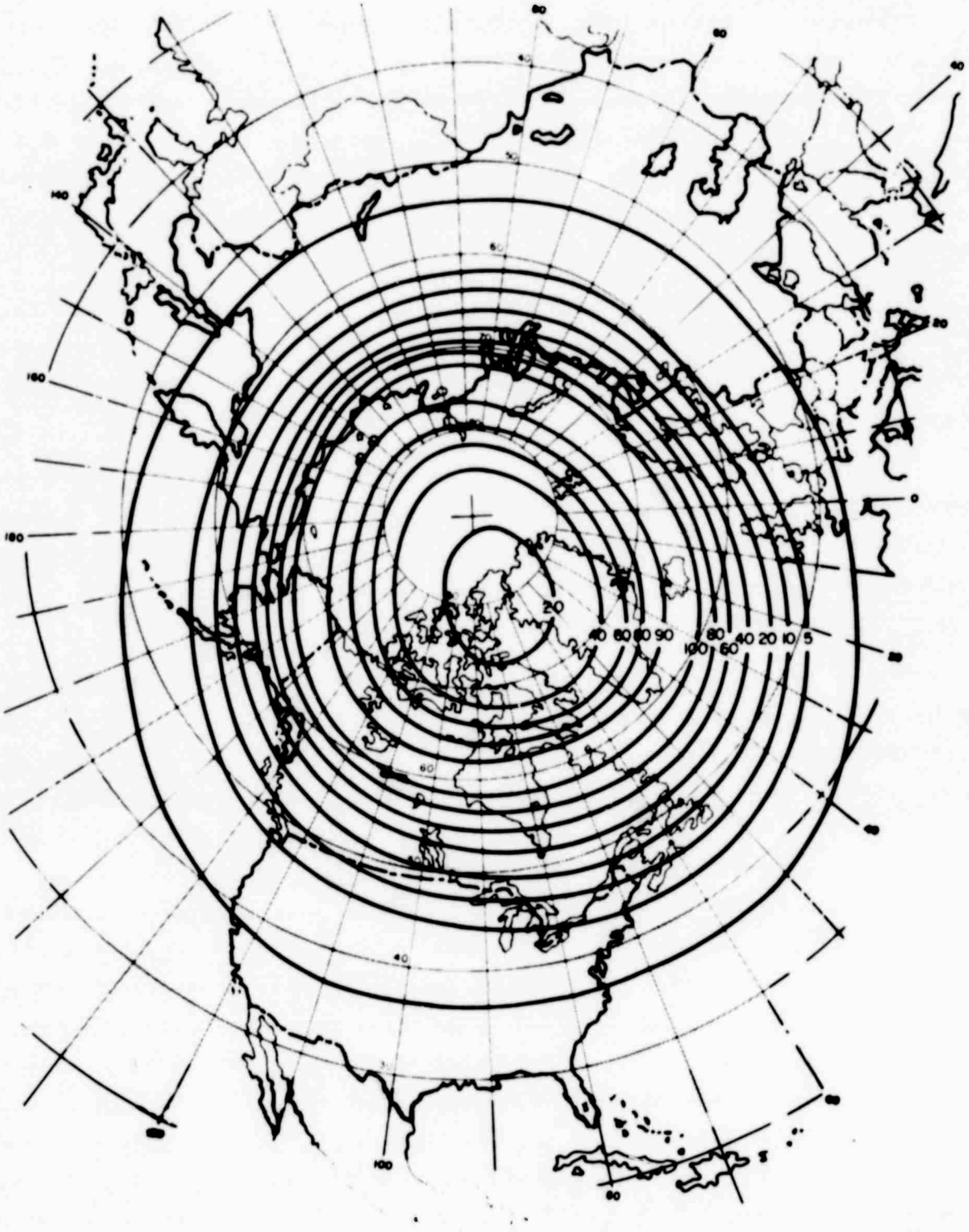

Figure A-1. Estimated Percentage-Frequency of Days with Occurrence of Aurora, Clear Dark Nights, Northern Hemisphere (after Vestine, 1944)

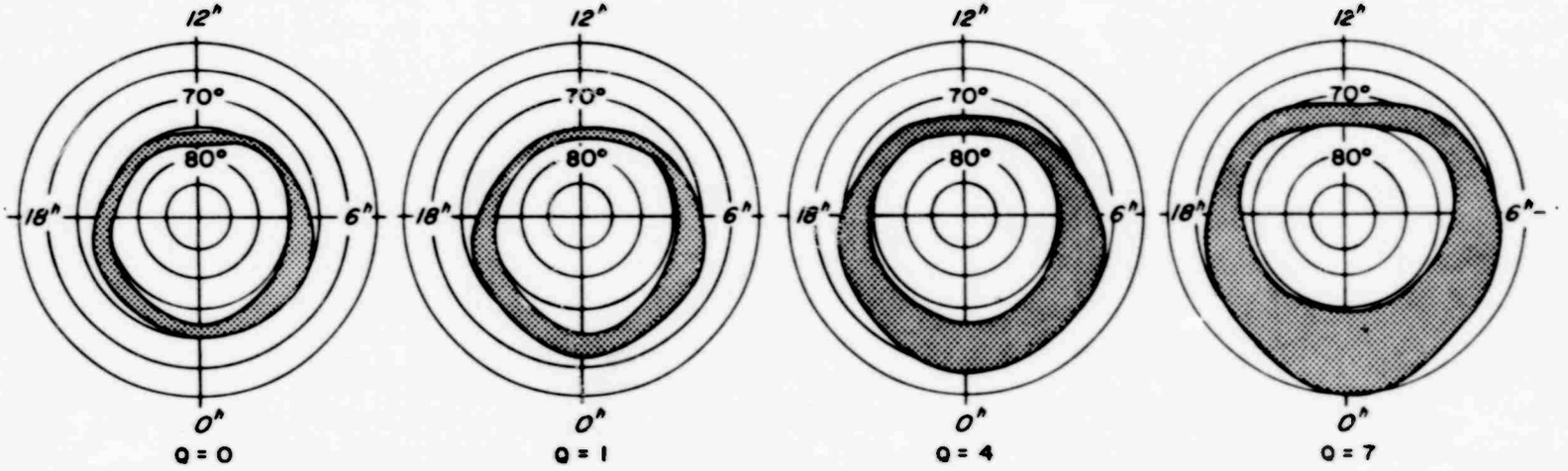

Figure A-2. Variation of the Auroral Belt with Magnetic Activity (after Feldstein and Starkov, 1967)

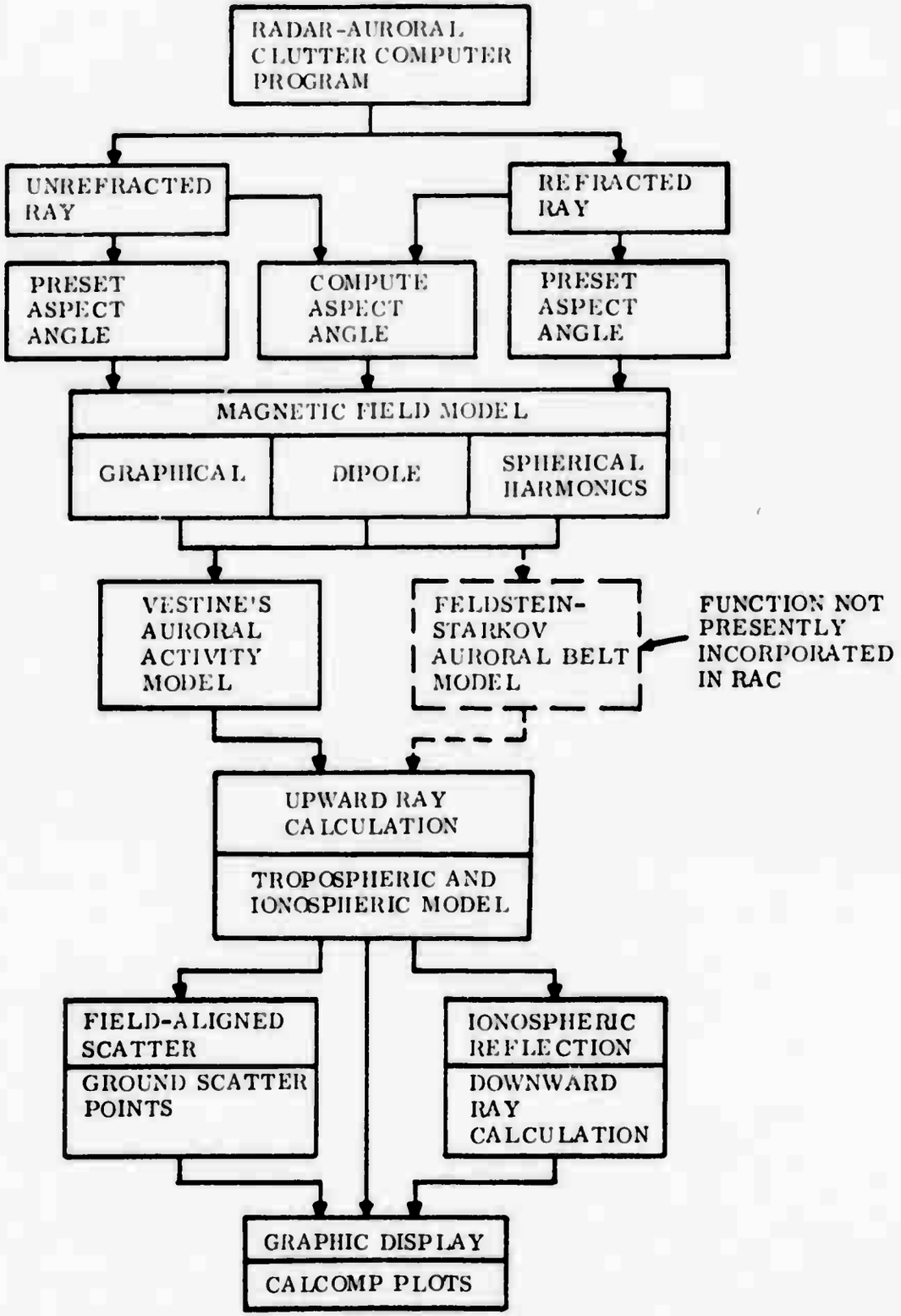

Figure A-3. Radar-Auroral Clutter (RAC) Computer Program Logic Diagram

APPENDIX B

MAGNETIC FIELD-BACKSCATTER GEOMETRY

In the study of radar-auroral reflections, it is desirable to determine the orientation of the lines of force of the earth's magnetic field for any geographic location, antenna azimuth bearing, elevation angle, and reflection height above the earth's surface.

It can be shown that the propagation angle θ (i.e., the angle between the direction of the magnetic lines of force and the direction of electromagnetic propagation), depicted in Figure B-1, can be expressed by the relationship (Millman, 1959)

$$\theta = \cos^{-1} [-\cos e \sin I - \sin e \cos I \cos (\gamma - D)] \tag{B-1}$$

where I and D are the magnetic inclination and declination angles, respectively. These parameters specify the direction of the total magnetic intensity vector in space.

The angle γ which is the geographic azimuth bearing of the observer's location as measured at the subionospheric point, i.e., the location on the earth's surface directly beneath the magnetic field intersection point, is defined by (Millman, 1958a)

$$\gamma = \tan^{-1} \left[\frac{\sin (\lambda_R - \lambda_P) \cos \phi_R}{\sin \phi_R \cos \phi_P - \cos \phi_R \sin \phi_P \cos (\lambda_R - \lambda_P)} \right] \tag{B-2}$$

where ϕ and λ are the geographic latitude and east longitude, respectively. The subscripts, R and P, refer to the transmission (or radar) site and the reflection point, respectively.

The angle e, which is the angle between the ray path and the zenith at the point of reflection, is given by

$$e = \sin^{-1} \left[\frac{r_o}{r_o + h} \cos E \right] \tag{B-3}$$

where r_o is the radius of the earth, E is the elevation angle of the antenna beam and h is the altitude above the earth's surface.

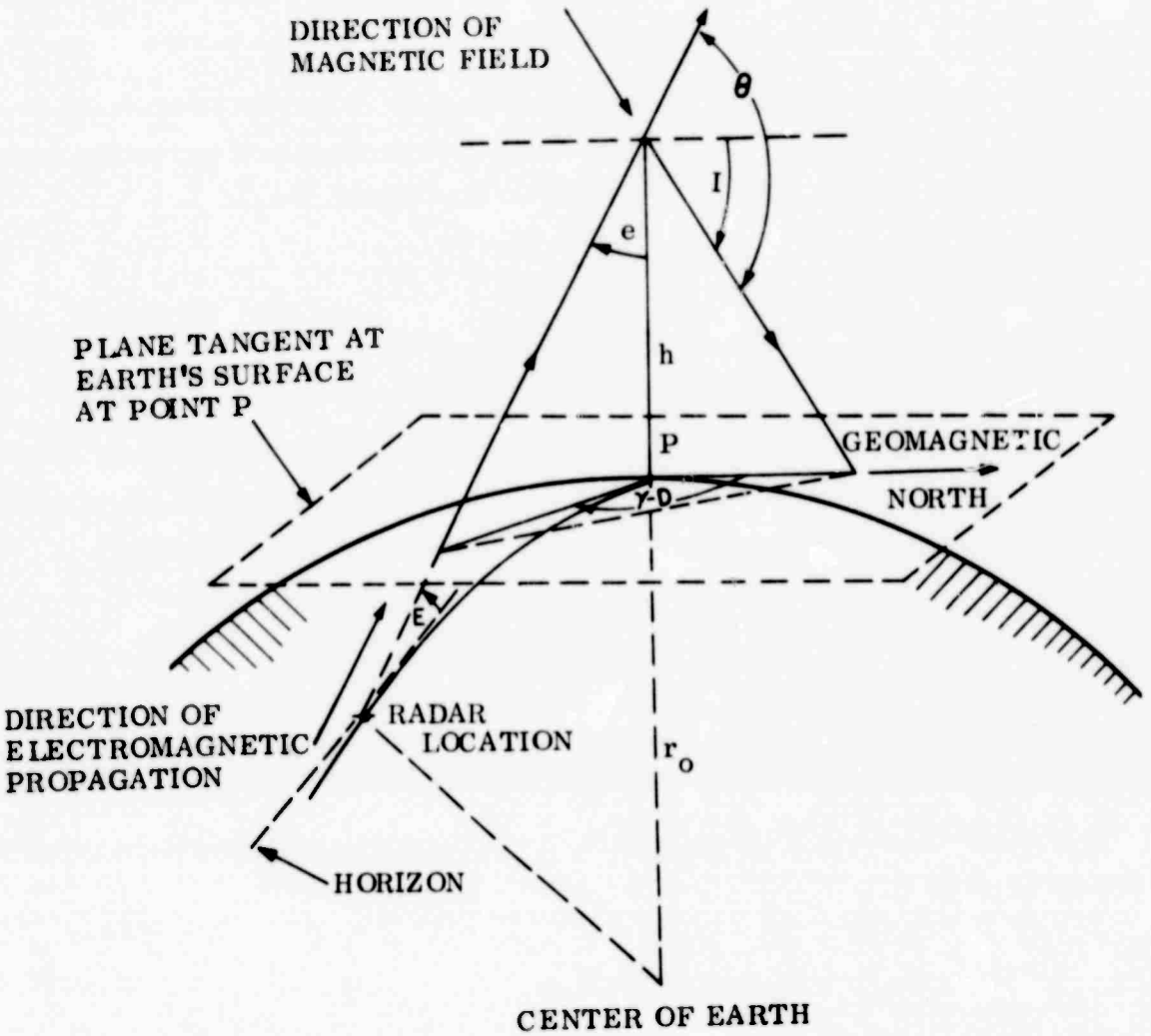

Figure B-1. Radar-Auroral Geometric Configuration

For the dipole model (i. e., earth's magnetic field approximated by a magnetic dipole having the geomagnetic north pole at 78.6°N, 70.1°W) the inclination, or magnetic dip, which specifies the direction of the total magnetic intensity vector with respect to the horizon and is measured positive in the downward direction, is given by (Chapman, 1951).

$$I = \tan^{-1} [2 \tan \psi_P] \tag{B-4}$$

where ψ is the geomagnetic latitude.

A simple transformation for expressing ψ_P in terms of geographic coordinates is given by (Millman, 1959)

$$\psi_P = \sin^{-1} [\cos (\lambda_M - \lambda_P) \cos \phi_M \cos \phi_P + \sin \phi_M \sin \phi_P] \tag{B-5}$$

where the subscript, M, refers to the geomagnetic pole.

The magnetic declination angle, which specifies the direction of the geomagnetic pole and is measured positive in a clockwise direction from geographic north, can be defined by the function (Millman, 1958a)

$$D = \tan^{-1} \left[\frac{\sin (\lambda_M - \lambda_P) \cos \phi_M}{\cos \phi_P \sin \phi_M - \cos (\lambda_M - \lambda_P) \sin \phi_P \cos \phi_M} \right] \tag{B-6}$$

It is of interest to note that, for the dipole model approximation, the inclination and declination are invariant with altitude.

Due to local magnetic anomalies on the earth's surface, there are large discrepancies and widespread departures from a simple dipole field. To take this into account, the earth's main field, i. e., the magnetic field which excludes such phenomena as magnetic disturbances and diurnal variations, can be represented by a regular or dipole field and an irregular field. A magnetic potential function for the main field over the earth's surface can be expressed in terms of a series of spherical harmonics (Chapman and Bartels, 1940) such as

$$V = \sum_{n=0}^{n=\infty} \sum_{m=0}^{m=n} \left(\frac{r_o}{r} \right)^{n+1} [g_{nm} \cos (m\lambda) + h_{nm} \sin (m\lambda)] \; P_n^m (\cos \phi') \tag{B-7}$$

where r is the distance from the center of the earth, ϕ' is the geographic colatitude, $P_n^m (\cos \phi')$ is the associated Legendre function of degree n and order m and g_{nm} and h_{nm} are the coefficients of the spherical harmonic expansion.

It should be noted that the first-degree harmonic terms in Equation (B-7), i.e., terms with n = 1 and m = 0, reduce to that of a dipole potential.

In practice, the magnetic potential is not a measurable quantity. The quantities which are measured are namely X, the northward horizontal component, Y, the eastward horizontal component, and Z, the downward vertical component of the total magnetic intensity, which are defined in terms of the magnetic potential by

$$X = \frac{1}{r} \frac{\partial V}{\partial \phi'} \tag{B-8}$$

$$Y = \frac{1}{r \sin \phi'} \frac{\partial V}{\partial \lambda} \tag{B-9}$$

$$Z = \frac{\partial V}{\partial r} \tag{B-10}$$

By definition, the magnetic inclination and declination angles are related to components of the total magnetic intensity by

$$I = \tan^{-1}\left[\frac{Z}{(X^2 + Y^2)^{\frac{1}{2}}}\right] \tag{B-11}$$

$$D = \tan^{-1}\left[\frac{Y}{X}\right] \tag{B-12}$$

It should be evident from Equations (B-7) through (B-12) that, for the spherical harmonic-magnetic field model, the parameters I and D are altitude dependent.

For a given set of spherical harmonic coefficients, the magnetic potential function, Equation (B-7), becomes specifiable. This function, in turn, is then employed to evaluate the spatial distribution of I and D.

The spherical harmonic coefficient models that are incorporated in the RAC computer program are listed in Table B-1.

TABLE B-1

SPHERICAL HARMONIC MODELS INCORPORATED
IN THE RAC COMPUTER PROGRAM

Model	Coefficients				
	Type Normalization	Epoch	Degree n	Order m	Total No.
Cain and Sweeney (1970)	Schmidt	1968.0	10	10	120
Fouguere (1965)	Gaussian and Schmidt	1960.0	8	7	77
Hendricks and Cain (1966)	Schmidt	1960.0	9	9	96
Hurwitz et al. (1966)	Schmidt	1965.0	12	12	155
International Geomagnetic Reference Field (1969)	Schmidt	1965.0	8	8	79
Jensen and Cain (1962)	Gaussian	1960.0	6	6	48

In the computation of the magnetic field-aspect angle, defined by Equation (B-1), 48 spherical harmonic coefficients ($n = 6$, $m = 6$) are only used although the international geomagnetic reference field (IGRF) derived by the International Association of Geomagnetism and Aeronomy (IAGA) and the models proposed by Cain and Sweeney (1970), Fouguere (1965), Hendricks and Cain (1966) and Hurwitz, et al. (1966) consist of a greater number of coefficients. The error introduced by neglecting the higher degree and order coefficients is of minor importance in geometric studies of field-aligned ionization.

According to Cain and Sweeney (1970) the IGRF model is inadequate when a high degree of accuracy is required especially at altitudes below 1000 km. For this condition, Cain and Sweeney (1970) recommend that models such as the one they propose be used.